Analysis, Modelling, and Control Strategy Development for Prosumer-based Heat Networks

Master Thesis

In partial fulfilment of the requirements for the degree
Master of Science in Power Engineering
at the Chair of Renewable and Sustainable Energy Systems
of the Technical University of Munich.

Advisor Prof. Dr. Thomas Hamacher

M.Sc. Thomas Lickleder er

Submitted by Ilya Elizarov

Munich, July 2020

Analyse, Modellierung und Entwicklung von Regelstrategien für Prosumer-basierte Wärmenetze

Masterarbeit

Wissenschaftliche Arbeit zur Erlangung des Grades
Master of Science in Power Engineering
an der Lehrstuhl für Erneuerbare und Nachhaltige Energiesysteme
der Technischen Universität München.

Betreut von Prof. Dr. Thomas Hamacher
M.Sc. Thomas Lickleder er

Eingereicht von Ilya Elizarov

München, Juli 2020

Abstract

A prosumer with an integrated heat source and load can produce and consume heat with respect to the heat network; thus, carrying out bidirectional heat flow. For this thesis, heat transfer to and from the network is performed by the means of the heat exchanger, which every prosumer is equipped with. The water flow in the network is non-directional, meaning that it could change the direction depending on the operating mode of prosumers. It was revealed that two major challenges were restricting energy and medium flow in the network: the exergy losses of the heat exchanger and the flow blocking caused by excessive pressure difference. A computer model written in the Modelica language and simulations performed in the Dassault Systèmes Dymola environment were used to investigate the thermohydraulic performance of three prosumers consolidated in the network. A stable heat flow with respect to the network following the reference value was the condition for an appropriate control strategy. As a response to the major challenges, a control strategy was suggested and tested. Heating curve switching and “suppression controller” are key elements of the developed control strategy. The first mechanism utilizes a heating curve with a higher supply temperature at the heat source for production to compensate for the exergy losses. The second is only activated in the blocking state, and it suppresses the shaft velocity of the feed-in pump that is producing excessive pressure. It is done by transmitting the velocity reduction signal. The control strategy was tested with a discrete heat flow reference with respect to the network under various scenarios. The capability of the control strategy to respond to the challenges is then demonstrated. However, some of the transient processes cause an undesired indoor air temperature drop and short-time heat flow rate overproduction in the network. The origin of these transient states was investigated for the future improvement of the control strategy.

MSE Munich School of Engineering
Technische Universität München

Bachelor's / Master's thesis

Modelling of innovative bidirectional heat networks

Motivation
Conventional heating networks distribute the energy unidirectionally from the central generation units to the consumers. The decentralisation of energy production and storage together with the progressive coupling of the heat and electricity sectors leads to the idea of a new type of heat network: From the network perspective, consumers become sector-coupled prosumagers (producer + consumer + storage) forming a technical welfare aggregate. They exchange energy bidirectionally within the closed heating network and with the public electricity network. Networking is intended to improve the overall performance of the aggregate in comparison to the loose totality of self-sufficient units. This requires adequate topologies and novel hydraulic infrastructures, which must be operated with appropriate control methods and strategies.

Working Environment
In the facilities of the Center for Energy and Information, an experimental network laboratory is currently under construction which will emulate an energy system consisting of 5 buildings including a connecting heating network and Smart Grid. The planned topology and hydraulics of the laboratory network will in the framewok of the thesis serve as a reference for future bidirectional heating networks.

The work is located in the MSE offices on the TUM campus in Garching near Munich. The support is provided by a scientific employee on site. A workplace is provided if required.

Main tasks
The aim of this thesis is to investigate the thermohydraulic behaviour of such bidirectional heat networks on the basis of models, to derive suitable operating strategies and possible improvement proposals for the design of such heat networks. Optionally, further control algorithms for the implementation of abstract optimized energy flows will be developed.

1. research on the planning, operation / control and modelling of heat networks
2. modelling of a bidirectional heating network based on the laboratory network in OpenModellica or a comparable software (Dymola, SimulationX, Simulink, TRNSYS etc.)
3. investigation of the thermohydraulic behaviour of the model, plausibility check of the results and development of operating strategies
4. identification of critical operation/control states
5. development of control concepts and recommendations for adapting the hydraulics / topology of the network for more efficient, stable operation
6. summary of the results in a scientific thesis

Requirements
- Enrolled student status at TUM
- A profound understanding of thermodynamics and fluid mechanics
- Experience in modelling and in dealing with corresponding software
- Programming experience desirable
- Reliable, independent and scientific way of working

What we offer
- Participation in research on the energy systems of the future
- Multidisciplinary working environment
- Theoretical task with practical relevance and relation to laboratory implementation
- Individual support by motivated scientists in a cooperative atmosphere
- Possibility of publication in international journals and conferences

Application
Please send your complete application documents with cover letter, curriculum vitae, diplomas and current overview of grades to **thomas.lickleder@tum.de.**

Statement of Academic Integrity

I,

Last name: Elizarov
First name: Ilya
ID No.: 03693486

Hereby confirm that the attached thesis,

Analysis, modelling, and control strategy development for prosumer-based heat networks

Was written independently by me without use of any sources or aids beyond those cited, and all passages and ideas taken from other sources are indicated in the text and given the corresponding citation. I confirm to respect the „Code of Conduct for Safeguarding Good Academic Practice and Procedures in Cases of Academic Misconduct at Technische Universität München, 2015", as can be read on the website of the Equal Opportunity Office of TUM. Tools provided by the chair and its staff, such as models or programmes, are also listed. These tools are property of the institute or of the individual staff members. I will not use them for any work beyond the attached thesis or make them available to third parties.

I agree to the further use of my work and its results (including programmes produced and methods used for research and instructional purposes.

I have not previously submitted this thesis for academic credit.

Munich, 15.07.2020

.....
(Author: Elizarov, Ilya)

Declaration for the Transfer of the Thesis

I agree to the transfer of this thesis to:

- Students currently or in future writing their thesis at the chair:
  - ☑ Flat rate by students
  - ☐ Only after particular prior consultation.
- Present or future employees at the chair:
  - ☑ Flat rate by employees
  - ☐ Only after particular prior consultation.

My copyright and personal right of use remain unaffected.

Munich, 15.07.2020

.....

(Operator: Elizarov, Ilya)

Contents

1. Introduction

Innovative prosumer-based heat networks allow deeper integration of renewable energy and waste heat sources for the heat supply of cities while remaining to be a cost effective solution. A conventional district heating system unites big generation centres and consumers by means of a heat network. However, with the prosumer technology, customers can participate in heat production and distribution as well. Potentially, together with energy sector coupling, widespread use of this technology can have the same impact on energy systems of cities as electricity generation from PV panels are promoted by a feed-in tariff policy in Germany.

With the state-of-the-art technology, the role of district heating in the future of the European energy system is evaluated, and the concept of prosumers, which is beyond the state-of-the-art, is then introduced in section 1.1. The problem definition, goals and objectives are explained in section 1.2 and in section 1.3. Section 1.4 describes applied scientific method. Finally, section 1.5 gives an overview about related works from the literature.

1.1. Context

This section provides a context for the topic of the thesis. The role of district heating in decarbonisation is examined in section 1.1.1, and a basic description of prosumers is given in section 1.1.2.

1.1.1. Role of District Heating in Decarbonisation

The European Union has been showing an intention to mitigate climate change. The goal is to cut greenhouse gas emissions by 80% by 2050 compared to 1990. This imposes serious challenges on the European energy system, since it is the main source of emissions [6]. Moreover, sustainability, energy security (reduction in import dependency), competitiveness are the other objectives of the EU energy policy [6].

Taking a closer look at the EU energy system from 2015 in fig. 1, heating and cooling accounted for the half of the final energy demand distribution. In this share, space heating was the most prominent end-use with a of share 27%.

The energy carriers that covered the final energy demand are given in fig. 2. Natural gas with a share of 42% was the main energy carrier for heating. In total, fossil fuels accounted for 66% of primary energy consumption share. This share mostly represented heat production in on-site boilers. Renewable energy covered only 13% of the total demand.

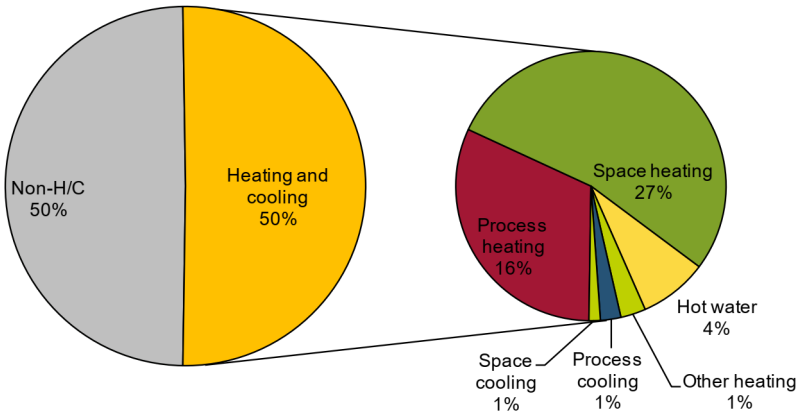

Figure 1: Final energy demand by end use in EU28 in 2015 [7]

.

The large share of the fossil fuel usage clearly demonstrates that transformations in the heating sector are necessary to reach the ambitious objective of decarbonisation. Special attention should be paid to space heating, which is the main application of heat in the end-use.

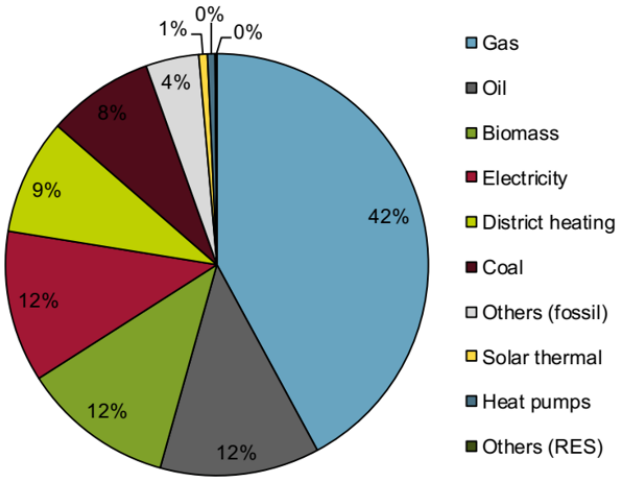

Figure 2: Primary energy consumption for heating in EU28 in 2015 [7]

.

Drastic decarbonisation in heating supply could be achieved by various measures e.g. introduction of a high share of renewable energy sources, reduction in final energy demand (energy saving) or building carbon capture storages. The main trend in literature focuses on electrification with extensive energy saving as the main technological change in the heating sector [5]. However, Colony et al. [5] investigates the role of a district heating expansion.

District heating expansion is relevant because of sufficient demand in many European cities (in 2014 approx. 73% of residents lived in cities, towns, and suburbs [11]). In 2015, district heating covered only 12% of final energy demand in EU28 as mention in fig. 2 and approx. 14% in Germany [7], so there was an unrealized opportunity for growth. In addition, 46% of waste heat and 31% of the heat demand is concentrated within densely populated areas [16]; therefore, cities possess one more potential heat source that can be effectively used in the heat network in the future.

The future district heating systems imply the substitution of individual fossil fuel boilers with a connection to the heat network [5]. As a consequence, customers could receive heat from local renewable and waste heat sources. Another trait of the future district heating system is decentralisation. Construction of new relatively small combined heat and power (CHP) plants will be required since heat production must be located near heat demand in urban areas [5].

According to [5], the motivation for the district heating expansion is the following. The EU energy system would be able to achieve the goal of greenhouse reduction with costs for heating that are 15% lower than without the expansion. Additionally, the annual costs would decrease by 7%. The estimations done in the research were based on contemporary heat supply technology.

In conclusion, district heating expansion complements the transition to renewable energy in a way that it connects consumers and renewable and waste heat sources in cities. This is a cost-effective solution that can be implemented with the current state-of-the-art in heat supply industry. Nevertheless, there is an opportunity to further integrate local heat sources by means of, so-called, prosumers.

1.1.2. Prosumers

Prosumer is a neologism made of the words producer and consumer, showing that a prosumer can produce and consume heat with respect to the heating network [2]. While remaining to be a cost-effective solution, the introduction of a prosumers-based heat network can promote district heating expansion, utilization of a higher share of renewables, and waste heat.

For example, a building with solar thermal collectors could be a prosumer if it was connected to the network. When heat supply surpasses the demand, the surplus could be fed into the network and vice versa. Other examples of potential prosumers, according to Kauko et al. [10], could be buildings with large chiller and refrigeration facilities, such as data centers, office buildings, or food retail stores. Such buildings may have a demand for heat at

low ambient temperature and surplus of heat at high ambient temperature.

The following benefits of prosumers were mentioned in [17]. Heat networks with prosumers could be especially relevant for densely populated areas since they lack areas for large solar thermal plants. Combining heat supply and feed-in in a customer's substation does not require to build additional connecting points to the district heat network. Moreover, existing hydraulic components of heating substations could be utilized. Thus, the introduction of prosumers is cost-effective.

A prosumer can produce and consume heat with respect to the heat network; thus, carrying out bidirectional heat flow. For this thesis, heat transfer to and from the network is performed by the means of the heat exchanger, which every prosumer is equipped with. The water flow in the network is non-directional meaning that it could change the direction depending on the operating mode of prosumers. To emphasize the requirements that prosumers impose, a comparison between conventional and prosumer-based networks is made in table 1.

Table 1: Comparison between conventional and prosumer-based heat networks, adapted from [3]

Conventional	Prosumer-based
Unidirectional energy flow Supply station transfers heat to the network. Customers receive heat from the network.	*Bidirectional energy flow* Some customers produce, the others consume heat with respect to the network. After some time their roles can interchange.
Directional medium flow Heat carrier is circulated in the network driven by pressure difference from the pumps installed at supply stations. Flow is directed from the production center to consumers; hence, the flow direction is the property of the network.	*Non-directional medium flow* Flow direction is not determiner by the network, but rather is determined by the operation mode of a customer.

To sum up, the introduction of prosumers can have some benefits, but it requires radical changes in heat networks.

1.2. Problem Definition

Operation of a heat network with a prosumer can affect both the heat network and an inner system of the prosumers [2]. The impact on the network can impair its ability to transmit the

required heat flow rate.

A review of the available literature, which will be given in later in this chapter, revealed that a control strategy was already suggested and tested for a prosumer; however, it was applied under the condition that the rest of the network consisted of conventional consumers. Therefore, a control strategy for the network that fully consists of prosumers has yet to be developed.

1.3. Goals and Objectives

The framework of this thesis is an experimental set up in the facilities of the center for Combined Smart Energy Systems (CoSES) at the Technical University of Munich.

The functional scheme of the prosumer substation in the CoSES center is given in fig. 3. Bidirectional heat flow takes place in the heat exchanger. The non-directional heat network is presented by "hot" and "cold" pipelines, where corresponding temperatures are sustained. A control valve on the primary side is modulated in consumption mode, and a feed-in pump is activated in production mode. Two pumps on the secondary side are production and consumption pumps that guarantee counter current flow at the heat exchanger with a respective mode of operation.

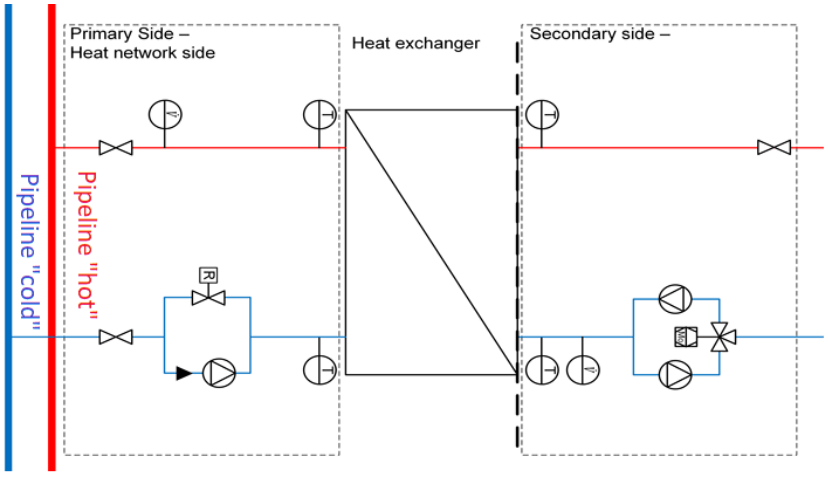

Figure 3: Functional scheme of the prosumer substation in CoSES center [19]

The goal of the thesis is to derive a suitable control strategy to provide a stable heat injection/extraction flow with respect to the network that consists of three prosumers.

The objectives of the thesis are:

1. Literature researching on the current state of a control strategy development for heat networks with prosumers

2. Modelling of a prosumer and a prosumer-based heat network
3. Developing and modelling control strategy
4. Performing simulations and investigation of thermohydraulic behaviour of the prosumer-based heat network
5. Identification of critical operation and control states
6. Investigating the potential of improvement for the control strategy

1.4. Method

Computer modelling and simulation of physical processes is the research method applied in the thesis. A model written in the Modelica language and simulations performed in the Dassault Systèmes Dymola environment were used to investigate the thermohydraulic performance. Fritzson [8] describes the Modelica language in the following paragraph.

Modelica has a major application in virtual prototyping of complex, multi-domain cyber-physical systems, which mix physical system dynamics with software. Based on the visual design of lego-like model building blocks, it is easy to use. Last, but not least, an open-source and free environment OpenModelica is used in academic and industrial environments. Although Modelica has certain benefits from other programming environments, it is not yet well-known.

The methodology of the thesis consists of the following steps.

1. Carrying out a preliminary analysis of the prosumer-based heat network to formulate a hypothesis
2. Developing the prosumer and prosumer-based heat network models
3. Investigating thermohydraulic performance to confirm the hypothesis from the preliminary analysis
4. Developing control mechanisms and their modelling
5. Validation and evaluating of control mechanisms to formulate consolidated control strategy
6. Investigating thermohydraulic performance under various scenarios to reveal critical operation and control states for the developed control strategy

1.5. Literature Review

Control strategy of an individual prosumer has strong impact on flow, pressure, and temperature of the network [2]. In this context, it is necessary to dedicate the literature review to both prosumer (see section 1.5.1) and heat network (see section 1.5.2) levels.

1.5.1. Control Strategy for a Prosumer

A control strategy for a prosumer was proposed by Rosemann et al. [17] The prosumer included three fundamental components: a heat source, a heat sink, and a connection to the network. The implementation of these fundamental components was the following.

- The heat source was a solar thermal system
- The heat sink was a consumer's heat supply system – combined space heating and domestic hot water supply
- Connection to the district heating network was made through a heat exchanger

The scheme of the prosumer is given in fig. 4. The variable speed feed-in pump is required to overcome pressure difference and provide required mass flow rate in the network. The control valve on the primary side sustains the necessary flow rate from the network. The purpose of two supplementary valves is to guarantee counter flow with the respect to the heat exchanger.

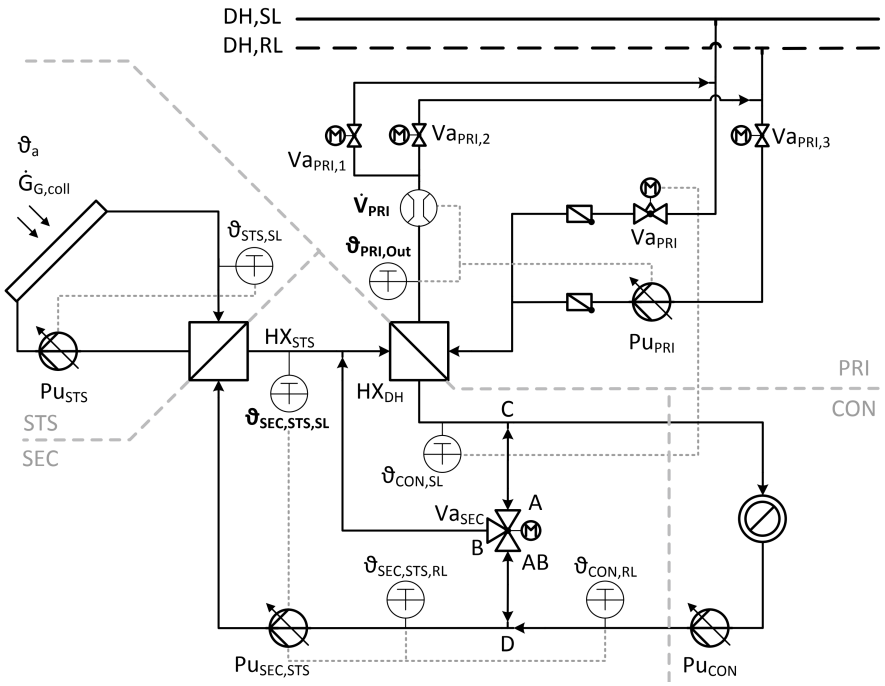

Figure 4: Functional scheme of a prosumer from [17]

The prosumer has four operating modes that explain its basic functioning (see table 2). Each mode is defined by heat flow from solar gain and the consumer's heat demand, which, in-turn, depends on the outdoor temperature.

A control mechanism of the feed-in pump has two differing tasks:

Table 2: Operating modes of the prosumer from [17]

Mode	Description
Supply	The demand is covered completely by the network
Combi-S	The demand is covered by the internal heat source and the district heating network
Feed-in	There is no demand from the consumer's side. Heat flow from solar gain is fed into the network

1. Overcoming the pressure difference of the heat network to generate mass flow rate
2. Controlling the feed-in supply temperature by varying the volume flow rate

A cascaded controller (see fig. 5) was used to achieve both tasks. The set point for the outer controller is given by a heating curve depending on the outdoor air temperature i. e. $T^{pri}_{hot,\,set} = f(\vartheta_o)$. The outer controller finds a solution for the equation eq. (1) by adjusting the volume flow set point $\dot{V}^{pri}$ of the inner controller. The inner controller compensates any changes of the pressure difference in the network, which act as a disturbance.

$$T^{pri}_{hot,\,set} = \frac{\dot{Q}_{STS}}{\dot{V}^{pri}\,\rho\,c_p} + T^{pri}_{cold} \tag{1}$$

where $\dot{Q}_{STS}$ is the reference heat flow rate with respect to the network.

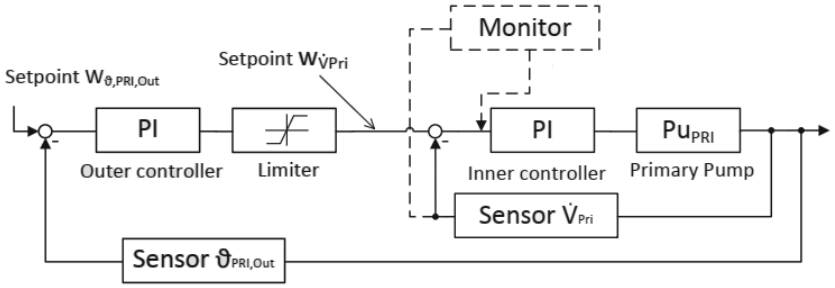

Figure 5: Cascade closed-loop controller of the feed-in pump [17]

The control strategy applied by Rosemann et al. was developed under the condition that the rest of the heat network consisted of conventional consumers.

1.5.2. Influence of Prosumers on Heat Network

In order to identify critical operation and control states influenced by a prosumer in the network, the following literature sources were found.

Heymann et al. [9] and Paulick et al. [15], identified crucial operating stages of decentralized feed-in substations from solar thermal collectors into a heat network. It was observed that when heat demand connected downstream lags feed-in output, a reversal of the flow direction upstream occurs. A border between two opposite mass flow rates was called the supply frontier [9]. In this region mass flow rate along supply and return lines is nearly zero. This effect was independent of network topology.

The same effect as supply frontier, but in terms of differential pressure, as was mentioned by [2]. After a certain threshold of injected heat flow rate, a prosumer creates its own pressure cone[1]. When a feed-in pump generates corresponding the mass flow rate that corresponds to the critical heat flow, the pressure difference in customers' proximity increases. Potentially, if a heat flow keeps on increasing, oncoming end of the pressure cone can even suppress the central producer or other decentralized heat generators [20]. Under normal operation, no pressure cone is created, and the network follows a pressure cone created by a centralized heat source. As a result, differential pressure gradually decreases from the source to the most distant point of the network.

A control mechanism of the main circulating pump typically utilizes differential pressure as a measured variable. The measurement of the pressure can be performed directly at the source or at some point in the network, usually, the most distant one. When the latter is performed, and a prosumer influences the pressure at this point. Thus, the main circulating pump decreases differential pressure at the source to keep to the reference. This has a negative effect on the areas of the network that are not reached by prosumers: differential pressure in these nodes also decreases [2].

Water stops in the supply frontier and cools down due to thermal losses in the network. There is no pressure gradient along the supply and return line in a network between consumers, but the pressure difference between supply and return pipelines is present. Supply frontier is not a static point in the network, but a movable one depending on the performance of feed-in's pump or pumps interaction in a particular network. When pressure conditions change, cool water volume in supply frontier starts to move along the network.

Finally, another problem was noticed in the pilot projects. Pump-to-pump interactions between prosumers might cause pressure and mass flow oscillations [20]. The problem is especially prominent when the prosumer with a larger feed-in pump affects another prosumer with smaller feed-in pump.

[1] Pressure cone represent pressure in supply and return lines along pipelines and can be used to indicate pressure difference

2. Fundamentals

This chapter presents essential background on hydronic heating systems mainly focusing on components of the prosumer given in section 1.3.

Governing equations of fluid dynamics are given in section 2.1, heat exchanger thermal analysis is presented in section 2.2, fundamentals for control valves and circulating water pumps are summarized in section 2.3 and section 2.4. 'Flow – head' diagram analysis for determining flow conditions in the network is described in section 2.7

In addition, a short introduction on heating load and heat supply are given in section 2.5 and section 2.6. At the end of this chapter some insights on modelling and simulation within the Modelica language are given in section 2.8.

2.1. Governing Equations of Fluid Dynamics

Dynamic modelling of a hydronic heating system, and especially a heat network requires at least a basic understanding of fluid dynamics. Three equations: material balance, momentum and energy equations describe the physics behind the liquid flow in hydronic systems.

For most applications in district heating, the heat carrier is water, and it can be considered incompressible i.e. $\rho = const$. The resulting material balance for every hydronic component is then simply:

$$0 = \dot{m}_{in} - \dot{m}_{out} \tag{2}$$

Obviously, the one-dimensional flow was enough for consideration since the thesis focuses on the overall hydro- thermodynamic behaviour. Under this assumption, the momentum equation of a finite liquid volume can be written as:

$$\rho \left(\frac{\partial v}{\partial t} + \frac{\partial v^2}{dx} \right) = -\frac{\partial p}{\partial x} + \mu \left(\frac{\partial^2 v}{\partial x^2} \right) + \rho s \tag{3}$$

where t is time; x is spatial coordinate; v is mean velocity; p is mean pressure; ρ is mean density; μ is kinematic viscosity.

The term s in eq. (3) represents acceleration due to body forces. The body forces acting on the liquid volume are:

- Gravity. Gravity does not act along the x-axis, but when a single pipe undergoes elevation, the gravitational term can be formulated as:

$$s_g = g \frac{dz}{dx} \tag{4}$$

Here, z is the elevation above the horizon.

- Friction. Friction can be expressed as a body source:

$$s_f = -\frac{1}{2} v|v| \left(f_D S + \zeta\right) \tag{5}$$

Fanning friction factor f_D depends on relative roughness of the pipe and Reynolds number: $f_D = f\left(\frac{\epsilon}{d}, Re\right)$. Fanning factor can be found in the literature depending on a specific task. Here ϵ is absolute roughness, S is the circumference of a pipe, and ζ is local loss coefficient.

Heat networks are characterized by turbulent flow region [4]. This means that the flow can be considered as inviscid where net viscous forces in eq. (3) are negligible i.e. $\mu\left(\frac{\partial^2 v}{\partial x^2}\right) \approx 0$, and the final version of the differential equation for momentum is obtained as:

$$\rho\left(\frac{\partial v}{\partial t} + \frac{\partial v^2}{dx}\right) = -\frac{\partial p}{\partial x} + \rho s \tag{6}$$

The general form of the energy equation for a finite liquid volume is:

$$\rho\left(\frac{\partial u}{\partial t} + \frac{\partial v\left(u + \frac{p}{\rho}\right)}{\partial x}\right) = v\frac{dp}{dx} + v\rho s_f + k\frac{\partial^2 T}{\partial x^2} + \dot{Q} \tag{7}$$

where u is specific internal energy; k is thermal diffusivity; $\dot{Q}$ is the source term that represents heat inflow or outflow to the liquid volume.

It is worth mentioning, that eq. (7) describes the effect of outlet temperature growth when the volume of the pipe is filled with liquid that temperature is different from the inlet.

2.2. Heat Exchangers

For the set up, a heat exchanger is responsible for bidirectional heat flow. The basic equations that describe its performance are given in this section. Exemplary flow scheme of the heat exchanger is shown in fig. 6.

The energy balance for primary and secondary side [1]:

$$\begin{cases} \dfrac{dU^{pri}}{dt} = \dot{m}^{pri} c_p^{pri} (T_{in}^{pri} - T_{out}^{pri}) + \dot{Q} \\ \dfrac{dU^{sec}}{dt} = \dot{m}^{sec} c_p^{sec} (T_{in}^{sec} - T_{out}^{sec}) + \dot{Q} \end{cases} \tag{8}$$

The terms on the left side demonstrate the change in internal energy with time:

$$\frac{dU}{dt} = \frac{dT_{out}}{dt}\left(m_w\, c_p + \frac{1}{2} m_{HEX} c_{p,\,HEX}\right) \tag{9}$$

where m_w is the mass of water volume; m_{HEX} is mass of the heat exchanger without water; $c_{p,\,HEX}$ is specific heat capacity of heat exchanger material.

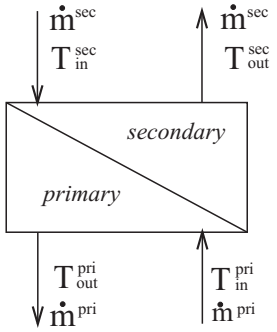

Figure 6: Heat exchanger flows scheme

The heat transfer rate $\dot{Q}$ can be calculated as following:

$$\dot{Q} = hA\Delta T_{LMTD} \tag{10}$$

where Δt_{LMTD} is logarithmic mean temperature difference (LMTD); h is overall heat transfer coefficient, and A is heat transfer area.

The counter flow arrangement was always applied in the considered prosumer set up. With this arrangement, LMTD for counter current flow is:

$$\Delta T_{LMTD} = \frac{\Delta T_1 - \Delta T_2}{ln\left(\Delta T_1 / \Delta T_2\right)} \tag{11}$$

where $\Delta T_1 = T_{hot,\,in} - T_{cold,\,out}$ and $\Delta T_2 = T_{hot,\,out} - T_{cold,\,in}$.

The problem with using eq. (10) and eq. (11) is that the temperature at minimum three nozzles must be known. However, for a prosumer, only two temperatures are known: inlet temperature on the secondary side and inlet temperature on the primary side. To avoid the problem, NTU-effectiveness (NTU-ε) method can be applied.

In NTU-ε method, heat transfer rate is expressed as:

$$\dot{Q} = \varepsilon\, C_{min}\left(T_{hot,\,in} - T_{cold,\,in}\right) \tag{12}$$

where ε is the effectiveness; C_{min} is the smaller heat capacity rate.

For a counter-flow arrangement, the effectiveness is:

$$\varepsilon = \frac{1 - e^{-NTU(1-R)}}{1 - Re^{-NTU(1-R)}} \tag{13}$$

The variables in eq. (13) are clarified below.

Number of transfer units NTU is given by:

$$NTU = \frac{hA}{C_{min}} \tag{14}$$

Heat capacity rate ratio R is calculated as:

$$R = \frac{C_{min}}{C_{max}} = \frac{\dot{m}_{max} c_{p,\,max}}{\dot{m}_{min} c_{p,\,min}} \tag{15}$$

where $\dot{m}_{max}$ is bigger mass flow rate; $\dot{m}_{min}$ is smaller mass flow rate; $c_{p,\,max}$ and $c_{p,\,min}$ are specific heat capacities for the flows.

With $R = 1$, the effectiveness is:

$$\varepsilon = \frac{NTU}{1 + NTU} \tag{16}$$

2.3. Control Valves

A regulating or control valve is another essential element of the set up. It regulates the flow rate coming from the heat network to fulfil heat demand in consumption mode of the prosumer. The flow properties of regulating valves are summarized in this subsection.

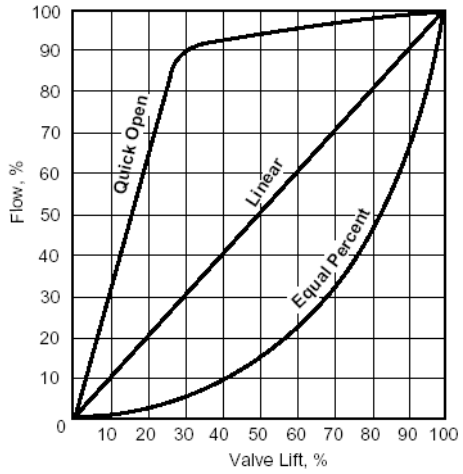

Figure 7: Typical characteristic curves of control valves (source: www.flowserve.com)

The volumetric flow rate through the valve can be determined as:

$$\dot{V} = K_{vs} \sqrt{\frac{\Delta p}{\rho / \rho_0}} \tag{17}$$

where K_{vs} is flow coefficient; Δp is the pressure loss at the valve; ρ is actual density of water flow; ρ_0 is water density at 20 ℃.

Depending on the characteristic curve, the flow rate is changed with the valve's opening in a different way (see fig. 7). A control valve used in the set up has an equal percentage characteristic curve. For this curve, the following relation could determine the actual flow coefficient [14]:

$$\frac{K_{vs}}{K_{vs,\,nom}} = e^{c(op/op_{nom} - 1)} \tag{18}$$

where $K_{vs,\,nom}$ is nominal flow coefficient; op is actual opening; op_{nom} is nominal opening.

Parameter c is calculated as [14]:

$$c = ln\, R_v$$

where R_v is the regulating ratio.

Result from eq. (18) does not show the minimal leakage value from the valve's data sheet when the valve is fully closed [14]. A polynomial function is required to fully describe the dependency of flow coefficient on the valve's opening for an equal percentage characteristic instead of eq. (18).

2.4. Circulating Water Pumps and Affinity Laws

A pump generates pressure difference to move water, which acts as a heat carrier, in a hydronic system. An overview of the main properties of circulating water pumps is provided in this subsection.

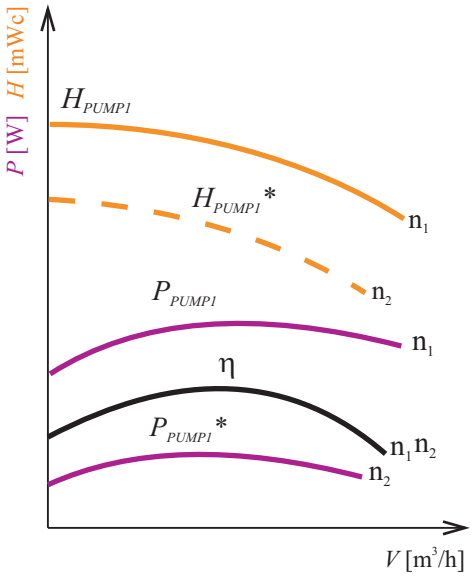

Figure 8: Pump characteristics

The performance of a pump is defined by empirical characteristic curves. The most important one is known as a volume flow – head curve. It describes the pressure generated by a pump as a function of the volume flow rate.

It is common practise to use the head, 'meters of water column' (mWC), as a measure for the pressure generated by a pump. The ratio between Pascals and mWc is:

$$H = \frac{p}{\rho g}$$

A general view of a pump characteristic diagram is given in fig. 8. A first group of curves determines the characteristic of the pump under nominal shaft velocity n_1. Among them are a curve H_{PUMP1} that determines the head of the pump, a curve P_{PUMP1} that represents electric power consumption, and η – efficiency.

Pumps in the set up are equipped with variable frequency drive (VFD) to vary shaft speed. The affinity laws allow prediction of the pump characteristics depending on the speed. They are given by the following equations:

$$\begin{aligned} \frac{\dot{V}_1}{\dot{V}_2} &= \frac{n_1}{n_2} \\ \frac{H_1}{H_2} &= \left(\frac{n_1}{n_2}\right)^2 \\ \frac{P_1}{P_2} &= \left(\frac{n_1}{n_2}\right)^3 \end{aligned} \tag{19}$$

where index 1 corresponds to nominal rotational speed, and index 2 for lower rotational speed.

The effect of speed reduction is also shown in fig. 8: H^*_{PUMP1} and P^*_{PUMP1} are the head characteristic and electric power consumption for slower velocity n_2.

The energy balance of the pump as a control volume can be written as:

$$\frac{dU}{dt} = \dot{m}\left(\left(u_{in} + \frac{p_{in}}{\rho}\right) - \left(u_{out} + \frac{p_{out}}{\rho}\right)\right) + \dot{W}_{flow} \tag{20}$$

where U is internal energy of the water volume inside a pump; $\dot{m}$ is mass flow rate generated by a pump; u_{in} and u_{out} are inlet and outlet specific internal energy, which determines temperature of the flow; p_{in} and p_{out} are inlet and outlet pressures; $\dot{W}_{flow}$ is flow power.

2.5. Heating Load and Heat Supply of Buildings

Heating load varies with weather. In order to sustain comfortable indoor air temperature, a heating system must counteract these variations.

For every type of hydronic device that is used for space heating, the heat flow rate can be expressed as [18]:

$$\dot{Q}_{in} = \frac{T_{in} - \vartheta_i}{\frac{1}{hA} + \frac{1}{2}\frac{1}{\dot{m}c_p}} \tag{21}$$

where T_{in} is inlet water temperature; ϑ_i is the room's air temperature; h – overall heat transfer coefficient for the heater; A is the heat transfer area of the heater; $\dot{m}$ – mass flow rate through the heater.

As a rule, design heating load $\dot{Q}_{l,\,d}$ for a building is known. This value is determined for design outdoor and indoor air temperature, which are $\vartheta_{o,\,d}$ and $\vartheta_{i,\,d}$. They are prescribed by building codes and regulations. In the thesis, $\vartheta_{o,\,d} = -16$ ℃ and $\vartheta_{i,\,d} = 23$ ℃ is taken.

The main influence on actual heating load $\dot{Q}_l$ has outdoor air temperature ϑ_o. Thus, the actual heating load can be determined as:

$$\dot{Q}_l = \dot{Q}_{l,\,d}\overline{Q} \tag{22}$$

Here $\overline{Q}$ is relative heating load that can be calculated as:

$$\overline{Q} = \frac{\vartheta_i - \vartheta_o}{\vartheta_{i,\,d} - \vartheta_{o,\,d}} \tag{23}$$

where ϑ_o is current outdoor air temperature.

2.6. Heat Supply Regulating and Heating Curve

This section is dedicated to weather compensation regulation and gives an overview of the heating curve, the technique to regulate heat input.

In practice, only two parameters from eq. (21), namely, T_{in} and $\dot{m}$ are used for regulating heat input to a building [18].

In contemporary systems, mass flow rate $\dot{m}$ through the heater is adjusted individually by means of thermostats; thus, the flow rate regulation is out of the scope of the collective control strategy for a prosumer-based heat network. For this reason and for simplicity, it is assumed that flow rate through the heater does not vary i.e. $\dot{m} \approx const$.

The heating curve is the graph of the supply $T_1^{h.c.}$ and return $T_2^{h.c.}$ water temperature depending on the outdoor air temperature for heat input regulation. The heating curve can be expressed as [18]:

$$T_1^{h.c.} = \vartheta_{i,\,d} + \Delta\vartheta_d\,\overline{Q}^{\frac{1}{m}} + \frac{1}{2}\delta T_d\,\overline{Q} \tag{24}$$

$$T_2^{h.c.} = T_1^{h.c.} - \delta T_d\,\overline{Q} \tag{25}$$

where m is the exponent for heat transfer, which depends on the type of a heater, for radiators $m = 1.3$ can be taken; the other variables are described below.

The design temperature difference between supply and return temperatures δT_d is given by:

$$\delta T_d = T_{1,\,d}^{h.c.} - T_{2,\,d}^{h.c.}$$

The design temperature difference between the heating surface and the room's air temperature $\Delta\vartheta_d$ can be calculated as follows:

$$\Delta\vartheta_d = \frac{T_{1,\,d}^{h.c.} + T_{2,\,d}^{h.c.}}{2} - \vartheta_{i,\,d}$$

Heating curves go by the names of their design supply and return temperatures. For instance, heating curve 50/30 ℃ has $T_{1,\,d} = 50$ ℃ and $T_{2,\,d} = 30$ ℃.

Two heating curves $70/30$ ℃ and $50/30$ ℃ are shown in fig. 9.

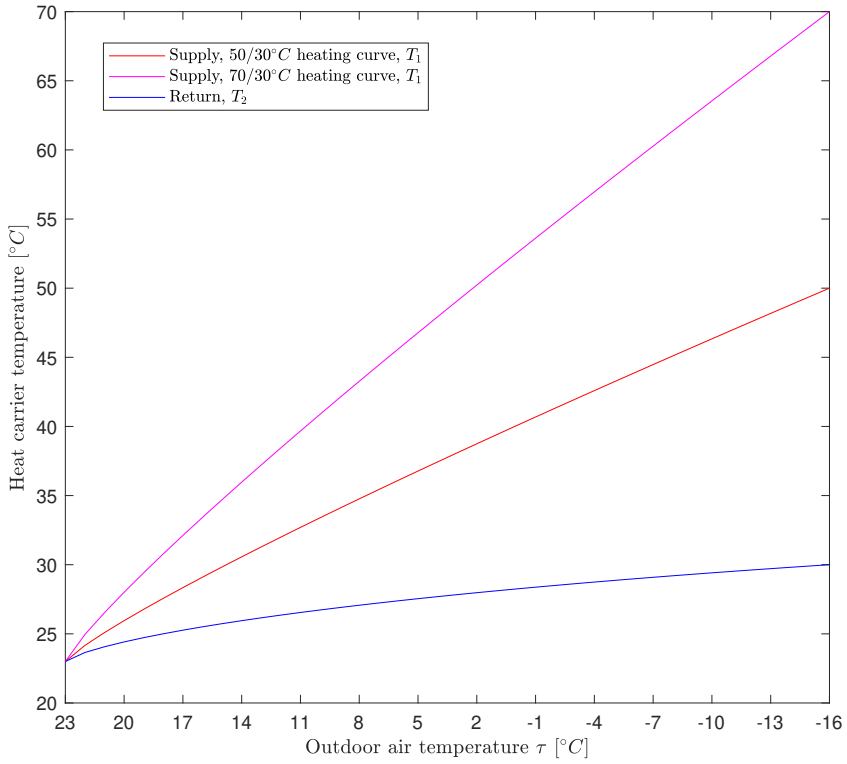

Figure 9: Heating curves: parameters are $\vartheta_{i,\,d} = 23$ ℃ , $\vartheta_{o,\,d} = -16$ ℃ , $m = 1.3$

2.7. 'Flow – Head' Diagram

Combination of a pump and network characteristic in the volume flow – head diagram (Q-H diagram) brings an intuitive way to estimate flow conditions in the network. This method of analysis is presented in this section.

Pressure loss of the network with respect to flow rate is called network characteristic. For steady state, eq. (6) integrated over the finite length define a relation for calculating the network characteristic:

$$\Delta p = \frac{4 \rho l f_D}{\pi d^3} \dot{V}^2 \tag{26}$$

where d is a diameter of the pipeline.

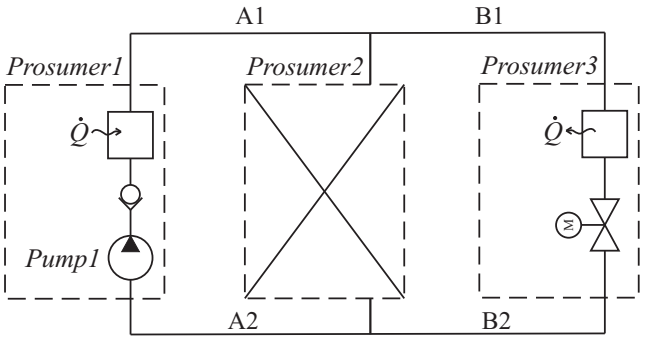

Figure 10: Prosumer-based heat network, configuration 1: prosumer 1 is in production mode; prosumer 2 is in idle mode (disconnected); prosumer 3 is in consumption mode

An exemplary flow – head diagram for the network from fig. 10 is given in fig. 11. The intersection of network characteristic for the sector A1-B1-B2-A2 H_{net1} and the pump characteristic H_{PUMP1} is called the working or operating point. The working point determines the head and flow rate of the pump: ΔH_{PROS1} and $\dot{V}_{PROS1}$. It must be enclosed within allowable operating range to prevent overheating of the pump, excessive vibration, and cavitation on the impeller.

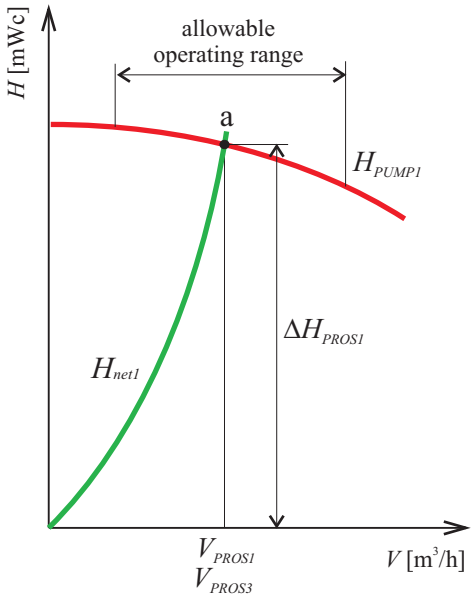

Figure 11: Exemplary flow–head diagram for the configuration 1 (see fig. 10)

2.8. Modelling and Simulation in Modelica

Extensive libraries, written in Modelica, include components for modelling hydronic systems and components for other domains e.g controllers. Every component in the libraries described with equations.

A diagram of the exemplary model in fig. 12 is built with IBPSA and Standard library com-

ponents. The components linked together with connectors. Between hydronic components, connectors transfer thermodynamic properties, e.g. mass, pressure, enthalpy. A common connecting point forms a node.

The following three conditions can be applied for the nodes.

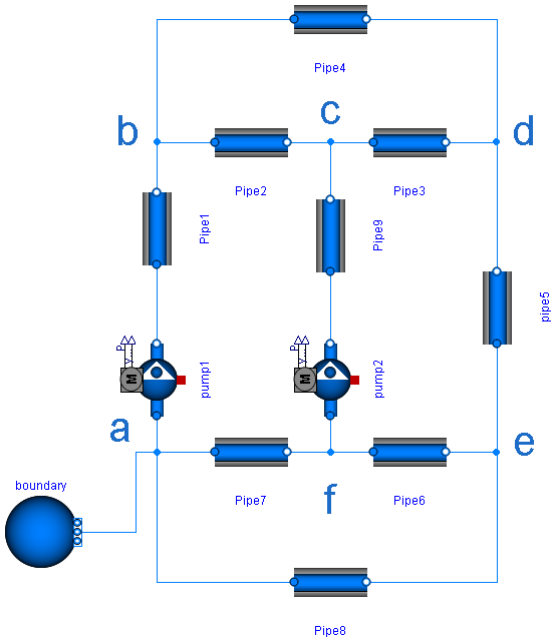

Figure 12: Exemplary heat network model in Modelica

Mass balance:

$$\sum_{i=1}^{n} \dot{m}_i = 0 \tag{27}$$

Pressure at all connectors connected to the same node is constant:

$$p_i = const \tag{28}$$

Energy balance:

$$\sum_{i=1}^{n} \dot{m}_i \, h_i = 0 \tag{29}$$

where i is a connector number; n is the number of connectors in the node.

The mass balance from eq. (27) can be rewritten as:

$$\sum_{i=1}^{n} \dot{m}_i = \sum_{i=1}^{n} v_i d_i^2 = 0$$

Energy balance can also be expressed as:

$$\sum_{i=1}^{n} \dot{m}_i \, h_i = \sum_{i=1}^{n} v_i d_i^2 T_i = 0$$

The system of equations that describes the heat network model in fig. 12 is then:

$$\frac{dv_1}{dt} = \frac{p_a - p_b + \Delta p_{pump\,1}}{\rho \, l_{pipe1}} - \frac{1}{2} v_1 |v_1| f_{D\,1} S_1$$

$$< \cdots >$$

$$
\begin{aligned}
\frac{dv_k}{dt} = \frac{p_{out} - p_{in} + \Delta p_{pump\,k}}{\rho\, l_{pipe\,k}} - \frac{1}{2} v_k |v_k| f_{D\,k} S_k \\
p_1 = const \text{ (boundary condition)} \\
\frac{l_{pipe1}}{v_1} \frac{dT_{1\,out}}{dt} = T_{1\,in} - T_{1\,out} \\
< \cdots > \\
\frac{l_{pipe\,k}}{v_k} \frac{dT_{k\,out}}{dt} = T_{k\,in} - T_{k\,out} \\
v_7 d_7^2 + v_8 d_8^2 + v_1 d_1^2 = 0 \\
v_1 d_1^2 + v_2 d_2^2 + v_4 d_4^2 = 0 \\
v_2 d_2^2 + v_3 d_3^2 + v_9 d_9^2 = 0 \\
v_3 d_3^2 + v_5 d_5^2 + v_4 d_4^2 = 0 \\
v_6 d_6^2 + v_8 d_8^2 + v_5 d_5^2 = 0 \\
v_6 d_6^2 + v_8 d_8^2 + v_5 d_5^2 = 0 \\
v_7 d_7^2 T_{7\,out} + v_8 d_8^2 T_{8\,out} - v_1 d_1^2 T_{1\,in} = 0 \\
T_{out\,1} = T_{in\,4} = T_{in\,2} \\
v_2 d_2^2 T_{2\,out} + v_9 d_9^2 T_{9\,out} - v_3 d_3^2 T_{3\,in} = 0 \\
v_4 d_4^2 T_{2\,out} + v_3 d_3^2 T_{9\,out} - v_5 d_5^2 T_{5\,in} = 0 \\
T_{out\,5} = T_{in\,6} = T_{in\,8} \\
T_{out\,6} = T_{in\,9} = T_{in\,7}
\end{aligned}
\tag{30}
$$

where k is pipe number; $\Delta p_{pump\,k}$ is the pressure difference generated by the pump in the branch.

There are 30 unknowns and 30 equations in the system. It belongs to non-linear differential algebraic equations (DAE) system type.

The system of equations in eq. (30) can be written in general as:

$$
\begin{aligned}
\dot{\mathbf{x}}(t) &= \mathbf{f}\left(\mathbf{x}(t), \mathbf{z}(t), \mathbf{p}, t\right) \\
0 &= \mathbf{g}\left(\mathbf{x}(t), \mathbf{z}(t), \mathbf{p}, t\right)
\end{aligned}
\tag{31}
$$

where $\mathbf{x}$ is a vector of differentiable variables:

$$
\mathbf{x}(t) = [v_1(t) \ldots v_k(t); T_{1\,out}(t) \ldots T_{k\,out}(t)]^T
$$

$\mathbf{z}$ is a vector of algebraic variables:

$$\mathbf{z}(t) = [p_a(t) \dots p_f(t); T_{1\,in}(t) \dots T_{9\,in}(t); \Delta p_{pump\,k}(t)]^T$$

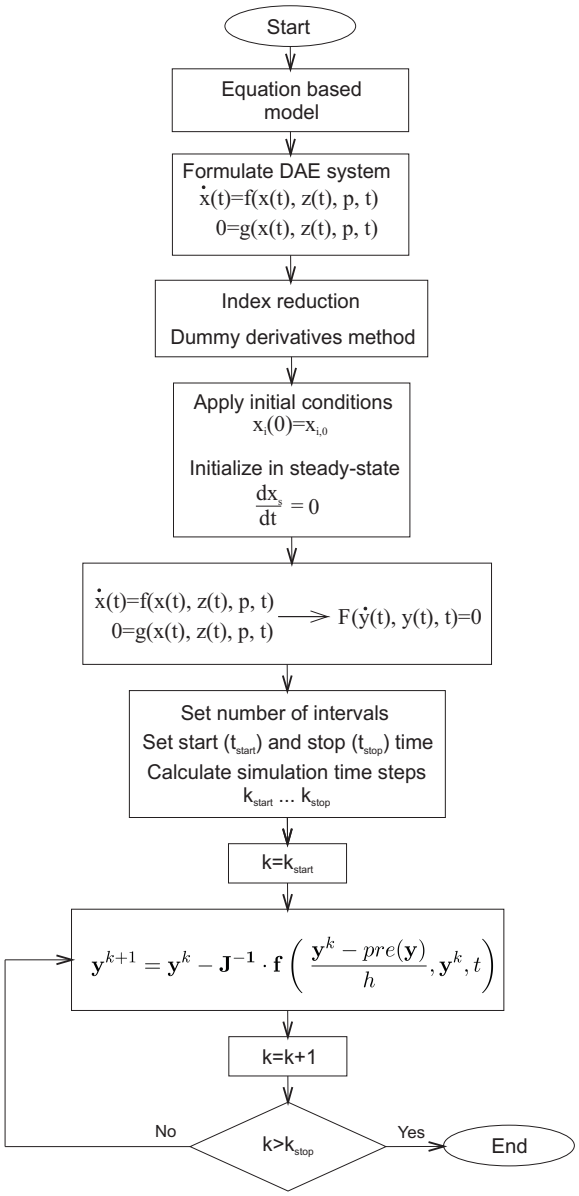

Figure 13: Simulation algorithm in Modelica

$\mathbf{p}$ is a vector of parameters, i.e. values that do not change during simulation:

$$\mathbf{p} = [d_1 \dots d_9; l_1 \dots l_9; S_1 \dots S_9; f_{D\,1} \dots f_{D\,9}]$$

Eq. 31 represents DAE system in semi-explicit form. The bottom equation is called the algebraic constrain. It arises from conservation laws.

Modelica utilizes DASSL solver to find numerical solution for the system of equations [13]. Two equations from eq. (31) must be combined in implicit DAE form for solving:

$$\mathbf{F}(\dot{\mathbf{y}}, \mathbf{y}, t) = 0 \tag{32}$$

where $\mathbf{y}$ is a vector of unknown variables $\mathbf{y} = [\mathbf{x}, \mathbf{y}]^T$.

Newton's method is used in DASSL algorithm for solving y from nonlinear systems [13]:

$$\mathbf{y}^{k+1} = \mathbf{y}^k - \mathbf{J}^{-1} \cdot \mathbf{f}\left(\frac{\mathbf{y}^k - pre(\mathbf{y})}{h}, \mathbf{y}^k, t \right) \tag{33}$$

where k is time step number; h is time step length; $pre(y)$ is a function of known values of y from the previous steps; J^{-1} is the matrix inverse of the Jacobian matrix.

The Jacobian matrix of $\mathbf{f}$ is [13]:

$$\mathbf{J} = \frac{d\mathbf{f}}{d\mathbf{y}} = \frac{\partial \mathbf{f}}{\partial \mathbf{y}} + \frac{1}{h}\frac{\partial \mathbf{f}}{\partial \dot{\mathbf{y}}} \tag{34}$$

An intermediate stage in between formulation of DAEs and applying DASSL algorithm is index reduction. Index of DAE is the minimum number of times the system eq. (31) needs to be differentiated to become an ordinary differential equations (ODE) system, which has index-0. The general form of ODE system is:

$$\dot{\mathbf{x}}(t) = \mathbf{f}\left(\mathbf{x}(t), \mathbf{z}(t), t\right)$$
$$\dot{\mathbf{z}}(t) = \mathbf{g}\left(\mathbf{x}(t), \mathbf{z}(t)\right)$$

Index reduction algorithm brings the DAE system to index-1 by replacing original constrain with the differentiated one. Numerical differentiation of constrains tends to drift and thereby cannot fulfil the original constrain. To prevent drifting, original constraints are added to the system, but it leads to the overdetermined system. The solution is to add more variables by replacing some of the derivatives with algebraic variables (dummy derivatives) i.e. $\frac{dx_i}{dt} \rightarrow der x_i$.

The summary of the simulation algorithm is shown in fig. 13.

3. Preliminary Investigation

Before starting the modelling, the fundamental traits that belong to prosumers heat network are presented in this chapter.

The toolbox that was used for the investigation was volume flow rate – head diagram (see section 3.1) and exergy analysis (see section 3.2). The first addresses medium flow conditions, the second analyses conditions for energy flow.

It is worth to mention what exergy is. In a nutshell, exergy in space heating can be interpreted as the ability of the heat carrier to warm up the air in the building. Exergy is associated with temperature: the higher the temperature is, the higher exergy is.

3.1. 'Flow – Head' Diagram Analysis

In this section, a volume flow rate – head diagrams for a prosumer-based heat network with radial topology are presented. A few operating modes were analysed, and critical states are pointed out.

The scheme of the heat network with the analysed flow conditions is shown in fig. 14.

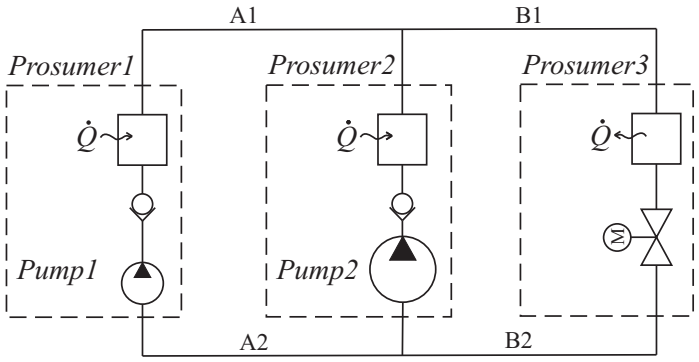

Figure 14: Heat network with three prosumers: prosumers 1 and 2 are in production mode; prosumer 3 is in production mode. Sizing of the pump 2 is bigger than the pump 1

The flow – head diagram for this case is shown in fig. 15. Characteristic curves of two pumps $H_{PUMP1}(\dot{V})$ and $H_{PUMP2}(\dot{V})$ were added together to get a total characteristic $H_{PUMP1'\,PUMP2}(\dot{V})$ since the pumps are working in parallel.

However, before addition, a characteristic curve of the feed-in pump 1 $H_{PUMP1}(\dot{V})$ was reduced with respect to the network characteristic of the segment A1-A2 $H_{A1-A2}(\dot{V})$:

$$H^{/}_{PUMP1}(\dot{V}) = H_{PUMP1}(\dot{V}) - H_{A1-A2}(\dot{V})$$

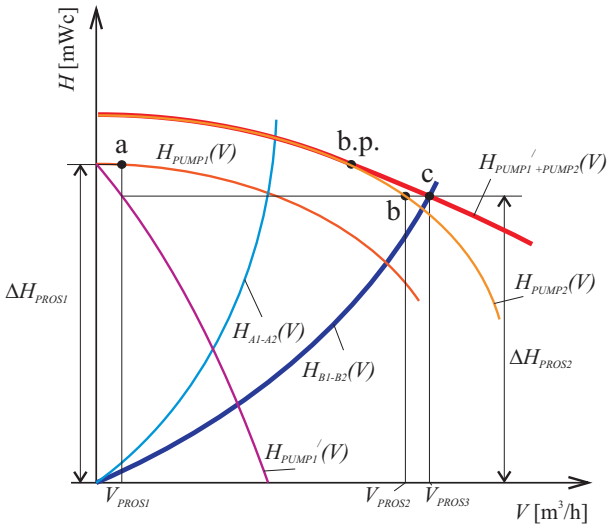

Figure 15: Flow–head diagram for the example in fig. 14: nominal state

The working point at the prosumer 2 (point c) is then given by the intersection of the segment B1-B2 network characteristic $H_{B1-B2}(\dot{V})$ and the total characteristic of the two pumps $H_{PUMP1'\,PUMP2}(\dot{V})$. Individual working points for feed-in pumps 1 and 2 are given by the points a and b respectively.

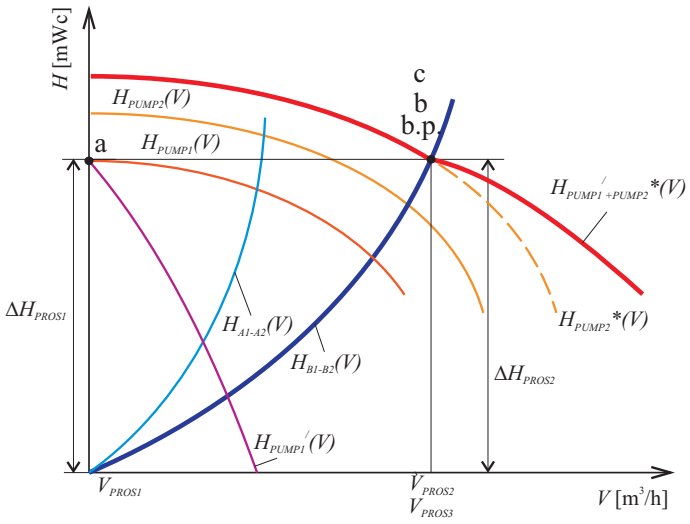

Figure 16: Flow–head diagram when the feed-in pump 2 is gaining speed

When the feed-in pump 2 is gaining speed, the overall flow – head characteristic undergoes changes, which can be seen in fig. 16. Characteristic curve of the feed-in pump 2 is increased according to the affinity law. This increase can reach the degree when feed-in

from prosumer 1 is not longer possible (working point a). The characteristic of the feed-in pump 2 that corresponds to this critical state is $H^*_{PUMP2}(\dot{V})$. The total working point (point c) coincides with individual working point of the feed-in pump 2 (point b). For this critical state, we define blocking point (point $b.p.$) as a local minimum on the total characteristic of the two pumps. At the intersection of blocking point and a network characteristic, the feed-in from a prosumer with a lower pump characteristic becomes blocked.

Up to this moment, the network characteristic at B1-B2 pipe section was assumed to be constant. This is only true if the control valve at prosumer 3 is not modulated. If the valve is being closed, the network characteristic $H_{B1-B2}(\dot{V})$ shifts to the left to become $H^*_{B1-B2}(\dot{V})$ as can be seen in fig. 17. The new total working can be found at the blocking point (point $b.p.$). Thus, the feed-in from the prosumer 1 can be blocked again.

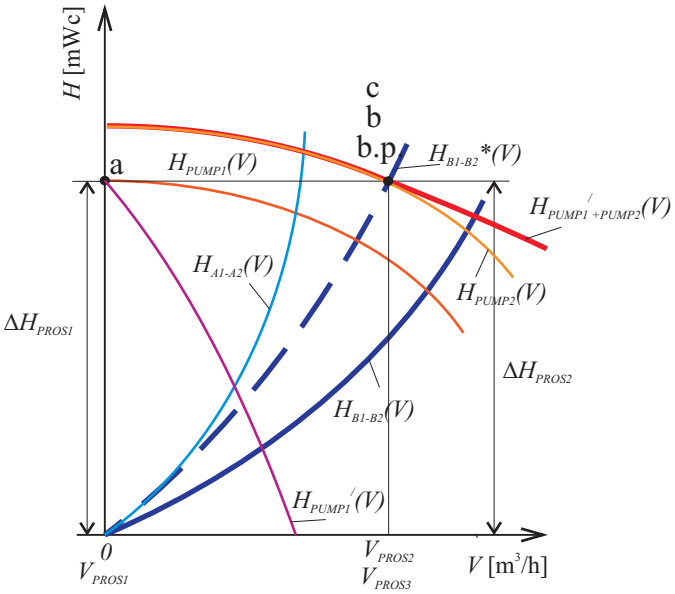

Figure 17: Flow–head diagram when the control valve at prosumer 3 is closing

To sum up, operating of the prosumers heat network has the following properties: a) *Operation of feed-in pumps strongly influence each other*: an increase in volume flow rate from a prosumer with bigger pump can block feed-in from other prosumers, and a working point of smaller sized pumps might shift away the from recommended area; b) *Modulation of control valves influence pumps performance*.

3.2. Exergy Analysis

For prosumers, the secondary side of the heat exchanger is connected to the space heating system. Heating system, in turn, is assembled for design inlet $T_{1,\,d}$ and outlet $T_{2,\,d}$ temperatures. For a conventional heating system, heat input from a source, e.g. a boiler, is controlled by the appropriate heating curve that is calculated for $T_{1,\,d}$ and $T_{2,\,d}$ as well.

If conventional control concept is utilized, the heat transmission between prosumers is be limited due to the exergy losses in heat exchangers. Let us consider two prosumers con-

nected in a heat network (see fig. 18): one is in production mode, the other is in consumption mode.

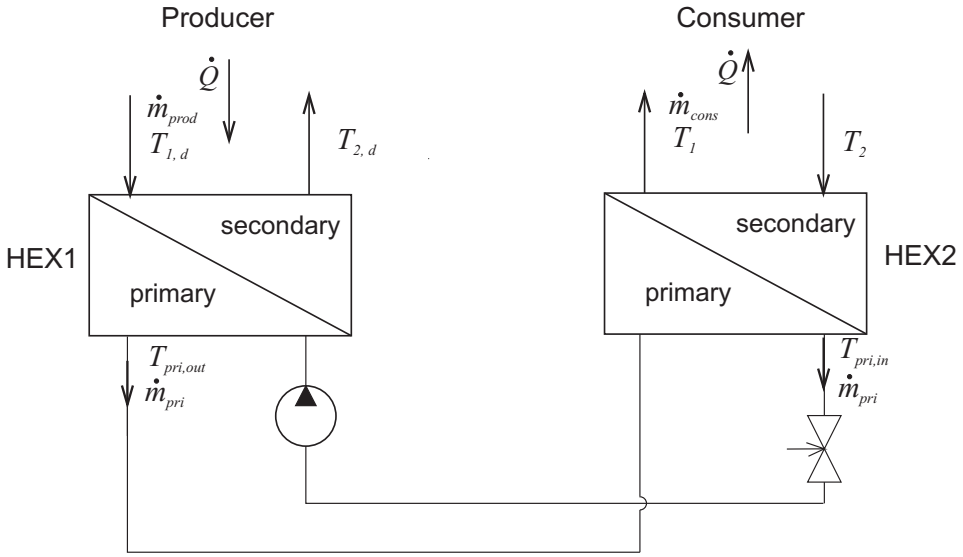

Figure 18: Functional scheme of two prosumers in the network: the first one is in production mode, the second is in consumption mode

The relation between exergy that is created and must be delivered to the prosumer in consumption mode is:

$$\begin{aligned} Ex_{prod} &= \dot{m}_{prod}\, c_p \left(T_{1,d} - T_{2,d} - \vartheta_{o,d} ln \frac{T_{1,d} + 273{,}15}{T_{2,d} + 273{,}15} \right) \\ Ex_{cons} &= \dot{m}_{cons}\, c_p \left(T_{1,d} - T_{2,d} - \vartheta_{o,d} ln \frac{T_{1,d} + 273{,}15}{T_{2,d} + 273{,}15} \right) \\ Ex_{prod} &= Ex_{cons} \end{aligned} \tag{35}$$

The exergy balance is:

$$Ex_{prod} - \Delta Ex_{loss,\,HEX1} - \Delta Ex_{loss,\,HEX2} = Ex_{cons} \tag{36}$$

where $\Delta Ex_{loss,\,HEX1}$, $\Delta Ex_{loss,\,HEX2}$ are the exergy losses in the heat exchangers that belong to prosumers. The graphical representation of the exergy balance is shown in fig. 19.

As a result, with a conventional control strategy, the heat demand of prosumer cannot be fulfilled because of finite temperature difference between primary and secondary sides of the heat exchanger i.e. $T_1 < T_{1,d}$.

Theoretically, there are two solutions to compensate the exergy losses:

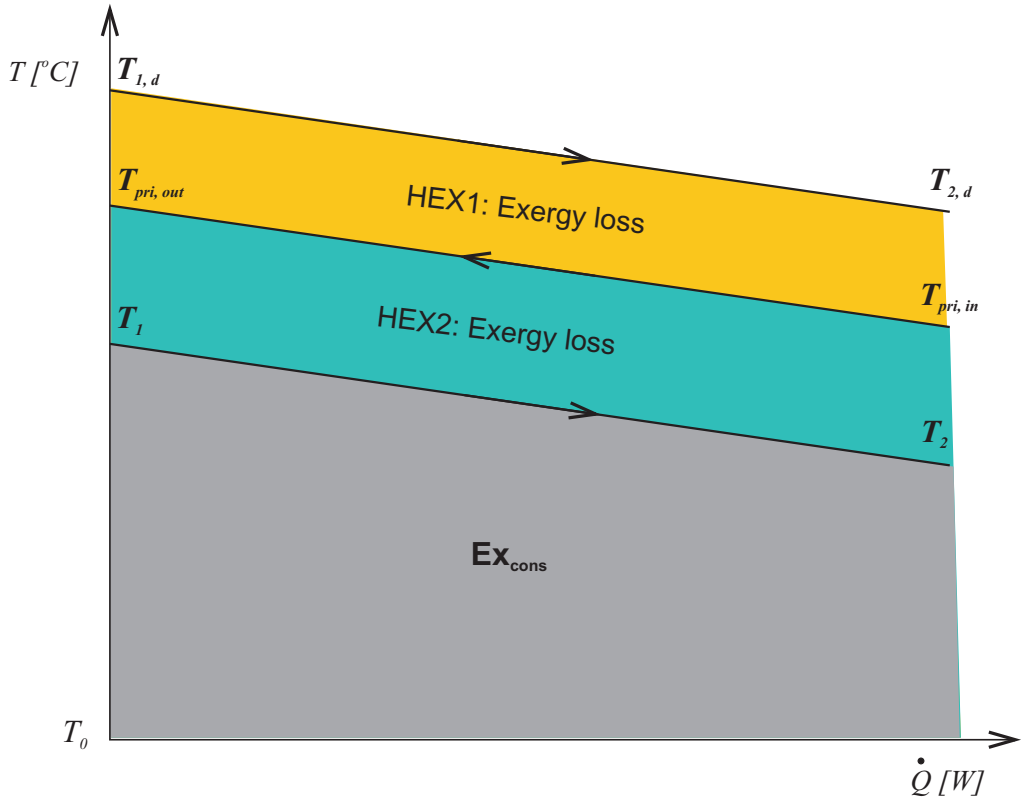

Figure 19: Q-T diagram of the exergy balance for the functional scheme in fig. 18

- Create more exergy in production mode:

$$Ex_{prod} = Ex_{cons} + (\Delta Ex_{loss,\,HEX1} + \Delta Ex_{loss,\,HEX2})$$

- Add exergy to the system from an exergy source, e.g. a heat pump ($Ex_{hea,\,pump}$).

$$Ex_{prod} + (Ex_{hea,\,pump} - \Delta Ex_{loss,\,HEX1} - \Delta Ex_{loss,\,HEX2}) = Ex_{cons}$$

The set-up given in the task was not equipped with a heat pump, so the only way to solve the exergy losses problem for the model was to increase exergy production at the heat source.

4. Modelling

This chapter presents mathematical modelling for this thesis. The approach to modelling is following bottom-up principle. The section 4.1 gives an overview of some important elementary blocks used in the model and assumptions. The section 4.2 describes a prosumer model. Finally, at the top of hierarchy stands the model of a heat network with prosumers formulated in section 4.3.

To avoid confusion, terms blocks and models are interchangeable. However, due to hierarchical approach, models on the lower level of hierarchy are called blocks.

4.1. Models of Basic Components

Most of the components used in the model were taken from public domain Modelica libraries:

- Standart Library (MSL), version 3.2.3
- Buildings library (IBPSA), version 6.0.0
- Library for district heating network (DisHeatLib)

Assumption taken for the prosumer and heat network models were expressed through parameterization of the components. The blocks that were developed especially for the thesis are described in more details.

4.1.1. Pipe

A pipe model is essential for modelling the heat network. Dynamic pipe model from MSL was used. This model is described with three equations: material balance (see eq. (2)), momentum (see eq. (6)) and energy (see eq. (7)) equations.

Assumption 1. The heat losses to the environment were considered negligible. Thus, 'use_HeatTransfer' flag was set to 'false'. These assumptions simplified heat flow analysis between prosumers, and allowed to evaluate control strategy with less computation difficulty.

4.1.2. Pump

A water centrifugal pump model was taken from the IBPSA library. It can be described by the energy balance equation from eq. (20). The following assumptions were applied to the pump model.

Assumption 2. The inner volume of all pumps was small compared to that of a prosumer and a heat network. As a result, the volume of the pumps was permanently in a

quasi steady-state, so in eq. (20) the term $\frac{dU}{dt} \approx 0$, and 'energyDynamics' flag was set to 'SteadyState'.

Assumption 3. The heat dissipation from the pumps was neglected, and the pumps were assumed to be isentropic. This meant that $u_{in} \approx u_{out}$, so 'AddPowerToMedium' flag was set to 'false'.

Electric power of the pumps is given by:

$$P = \frac{\dot{W}_{flow}}{\eta_{mot}\,\eta_{hyd}} \tag{37}$$

where η_{mot} is the motor efficiency; η_{hyd} is the hydraulic efficiency. Both coefficients were taken as $\eta_{hyd} = \eta_{mot} = 0.7$.

The pumps on the secondary side were implemented through the mass prescribed pump block 'FlowControlled_m_flow', and do not require a characteristic curve. On the contrary, the feed-in pumps used normalized speed pump models 'SpeedControlled_y', and require characteristic curves to describe their performance.

The pump curves are shown in fig. 20. Actual curves were approximated with linear functions that are put above. A curve *feedIn1* represents a hypothetical feed-in pump for prosumer 1.

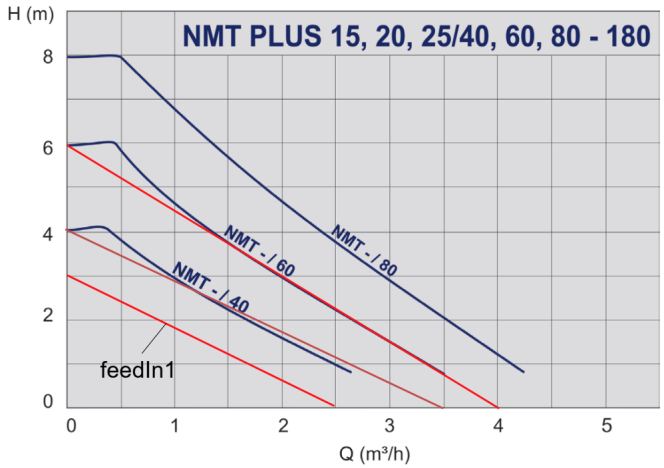

Figure 20: Characteristic curves of feed-in pumps (source: IMPPumps catalogue)

The pump characteristics assigned to the prosumers are shown in table 3.

The dynamics of the pumps is modelled through the following differential equation:

$$\tau_{pump}\frac{d\,n_f}{d\,t} = n_f - n_i \tag{38}$$

where τ_{pump} is the time constant that depends on the sizing; n_f is the modulated rotational speed; n_i is the initial rotation speed.

Table 3: Feed-in pumps installed at the prosumers

Prosumer	Pump model	Pump curve from fig. 20
Prosumer 1	Hypothetical pump	feedIn1
Prosumer 2	IMP NMT PLUS ER 25/60 180	NMT -60
Prosumer 3	IMP NMT PLUS ER 25/40 180	NMT -40

4.1.3. Control Valve

The control valve model was taken from the IBPSA library and is called 'TwoWayEqual-Percentage', which, obviously, describes an equal percentage opening characteristic.

The control valve requires time to open or shut down. Its dynamic behaviour is expressed as:

$$\tau_{valve} \frac{d\, op_f}{d\, t} = op_f - op_i \tag{39}$$

where τ_{valve} is the time constant that depends on the valve's actuator and thread lead; op_f is the opening modulated by the actuator; op_i is the initial opening.

4.1.4. Heat Exchanger

Assumption 4. It was assumed that the heat exchangers was operating under quasi steady-state. Considering a plate heat exchanger, the inner volume was low compared to that of the prosumer and heat network, and consequently, the water m_w and empty heat exchanger mass m_{HEX} from eq. (9) were negligible. Therefore, the dynamics of the heat exchanger can be neglected: $\frac{dU}{dt} \approx 0$. Rewritten energy balance is then:

$$\dot{m}^{pri} c_p^{pri} (T_{in}^{pri} - T_{out}^{pri}) = \dot{m}^{sec} c_p^{sec} (T_{in}^{sec} - T_{out}^{sec}) = \dot{Q} \tag{40}$$

For this reason, a static heat exchanger model 'PartialEffectivenessNTU' from the IBPSA library was used. However, it has a disadvantage that it does not calculate overall heat transfer coefficient h under various flow rates through the heat exchanger. To solve this problem, a model 'HAPlateHE' was written (see fig. 21).

'HAPlateHE' determines the product of convection heat transfer coefficient and heat transfer area for primary *alphaA_1* and secondary *alphaA_2* side of a heat exchanger. These

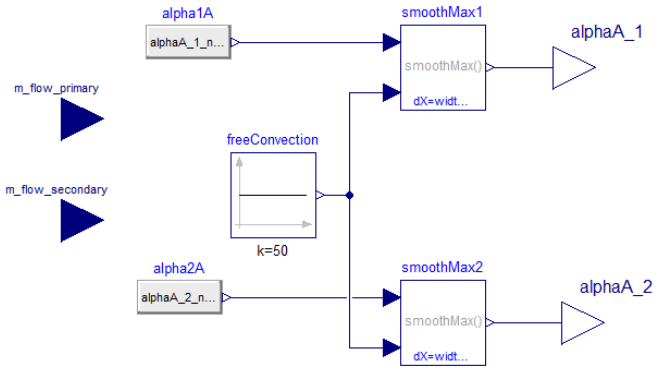

Figure 21: Diagram of 'HAPlateHE' block

values are required for 'PartialEffectivenessNTU' block. The product is calculated in expressions *alpha1A* and *alpha2A*. The derivation for these expressions is given below.

Usually, characteristics of a heat exchanger are given in the specification sheet in the nominal mode as it is shown in table 4.

Table 4: Main characteristics of a heat exchanger for nominal mode

$\dot{Q}_{nom}$	
h_{nom}	
A	
Primary side	Secondary side
$\dot{m}^{pri}_{nom}$	$\dot{m}^{nom}_{cold}$
$T^{pri}_{nom\,in}$	$T^{sec}_{nom\,out}$
$T^{pri}_{nom\,out}$	$T^{sec}_{nom\,in}$

A prosumer operates in large variety of mass flow rates and temperatures. It means that all parameters in table 4, except for the heat transfer area A, vary.

The overall heat transfer coefficient is given by:

$$h = \frac{1}{\frac{1}{\alpha^{pri}} + \frac{\Delta x}{k} + \frac{1}{\alpha^{sec}}} \approx \frac{1}{\frac{1}{\alpha^{pri}} + \frac{1}{\alpha^{sec}}} \tag{41}$$

where α^{pri} and α^{sec} are convection heat transfer coefficients; Δx is the wall thickness; k is the thermal conductivity of the wall.

The thermal resistance due to conduction $\frac{\Delta x}{k}$ is small compared to the convection terms, so it can be neglected in eq. (41).

With the existing correlations between Nusselt Nu, Reynolds Re, and Prandtl Pr numbers, α can be determined. Considering that the set up is equipped with the heat exchanger with the chevron angle[2] 60° for the plates, the appropriate correlation is [21]:

$$Nu = \frac{\alpha\, l}{k} = 1.112 Re^{0.6} Pr^{0.5} \tag{42}$$

where l is the characteristic length.

For α that is changing with respect to its nominal value α_{nom}, the following is relevant:

$$\frac{Nu}{Nu_{nom}} = \frac{\alpha}{\alpha_{nom}} = \left(\frac{Re}{Re_{nom}}\right)^{0.6} \left(\frac{Pr}{Pr_{nom}}\right)^{0.5} \tag{43}$$

Prandt number represents physical properties of the liquid in eq. (43). It is reasonable to assume that the physical properties do not change significantly in the operating range of prosumers. Therefore, the ratio between Prandt numbers is $\frac{Pr}{Pr_{nom}} \approx 1$. Reminding that $Re = \frac{\rho v D}{\mu}$ and leaving α on the left side, eq. (43) can be rewritten as:

$$\alpha = \alpha_{nom} \left(\frac{v}{v_{nom}}\right)^{0.6} \sim \alpha_{nom} \left(\frac{\dot{m}}{\dot{m}_{nom}}\right)^{0,6} \tag{44}$$

where v and v_{nom} are the average water velocity in the channels of the heat exchanger under current and nominal conditions.

At nominal conditions, α_{nom}^{pri} and α_{nom}^{sec} can be derived from h_{nom} as [12]:

$$\begin{aligned} \alpha_{nom}^{pri} &= (r+1) h_{nom} \\ \alpha_{nom}^{sec} &= \frac{r+1}{r} h_{nom} \end{aligned} \tag{45}$$

where r is the ratio between convective heat transfer coefficients:

$$r = \frac{\alpha_{nom}^{pri}}{\alpha_{nom}^{sec}} \sim \left(\frac{\dot{m}_{nom}^{pri}}{\dot{m}_{nom}^{sec}}\right)^{0,6} \tag{46}$$

In conclusion, to calculate the overall heat transfer coefficient h for every flow rate, convective heat transfer coefficients α_{nom} for nominal mode has to be found with the help of eq. (46) and eq. (45). Then, α for the current flow rate must be calculated with eq. (44) and, finally, h is given by eq. (41).

To validate the proposed approach, a comparison with the reference results that were obtained from the manufacter is made in fig. 22. The tendency between proposed formula

[2]TH designation in the specification sheet corresponds to high chevron angle 60°

and the reference, in general, is aligned. The coefficient of determination R^2 is closest to unity for relatively high flow rates on the secondary side, but for lower flow rates the values predicted by the formulas eq. (44), eq. (41) are less accurate.

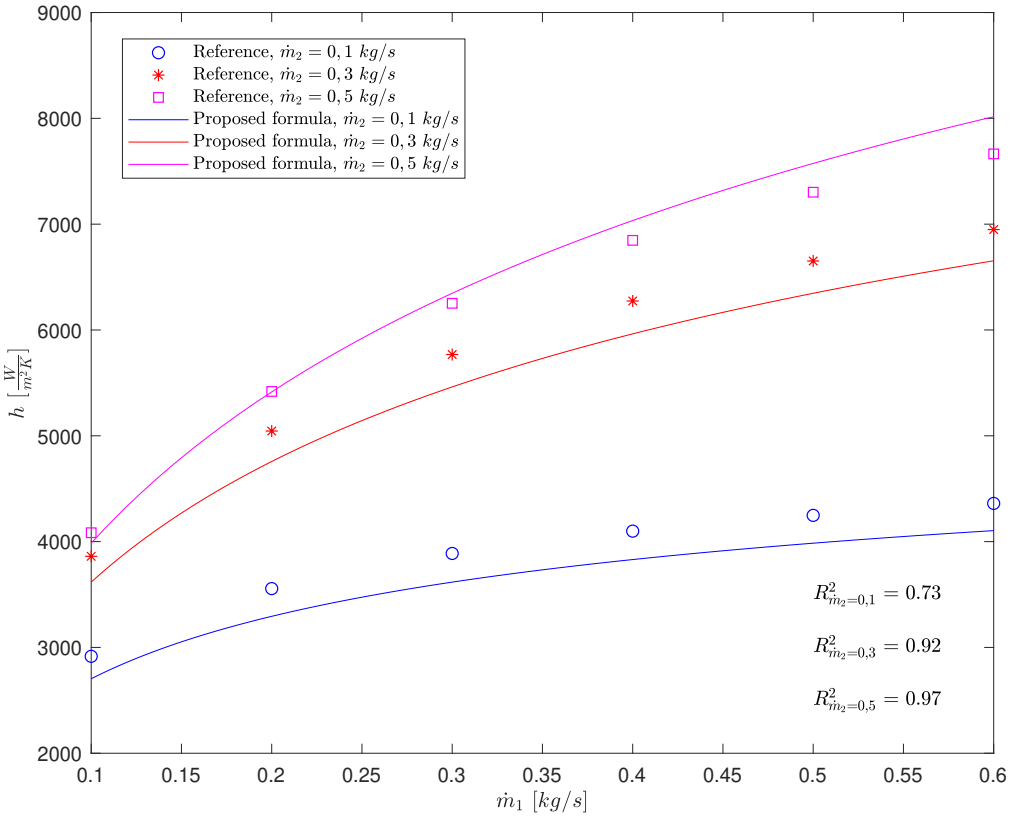

Figure 22: Overall heat transfer coefficients under various flow rates. The heat exchanger's model is HH08-32-16/1-11-TL, manufacturer is Danfoss. Indices 1 and 2 stand for primary and secondary sides. The nominal conditions are: $\dot{Q}_{nom} = 33.9\,kW$; $h_{nom} = 6116\,W/(m^2K)$; $A = 0.76\,m^2$; $\dot{m}^{pri}_{nom} = \dot{m}^{sec}_{nom} = 0.358\,kg/s$

4.2. Prosumer Model

The prosumer model is presented in appendix A. The model is complex, so it was reasonable to split it into parts that perform a specific function within the individual prosumer. The following six modules were distinguished:

1. *Thermal model of the building* imitates the heat losses and dynamics of the room's air

temperature.

2. *Mode definer* receives the reference heat flow rate with respect to the network and transfers it further. Moreover, this module defines the operating mode of a prosumer.
3. *Domestic heat input* defines thermal power of the heat source depending on the current heat losses and the reference with respect to the network. It uses outdoor air temperature as an input for calculations. The active heating curve is chosen in this module as well.
4. *Heat source – sink* forms inner hydronic system of the prosumer. It consists of the heat sink and the heat source.
5. *Secondary side* module includes every hydronic component on the secondary side from the heat exchanger.
6. *Primary side* module is connected directly to the heat network. It includes a feed-in pump and a control valve.

In sections 4.2.1 – 4.2.6, the modules given above, are described in more details. Please, go to appendix A when particular components are mentioned.

4.2.1. Thermal Model of the Building

A simple differential equation can be used to describe the room's air temperature ϑ_i dynamics:

$$\frac{dU_{air}}{dt} = \rho_{air} V_{air} c_{p\,air} \frac{d\vartheta_i}{dt} = \dot{Q}_r - \dot{Q}_l \tag{47}$$

where ϑ_i is indoor air temperature; $\dot{Q}_r$ is heat flow rate from the radiator; $\dot{Q}_l$ is the current heating load; V_{air} is the inner air volume of the building.

The current heating load for the radiator block *rad* is expressed as:

$$\dot{Q}_l = G\,(\vartheta_i - \vartheta_o) \tag{48}$$

where G is a parameter that determines thermal conductance:

$$G = \frac{\dot{Q}_{l,\,d}}{\vartheta_{i,\,d} - \vartheta_{o,\,d}}$$

where $\dot{Q}_{l,\,d}$ is design heating load; $\vartheta_{i,\,d}$ is design indoor air temperature, 23 ℃ was taken; $\vartheta_{o,\,d}$ is design outdoor air temperature, -16 ℃ was taken.

A block *volBuilding* represents the air volume V_{air}. Heat outflow $\dot{Q}_l$ is generated by a block *thermalLosses*, and heat inflow $\dot{Q}_r$ is received from the block *rad*.

4.2.2. Mode Definer

The main reference for the prosumer model is the heat flow rate $\dot{Q}_{net,\,ref}$ with respect to the network. Positive value corresponds to heat extraction, negative – to heat injection, and the prosumer operates in consumption or production mode respectively. The third mode, when the reference is zero, is called idle mode. The summary of the modes is given in table 5.

Table 5: Prosumer operating modes

Mode	Logical blocks	
	modeProd	*modeCons*
Production	True	False
Consumption	False	True
Idle	False	False

The module *mode definer* imitates thermal inertia of the heat source by imposing the first order system between the reference $\dot{Q}_{net,\,ref}$ and the value of heat flow rate $\dot{Q}^{w/\,inert}_{net,\,ref}$ transferred to the *domestic heat input* module. The dynamics are modelled through *inertiaQ* block, and is given by the following differential equation:

$$\tau_{b,\,Q}\frac{d\,\dot{Q}^{w/\,inert}_{net,\,ref}}{d\,t} = \dot{Q}^{w/\,inert}_{net,\,ref} - \dot{Q}_{net,\,ref,\,i} \tag{49}$$

where $\tau_{b\,Q}$ is the time constant; $\dot{Q}_{net,\,ref,\,i}$ is the initial value of the reference.

In addition, *mode definer* uses simple algebraic clauses to evaluate $\dot{Q}^{w/\,inert}_{net,\,ref}$ for determining operating mode. Threshold value ($\delta = 0.1$ W) was necessary to avoid the influence of numerical noise around zero.

4.2.3. Domestic Heat Input

The first task for the *domestic heat input* is to compute the thermal power set point for the heat source:

$$\dot{Q}_{b,\,set} = \dot{Q}_l - \dot{Q}^{w/\,inert}_{net,\,ref} \tag{50}$$

Since the current heating load $\dot{Q}_l$ varies linearly with the outdoor temperature ϑ_o, the range of available values for $\dot{Q}_{net,\,ref}$ is naturally limited (see fig. 23).

The second task for this module is to provide the temperature set points from the heating curves. The blocks *heaCurve70_30* and *heaCurve50_30* calculate supply $T_1^{h.c.}$ and return $T_2^{h.c.}$ temperatures for the "upper" and "lower" heating curves. These values are used as the temperature set point for *heatSource* (T^b_{set}) and "heat extraction controller" (*contExtr* block).

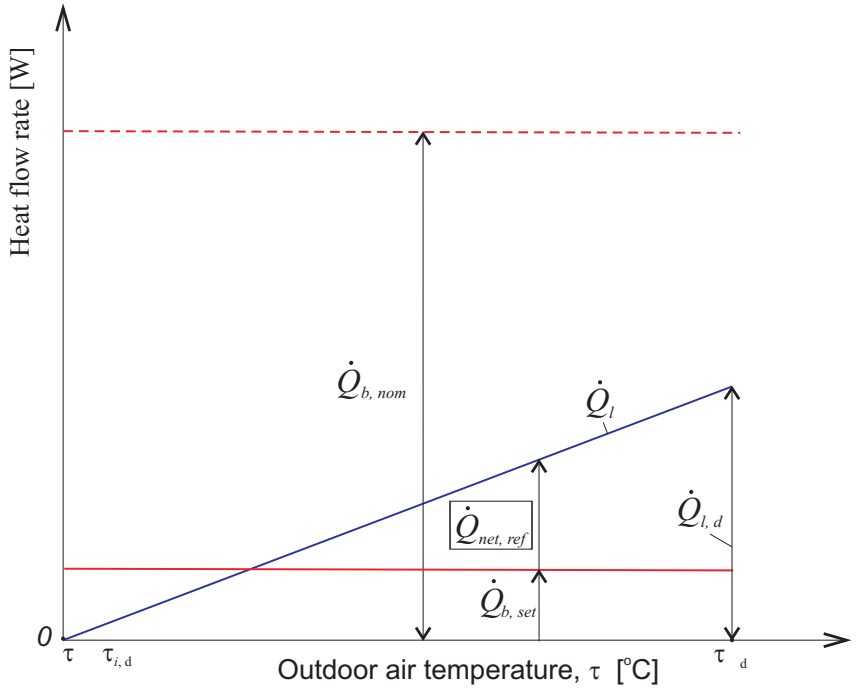

Figure 23: Diagram for determining thermal power of the heat source (here $\dot{Q}_{b,\,nom}$ is nominal thermal power of the heat source)

4.2.4. Heat Source – Sink

The *source – sink* module represents the core hydronic elements where heat flow rate targeted to the network is generated.

Heat sink for hydronic part of the prosumer model is a radiator block *rad*. Heat flow rate from the radiator can be written as following:

$$\dot{Q}_r = (h\,A)_r \left(T^r_{surf} - \vartheta_i\right)^m \tag{51}$$

where T^r_{surf} is the mean temperature on the radiator surface; m is the exponent for the heat transfer, which depends on the type of the radiator ($m = 1.3$ was taken).

The product $(h\,A)_r$ of the overall heat transfer coefficient and area is conveniently determined through the design values:

$$(h\,A)_r = \frac{\dot{Q}_{l,\,d}}{\frac{T^r_{1,\,d}+T^r_{2,\,d}}{2} - \vartheta_{i,\,d}} \tag{52}$$

where $T^r_{1,\,d}$, $T^r_{2,\,d}$ are design inlet and outlet temperatures for the radiator. The following values were taken: $T^r_{1,\,d} = 50$ ℃ and $T^r_{2,\,d} = 30$ ℃ . This is the most widespread temperature

span for the floor heating.

In the model, the heat source is the hypothetical element that is not tied to a specific technology and uses heat flow rate $\dot{Q}_{b,\,set}$ as an input. This assumption has a benefit that it brings a compatibility with external models for a heat source, e.g. gas boilers, solar thermal collectors, heat pumps, etc.

The *heatSource* block is based on the model from the DisHeatLib library. The inner structure of this block is given in fig. 24. The *heater* block is a control volume model with prescribed outlet temperature T^b_{set} received from the input connector *TSet*. The *heater* imitates thermal inertia with regard to the outlet temperature T^2_b:

$$\tau_{b,\,T}\frac{d\,T^b_2}{d\,t} = T^b_2 - T^b_{set,\,i} \tag{53}$$

where $\tau_{b,\,T}$ is the time constant; $T^b_{set,\,i}$ is the initial value of the reference.

A block *conPID* receives the set point $\dot{Q}_{b,\,set}$ through *QSet* connector and adjusts mass flow rate of a *pump* block, so that it follows the formula:

$$\dot{m}^b = \frac{\dot{Q}_{b,\,set}}{c_p\,(T^2_b - T^b_1)} \leq \dot{m}^b_{max} \tag{54}$$

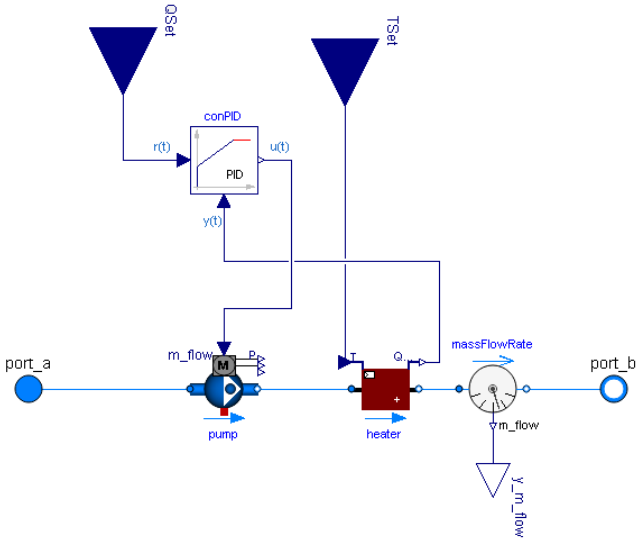

Figure 24: Diagram of the *heatSource* block

The thermal power of the source was limited by its nominal value. Since *heater* has

unlimited capacity, heat flow that water receives was limited by the mass flow rate:

$$\dot{m}^b_{max} = \frac{\dot{Q}_{b,\,nom}}{c_p\,(T^b_{1,\,d} - T^b_{2,\,d})} \tag{55}$$

Water circulation through the radiator block *rad* is driven by the radiator pump *pumpRad*. The mass flow rate is sustained permanently :

$$\dot{m}^r = \frac{\dot{Q}_{l,\,d}}{c_p(T^r_{1,\,d} - T^r_{2,\,d})} \tag{56}$$

The crossover connection around the radiator, a bypass, imitates a hydraulic separator.

4.2.5. Secondary Side

Secondary side module includes two more pumps: a production pump *pumpProd* and a consumption pump *pumpCons*. To formulate operating model of these pump, the analysis of the flow streams on the secondary side was required.

The scheme of flow streams in *secondary side* module is shown in fig. 25: $\dot{m}^p$ and $\dot{m}^c$ are mass flow rates generated by the production pump and the consumption pumps.

In production mode, *pumpProd* is active. The mass flow rate through the boiler is then:

$$\dot{m}^b = \dot{m}^p + \dot{m}^{heaSys} \tag{57}$$

In consumption mode, on the contrary, *pumpCons* is activated, and the mass balance is:

$$\dot{m}^{heaSys} = \dot{m}^b + \dot{m}^c \tag{58}$$

For idle mode, the mass balance in the system is simply:

$$\dot{m}^b = \dot{m}^{heaSys} \tag{59}$$

Mass flow rate through the heating system is:

$$\dot{m}^{heaSys} = \dot{m}^r - \dot{m}^{bypass} \tag{60}$$

As can be seen from eq. (60), water flows through the bypass only if $\dot{m}^{heaSys} \neq \dot{m}^r$. For the prosumer model, this happens if the inlet radiator temperature T^r_1 does not coincide with the outlet heat source temperature T^b_2.

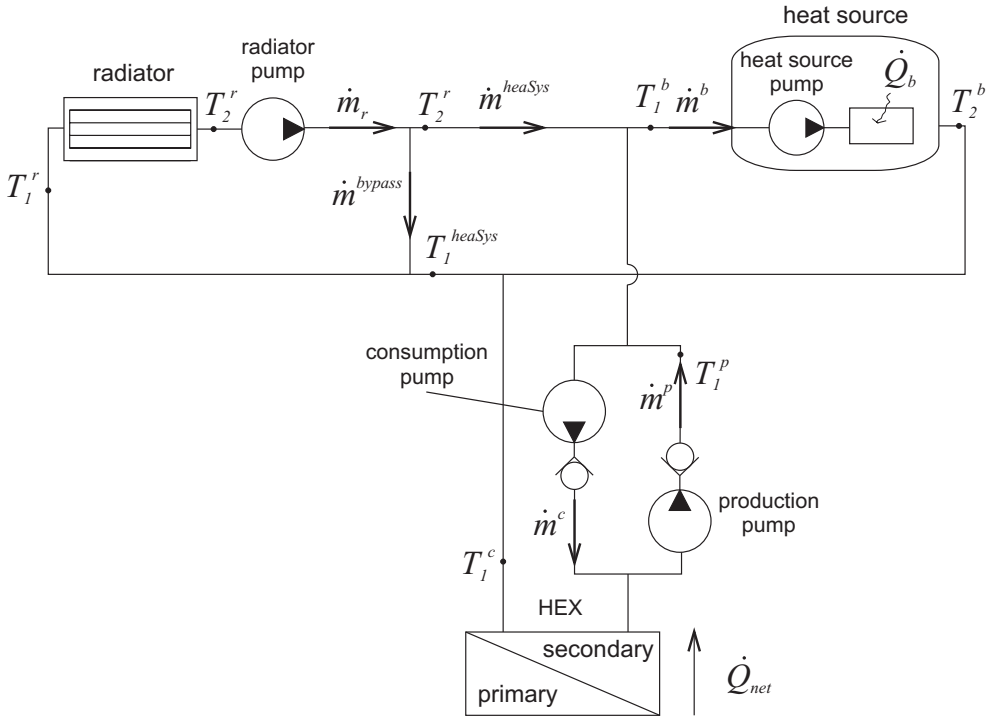

Figure 25: Scheme of mass flow streams on the secondary side

By solving for $\dot{m}^p$ and $\dot{m}^c$ from eq. (57) and eq. (58), mass flow control model for production and consumption pump can be formulated. Notice that $\dot{m}^b$ is measured by a flow meter block *massFlowRate* from fig. 24, and the signal is transmitted to the secondary side pumps controller *contSecPumps* (see fig. 26).

The content of *contSecPumps* controller is given in fig. 26. It uses simple algebra to calculate the set point for the pumps. The input from two boolean connectors *u_modeCons* and *u_modeProd* defines which pump is currently on.

4.2.6. Primary Side

The main components located on the primary side are a control valve *mainVal* and a feed-in pump *feedPump*.

Heat extraction from the network is regulated by varying the mass flow through the control valve *mainVal*. The control valve, in turn, is operated by "heat extraction controller" *contExtr*, which is described in section 5.2.1. The feed-in pump (*feedPump*) is a normalized speed pump. The input to the block can vary with a range $0 \dots 1$, where one corresponds to the nominal rotational speed.

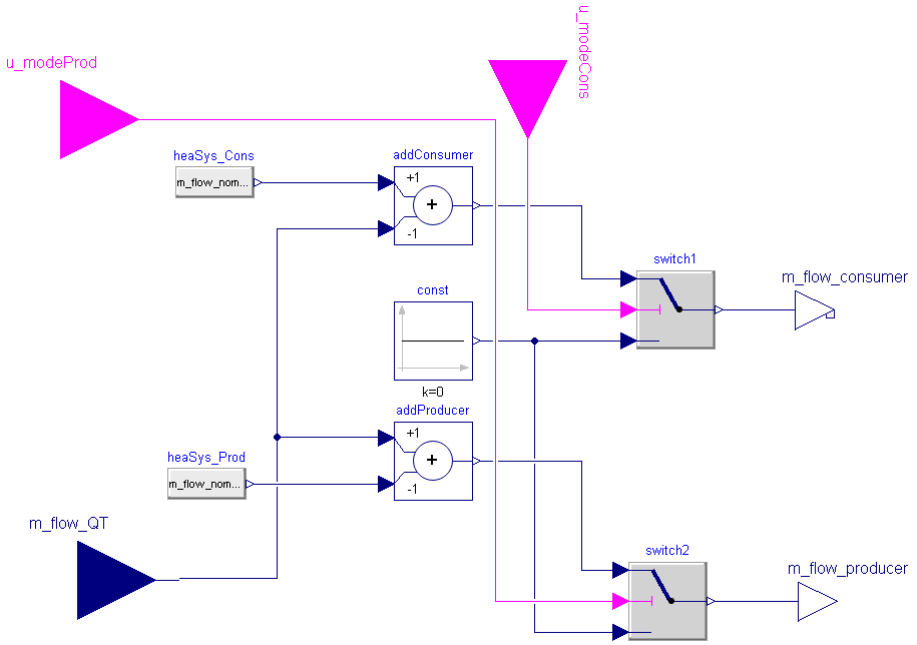

Figure 26: Diagram of production and consumption pumps controller *contSecPumps*

4.3. Heat network model

The heat network model was the final part of the modelling.

Two network topologies were modelled: radial and meshed. They are given in fig. 27.

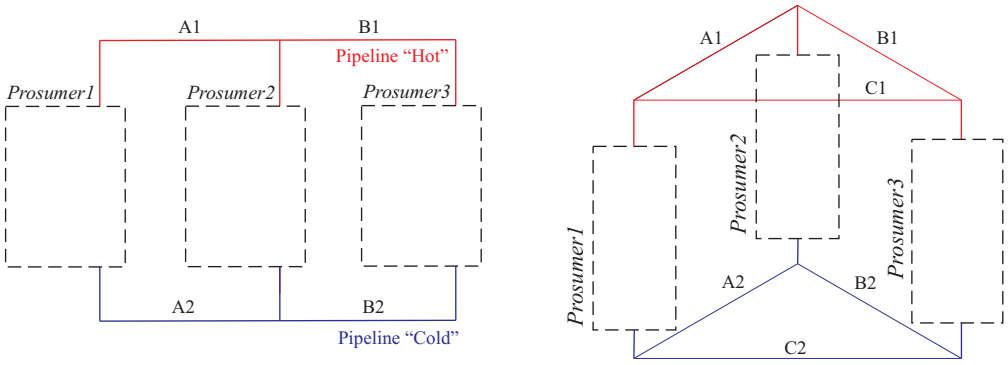

Figure 27: Investigated network topology: radial (left), meshed (right). A1, B1, C1 and A2, B2, C2 are the segments with the following lengths: $l_{A1,\,A2} = 50\,\text{m}$, $l_{B1,\,B2} = 100\,\text{m}$, and $l_{C1,\,C2} = 127\,\text{m}$; all the segments have the same inner diameter $d_{in} = 22\,\text{mm}$

The network model for radial topology is given in fig. 28. Prosumer model developed in the

appendix A is enclosed in a form of the block ($prosumer1 \ldots prosumer3$). According to the hierarchical approach, two fluid connectors *port_a* and *port_b* were added to the prosumer model in the appendix A, so it could be connected on the higher level of the hierarchy.

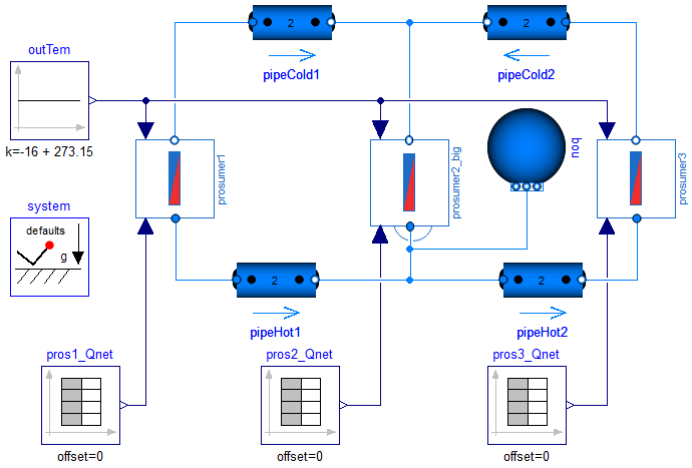

Figure 28: Prosumer-based heat network with radial topology

The heat network model utilizes unified outdoor air temperature ϑ_o for all prosumers. Its value is given by constant *outTem*. The reference heat flow rate with respect to the network, $\dot{Q}_{net,ref}$ is provided by the time-series tables *pros1_Qnet* ... *pros3_Qnet*. The block *bou* determines the static pressure in the network.

5. Control strategy

In this chapter, a summary of the control strategy development is presented. Challenging states for proper operation of prosumers are identified in section 5.1. As a response to the challenges, appropriate control mechanisms are offered in section 5.2, then validated in section 5.3. In section 5.4, control mechanisms are evaluated, and the eventual control strategy is adopted.

5.1. Challenging operating states

Two fundamental properties of prosumer-based heat networks were formulated in section 3: a) the exergy losses restrain energy flow; b) flow conditions put a bound on feed-in pumps. In order to demonstrate how these properties affect the heat transfer, simulations were performed.

To show the exergy losses problem, a heat network model with two prosumers was modelled (see fig. 29), and the prosumer model from appendix A is modified in fig. 30.

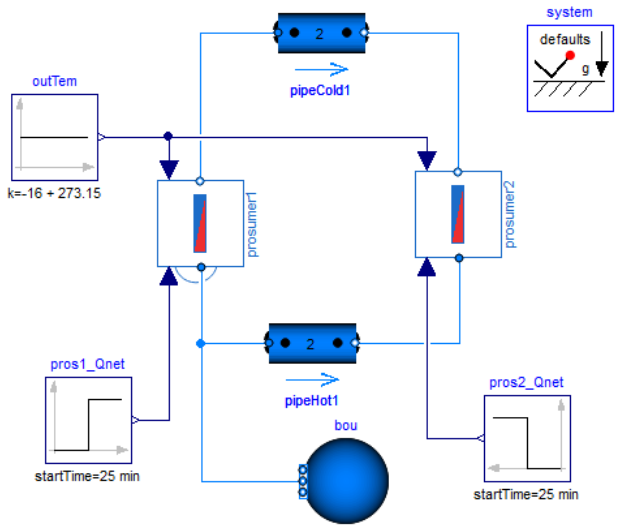

Figure 29: Diagram of the network with prosumers for the exergy losses problem

For simplicity, the outdoor temperature, *outTem*, was set to the design value, i.e. $\vartheta_{o,d} = -16\,°\text{C}$, so that the current heating load was $\dot{Q}_{l,d} = 28000\,\text{W}$. The reference value $\dot{Q}_{net,ref}$ of heat flow with respect to the network was given by time-series in *pros1_Qnet* and *pros2_Qnet* blocks. A single heating curve 50/30 ℃ was used for prosumer 1 and prosumer 2 as a set point temperature for *heatSource* block in appendix A.

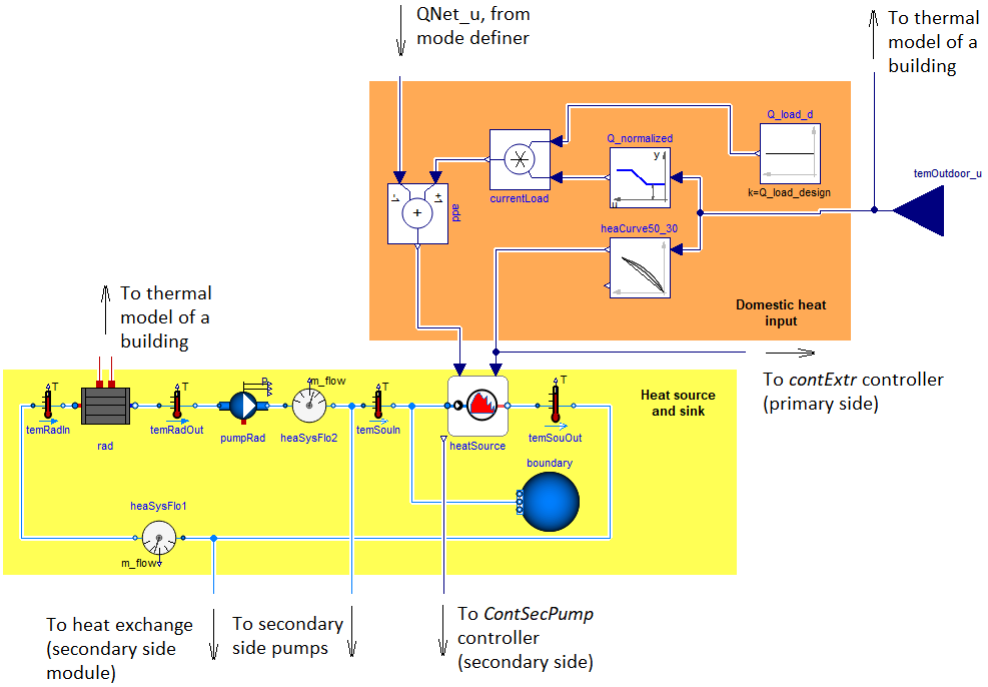

Figure 30: Modified fragment of the prosumer model for demonstrating the exergy losses problem (the remaining components are consistent with appendix A)

The heat flow rate plot obtained from the simulation is shown in fig. 31. Initially, the prosumers were in idle mode. Starting from 25 min, prosumer 1 was switched to production mode with $\dot{Q}_{net,ref} = -17500\,\text{W}$, and prosumer 2 inversely, was turned into consumption with $\dot{Q}_{net,ref} = 17500\,\text{W}$. As it can be seen, at the steady state, the reference values were not met. This is due to the exergy losses in the heat exchangers.

It is not shown in the plots, but according to multiple preliminary simulations, the extent to which actual heat flow rate $\dot{Q}_{net}$ deviates from the reference $\dot{Q}_{net,ref}$ depends on the value of the reference itself. For small $\dot{Q}_{net,ref}$ compared to the load $\dot{Q}_l$, the deviation can be as low as one Watt.

The exergy losses are caused by water temperature degrading. It is seen that the temperature is degrading from the secondary side (curve "Pros. 1, temSecHot") of the producing prosumer to the secondary side (curve Pros. 2, temSecHot") of the consuming prosumer in the temperatures plot in fig. B.4. The temperature was falling from 50 ℃ to 38.7 ℃. Again, the required temperature at the radiator's inlet was $T_1^r = 50\,^\circ\text{C}$. Thus, the "heat extraction controller" *contExtr* in appendix A could not meet the reference at prosumer 2, and the heat demand was not fulfilled.

The diagram of the heat network model for the flow conditions problem is given in fig. 28.

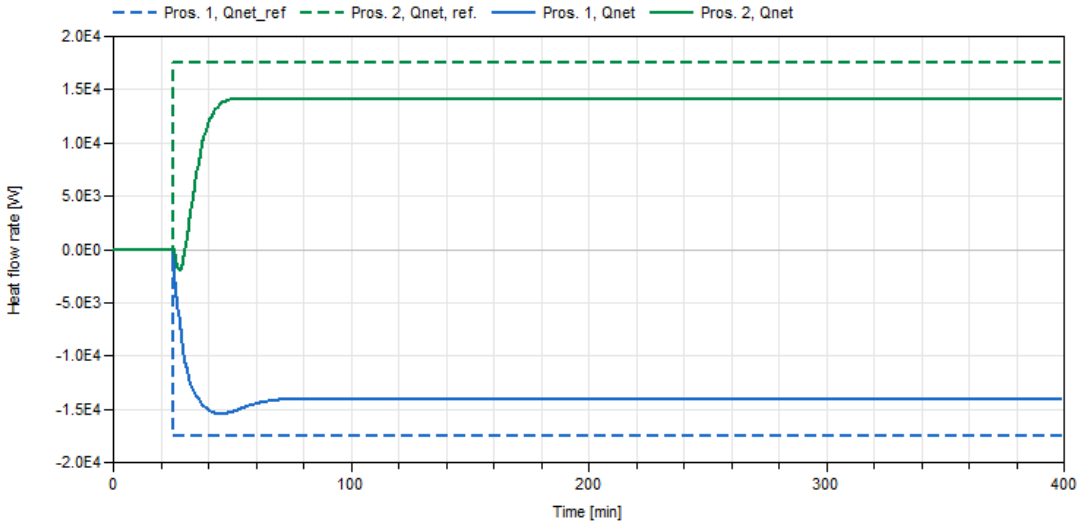

Figure 31: Heat flow rate with respect to the network for the exergy losses problem

This setting imitates conventional flow control strategy with a constant head as a set point. A feed-in pump at prosumer 2 has bigger sizing, so it develops higher nominal pressure and volume flow rate. The feed-in pump that belongs to prosumer 1, in turn, had lower sizing and lower nominal performance. The characteristic of both pumps were given in section 4.1.2. The design heating load for prosumer 1 is $\dot{Q}_{l,d} = 17500\,\text{W}$; for the other two prosumers, it is $\dot{Q}_{l,d} = 28000\,\text{W}$. Outdoor temperature *outTem* was the same as for demonstrating the exergy losses problem above. The reference $\dot{Q}_{net,net}$ was provided by time-series from *pros1_Qnet*, *pros2_Qnet*, and *pros3_Qnet* time tables.

The heat flow rate plot for the flow conditions problem is shown in fig. 32. Starting from 0 min, the prosumers were in idle mode. At 25 min, prosumers 1 and 3 were switched to production and consumption modes respectively with the reference $\dot{Q}_{net,ref} = -15000\,\text{W}$ and $\dot{Q}_{net,ref} = 15000\,\text{W}$. At 540 min, prosumer 2 joins the network with $\dot{Q}_{net,ref} = -4000\,\text{W}$ in production mode and stays in this mode until 1000 min. It is seen that the heat flow rate from prosumer 1 is interrupted and falls to zero, so the heat demand of prosumer 3 was not fulfilled between 540 min and 1000 min.

Note that the solution for the exergy losses problem was already applied in the model for the flow conditions problem. That is why between 120 min and 540 min $\dot{Q}_{net}$ finally arrives at the reference value.

A short explanation dedicated to this problem is accompanied by the plot in fig. 33. At 25 min, a feed-in pump at prosumer 1 starts to generate mass flow. Target head for the pump was 26 kPa. At 540 min, a feed-in pump from prosumer 2 cuts in. The target for the

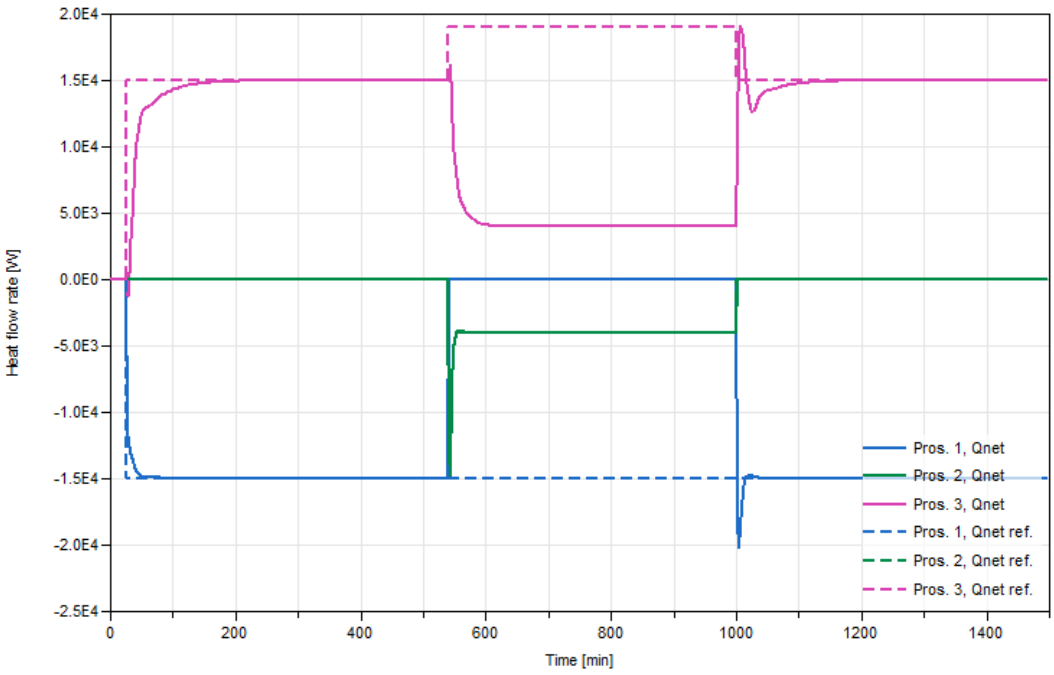

Figure 32: Heat flow rate between prosumers and heat network for the flow conditions problem

second pump is 50 kPa. As a result, the feed-in pump of prosumer 1 cannot overcome the pressure difference in the network. The check valve *cheVal1* in appendix A closes to prevent flow reversal, and the flow becomes blocked, and the heat transfer from prosumer 1 is not longer possible. At 1000 min, the feed-in pump of prosumer2 is switched off, and prosumer 1 comes back to normal operation.

Through the multiple preliminary simulation, it was found that the flow blocking is a special case of flow reduction problem. For the feed-in pumps that were already in operation, switching-on of prosumers with a head set point led to shifting of their pump working points to the left. This caused mass flow rate reduction, not necessary to the extent where the flow was blocked. A specific outcome depended on a pump curve and a characteristic of the network.

To sum up, it does not seem possible to avert the exergy losses and the flow blocking or reduction problem without new control mechanisms.

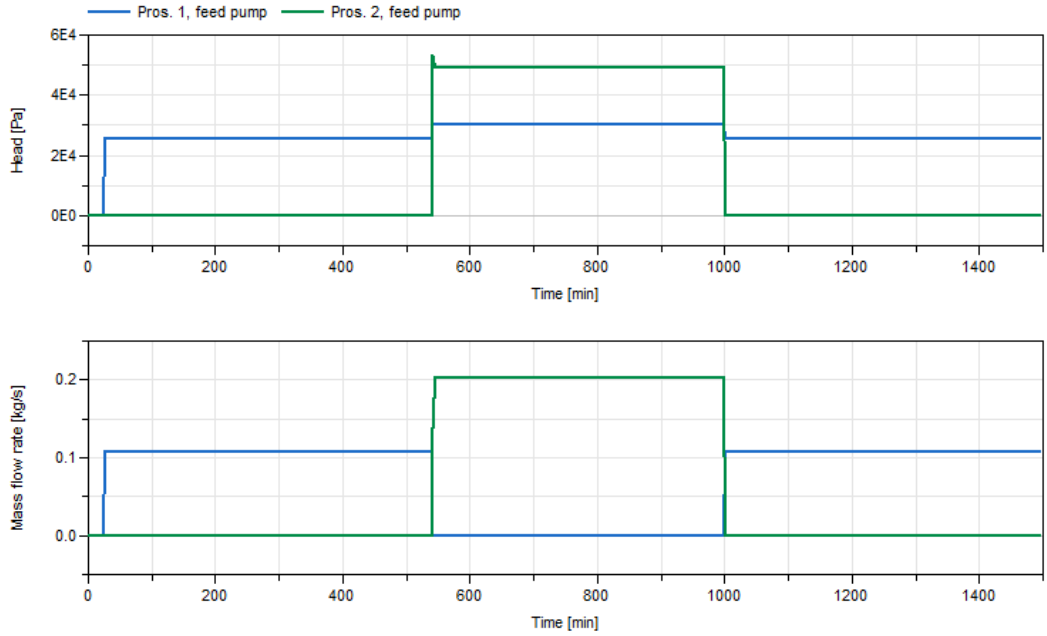

Figure 33: Head and mass flow rates of the feed-in pumps for the flow blocking

5.2. Proposed control mechanisms

This section is dedicated to the control mechanisms that target challenging operating states.

In the network, mass flows can be maintained by feed-in pumps and control valves. For the proposed control strategy, flow controllers provide a range of hydraulic conditions for all prosumers to operate in production mode. Then "heat extraction controllers" by means of control valves adjust this range to a more narrow one. Eventually, the two form a thermohydraulic state that satisfies goals of the control strategy.

An overview of "heat extraction controller" is given in section 5.2.1. Solution for the exergy losses problem is addressed in section 5.2.2. Three different control mechanisms are proposed for the flow condition problem in section 5.2.3.

5.2.1. "Heat extraction controller"

The task of "heat extraction controller" (*contExtr* block in appendix A) is to sustain heat flow $\dot{Q}_{net,ref}$ from the network to cover the heat demand created by the *source – sink* module. This type of controllers is widely used in contemporary heating systems. The implementation in Modelica is given in fig. 34.

The controller becomes activated through the *modeCons_u* connector only in consump-

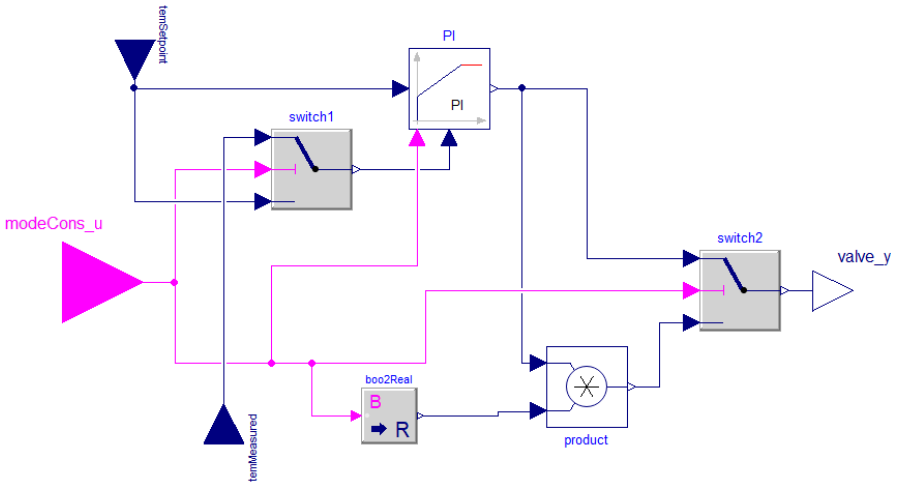

Figure 34: Diagram of "heat extraction controller"

tion mode. Supply temperature $T_1^{h.c.}$ of a "lower" heating curve 50/30 ℃ in appendix A serves as a set point. Outlet temperature T_1^c on the secondary side of the heat exchanger is received by *temMeasured* connector. The opening of the control valve (*valve_y*) acts as a manipulating variable.

5.2.2. Heating curve switching

The proposed control mechanism that targets the exergy losses problem is heating curve switching. By utilizing a "higher" heating curve, more exergy is generated at the heat source to compensate its losses in the heat exchangers. Note that it corresponds to the inlet temperature T_1 increase in the exergy generation formula (see eq. (35)).

Heating curve switching has been already implemented in the general prosumer model in appendix A. Heating curve 50/30 ℃ (*heaCurve50_30*) is used in consumption and idle modes, and for production mode, heating curve 70/30 ℃ (*heaCurve70_30*) is used instead. The switching between the two is controlled by the *mode definer* module and performed in the *heaCurveSwitch* block in *domestic heat input* module.

The heating system require to undergo changes at *heat source – sink* module. The issue was that the outlet temperature of the heat source is higher that the required inlet of the radiator, i.e.ṫhe radiator permanently operates with the "lower" heating curve 50/30 ℃. This led to overheating of room air temperature in production mode. To avoid this problem, the inlet water temperature is cooled by mixing with outlet water from the radiator. In the model in appendix A, it is done though a bypass. From the exergetic view, this is equivalent to

exergy destruction.

In production mode, mass flow rate through the heating system $\dot{m}^{heaSys}$ was less than design mass flow though the radiator $\dot{m}^{r}$. The ratio between the two is the following:

$$\dot{m}^{heaSys} = \dot{m}^{r} \frac{T^{r}_{1\,d} - T^{r}_{2\,d}}{T^{b}_{1\,d} - T^{r}_{2\,d}} = \dot{m}^{r} \frac{50 - 30}{70 - 30} = 0{,}5\,\dot{m}^{r} \tag{61}$$

where $T^{h.c.}_{1,\,d}$ is design supply temperature of the "higher" heating curve.

5.2.3. Flow control mechanisms

Three flow control mechanisms are proposed. The first is a controller by Rosemann et. al. in section 5.2.3. The second and the third control mechanisms, which were developed for this thesis, are the "minimal flow controller" (see section 5.2.3), and the "suppression controller" (see section 5.2.3). All the flow control mechanisms are only active in production mode.

Rosemann's controller The Rosemann's controller was initially designed for bidirectional heat transfer between a single substation and a conventional heat network [17]; however, in this thesis, an attempt was made to apply it in the prosumer-based heat network. A comprehensive description of this controller was already given in section 1.5.1.

The Rosemann's controller utilizes thermodynamic equilibrium to operate. For small deviations from the steady state, heat flow $\dot{Q}_{net}$ with respect to the network can be expressed as:

$$\dot{Q}_{net} = c_p\,\dot{m}^{pri}\,(T^{pri}_{hot} - T^{pri}_{cold}) \tag{62}$$

where $\dot{m}^{pri}$ is the mass flow rate though a feed-in pump.

When a flow from one of the prosumers is blocked, heat demand becomes higher than supply, and the temperature T^{pri}_{cold} in a "cold" pipeline decreases. Since temperature T^{pri}_{hot} in a "hot" pipeline is kept constant by the controller, to transfer the same $\dot{Q}_{net}$, inner controller decreases $\dot{m}^{pri}$. As a result, the new working point with lower pressure difference is obtained, and the blocked prosumer is released.

An implementation of Rosemann's controller is presented in fig. 35. In Rosemann et al. notation, the inner controller is *contTem*, the outer is *contFlow*. Connector *FlowRate_u* receives measure mass flow rate, and *TemOut_u* receives "hot" outlet temperature on primary side of a prosumer. *TemOutRef_u* receives a set point from a heating curve. Output connector *feedPump_y* transmits the manipulated variable (normalized shaft speed y) to a feed-in pump. Finally, the controller becomes activated through *modeProd_u* connector.

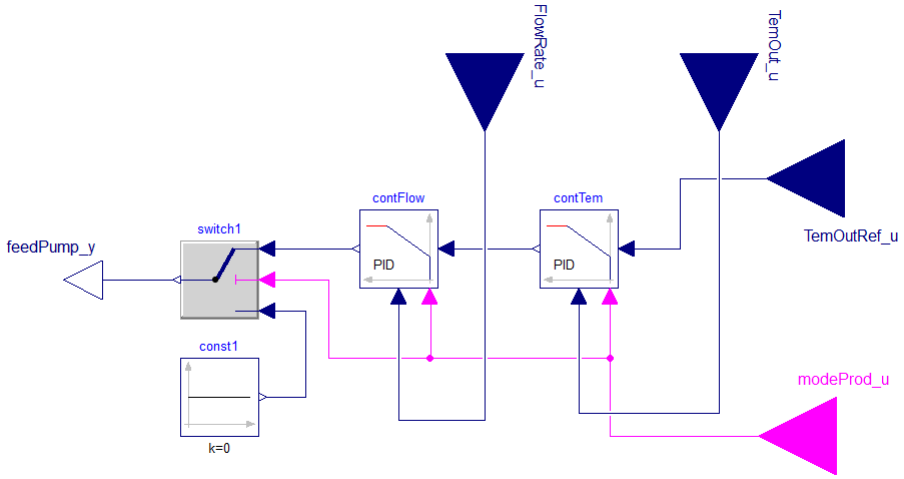

Figure 35: Diagram of the Rosemann's controller

Since pumps usually demonstrate unstable flow at low shaft velocities [18], the bottom output of *contFlow* controller was limited to 0.1. The reset was added to the PID controllers due to the integration wind up caused by switching between the modes.

"Minimal flow controller" The idea behind the "minimal flow controller" is the following. The certain minimum value $\dot{m}^{pri}_{min}$ of the flow exists on the primary side that sustains heat transfer for the reference $\dot{Q}_{net,\,ref}$. For this controller, mass flow through the primary side $\dot{m}^{pri}_{min}$ is sustained lower than mass flow $\dot{m}^{p}$ on the secondary side.

Keeping $\dot{m}^{pri}_{min}$ at every prosumer, brings about the flow conditions when excessive pressure difference tends not to appear in the network. In order to calculate $\dot{m}^{pri}_{min}$, the following formulas are used.

To begin with, the maximum allowed inlet temperature was derived for the heat source from eq. (54) and (55):

$$T^{b}_{1,\,max} = T^{b}_{set} - \frac{\dot{Q}^{b}_{set}}{\dot{m}^{b}_{max}} \tag{63}$$

As a reminder, T^{b}_{set} is determined by the supply temperature $T^{h.c.}_{1}$ of the heating curve.

In production mode, the inflow for the heat source is a mixture of the heating system flow $\dot{m}^{heaSys}$ with the flow $\dot{m}^{p}$ from the secondary side of the heat exchanger (see the scheme in fig. 25 and eq. (57). The energy balance expressed for the outlet water temperature on

the secondary side is given by:

$$T^{p}_{cold,\,max} = \frac{T^{b}_{1,\,max}\,\dot{m}^{b}_{max} - T^{heaSys}_{2}\,\dot{m}^{heaSys}}{\dot{m}^{b}_{max} - \dot{m}^{heaSys}} \tag{64}$$

where T^{heaSys}_{2} is equal to the temperature $T^{h.c.}_{2}$ of the heating curve.

According to eq. (40) and assuming that $c_{p,\,pri} \approx c_{p,\,sec}$, the energy balance for the heat exchanger can be expressed as:

$$\dot{m}^{pri}_{min} = \frac{\dot{m}_{p}(T^{b}_{set} - T^{p}_{cold,\,max})}{T^{pri}_{hot} - T^{pri}_{cold}} \tag{65}$$

Combining eqs. (40) and (13), the effectiveness can be formulated in terms of temperatures:

$$\varepsilon = \frac{T^{pri}_{hot} - T^{pri}_{cold}}{T^{b}_{set} - T^{pri}_{cold}} \tag{66}$$

While $\dot{m}^{pri}_{min}$ is declining compared to $\dot{m}^{p}$ as described in the beginning, it can be written for heat capacity ration from eq. (15) that $R \to 0$ (see eq. (15)). Thus, expression eq. (66) can be rewritten as:

$$T^{pri}_{hot} = T^{b}_{set} \tag{67}$$

By substituting eq. (67) into eq. (65), the minimum value of the mass flow can be calculated as following:

$$\dot{m}^{pri}_{min} = \frac{\dot{m}_{p}(T^{b}_{set} - T^{p}_{cold\,max})}{T^{b}_{set} - T^{pri}_{cold}} \tag{68}$$

Minimal flow $\dot{m}^{pri}_{min}$ depends on heat flow rate $\dot{Q}^{b}$, outlet temperature T^{b}_{set} at the heat source, and inlet temperature on the primary side of the heat exchanger T^{pri}_{cold}. Note that T^{b}_{set} is given by the heating curve, and; consequently, is defined by the outdoor temperature ϑ_{o}.

In order to evade deviations from above mentioned assumptions, a set point for the minimal flow is taken with a redundancy coefficient k_{r}:

$$\dot{m}^{pri}_{min,\,set} = k_{r}\,\dot{m}^{pri}_{min} \tag{69}$$

Coefficient k_{r} can take values between 1 and $k_{r,\,max}$, which is defined by the nominal

mass flow rate of the feed-in pump $\dot{m}^{f}_{nom}$:

$$k_{r,\,max} = \frac{\dot{m}^{f}_{nom}}{\dot{m}^{pri}_{min}} \tag{70}$$

It is expected that prosumers with high values of k_r will tend to block or reduce the flow from feed-in pumps with smaller sizing. In turn, $k_r = 1$ will worsen heat transfer to the network.

An implementation of "minimal flow controller" is demonstrated in fig. 36. A block *minMassFlow* utilizes eq. (63) – (68) to calculate minimum flow $\dot{m}^{pri}_{min}$. The block takes $\dot{m}^{b}_{max}$ from eq. (55) and $\dot{m}^{heaSys}$ from eq. (61) as parameters. The description of input variables for *minMassFlow* is shown in table 6. A PID controller is used to sustain $\dot{m}^{pri}_{min,\,set}$. Input connector *flowRate_* transfers measured variable (mass flow rate $\dot{m}^{pri}$) to *contFlow*.

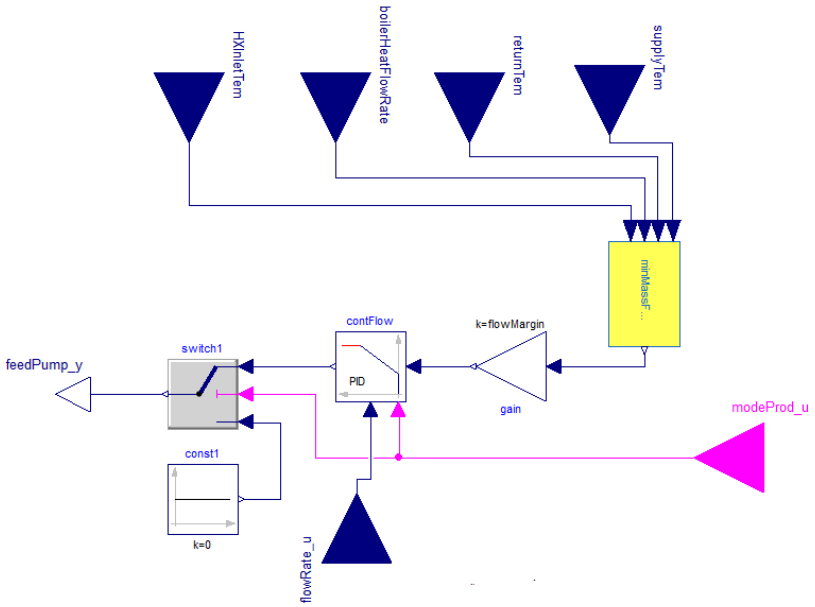

Figure 36: Diagram of "minimal flow controller"

Table 6: Description of input connectors to *minMassFlow* block

Connector	Variable	Description
HXInletTem	T_{cold}^{pri}	Inlet water temperature on secondary side
boilerHeatFlowRate	$\dot{Q}_{set}^{b}$	Heat flow rate set point for the heat source
returnTem	T_{2}^{heaSys}	Return temperature from the heating system
supplyTem	T_{set}^{b}	Outlet temperature from the heat source

"Suppression controller" This controller suppressed shaft velocity of the feed-in pumps that generate excessive pressure to keep other prosumers away from blocking. Out of the blocking states, the feed-in pumps operate with nominal shaft velocity, i.e. $y_{nom=1}$. The "suppression controller" becomes activated when pressure difference in the network becomes bigger or equal than shut-off head of the pump. The controller switches to inactive mode when an "event impulse" is received. The "event impulse" is formed when flow conditions change in the network, namely, a feed-in pump is commanded to shut off regardless of its location and blocking status.

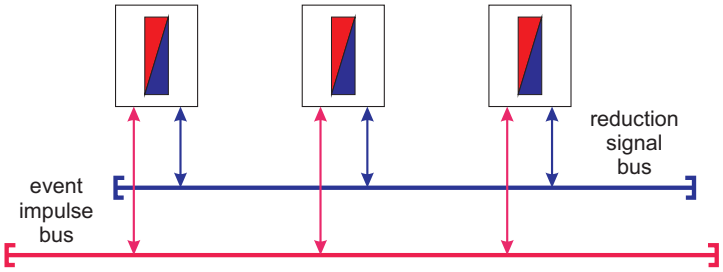

Figure 37: Diagram of communication lines between prosumers for the "suppression controller"

The "suppression controller" is based on a PID control mechanism. As a measured variable, it utilizes mass flow rate $\dot{m}^{pri}$ on the primary side of the prosumer undergoing blocking. As a set point, the controller uses minimal mass flow rate $\dot{m}_{min}^{pri}$ from "minimal flow controller". The manipulated variable is shaft speed velocity reduction signal. Reduction signal and "event impulse" are transferred to all other prosumers through the communication lines (see fig. 37).

The working principle of "suppression controller" is shown in the following volume flow – head diagrams. Network configuration from fig. 14 is considered. At first, prosumer 2 was in production mode (point *b*) with nominal shaft velocity (y_{nom}). Shortly after, prosumer 1 with smaller pump sizing switches from idle to production mode. The working state of the

feed-in pumps for this case is shown in fig. 38. Prosumer 1 immediately becomes blocked due to the excessive pressure difference (point a). The head at the point a is shut off head; therefore, the suppression controller becomes activated.

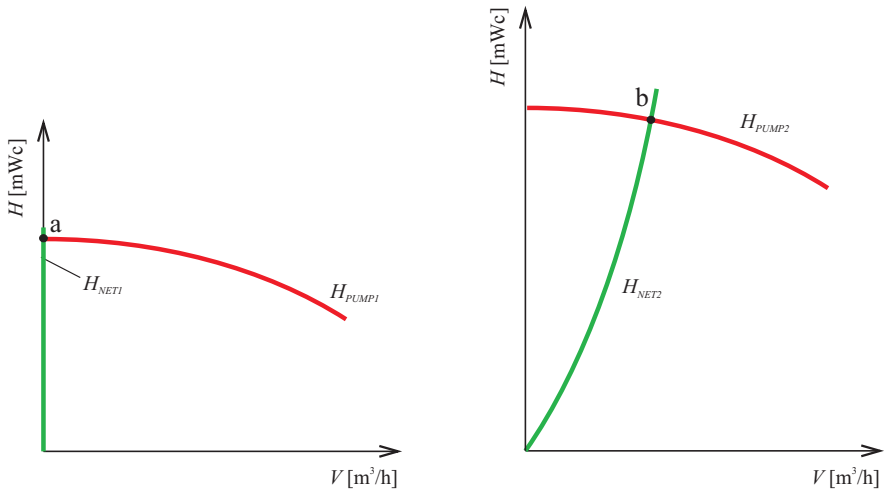

Figure 38: Volume flow – head diagrams before activation of "suppression controller": prosumer 1 (left); prosumer 2 (right)

The volume flow – head diagram after the activation is shown in fig. 39. The "suppression controller" sustains flow rate $\dot{m}^{pri}_{min,\,set}$ (point *c*) at prosumer 1. It is sending the reduction signal to prosumer 2 to, and thus, the pump's curve is lowering, and a new working point (point *d*) with lower pressure difference is achieved in the network as it shown in fig. 39. Now, both prosumers can generate mass flow to the network, and required heat flow rate is received by the load.

The model of "suppression controller" is shown in fig. 40. The reduction signal is received from (*bus_u*). A block *const_y_nom* defines nominal shaft velocity (y_{nom}), which the feed-in pump achieves without a reduction signal. Addition of velocity reduction signal from input *bus_u* and y_{nom} is performed in *addBus*. An input connector *dp_u* receives measured pressure difference Δp from the network. A block *activator*, developed for this theses, identifies if the feed-in pump approaches blocking state. Once Δp crosses shut off value H_{max}, *contPID* becomes unleashed from short circuit by a switch *switchCont*. The PID controller uses $\dot{m}^{pri}_{min,\,set}$ value calculated in *minMassFlow* as a set point. The measured value of flow rate $\dot{m}^{pri}$ on the primary side is received through *flowRate_u* connector. Reduction signal (manipulated variable) is sent through *bus_y* to other prosumers.

When activated, the controller ignores the input reduction signal by multiplying it with zero value from *true0False1*. When the controller is inactive, the output reduction signal is zero.

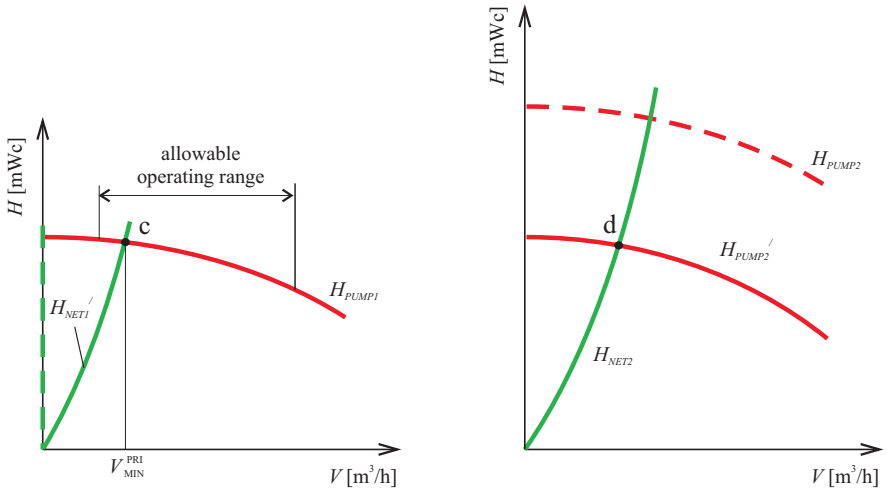

Figure 39: Volume flow – head diagrams before activation of the "suppression controller" for: prosumer 1 (left), prosumer 2 (right)

A block *fallingEdge* generates the "event impulse" when production mode is not longer on. The "event impulse" is received through *reset_u*, then *activator* is switched from 'true' to 'false' if it was previously activated. Through *reset_y* the "event impulse" is sent to the other prosumers.

Note that pressure differences H_{max} corresponds to point a in fig. 38.

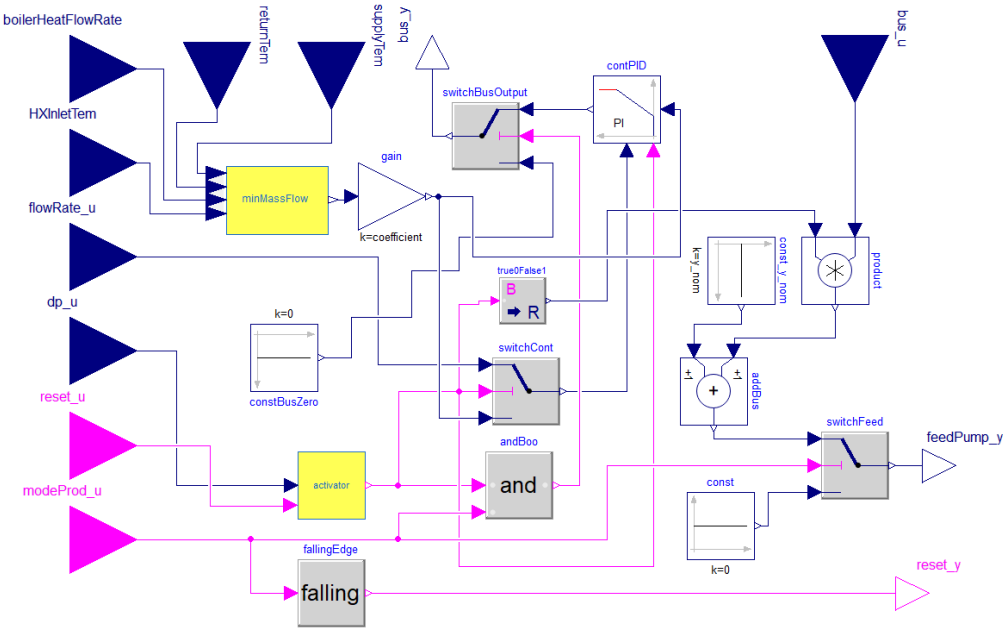

Figure 40: Diagram of "suppression controller"

5.3. Validation of control mechanisms

For validation, a general prosumer model was equipped with offered control mechanisms. A conclusion on how successfully they cope with the challenges is then based on comparison between simulation results from section 5.1 and simulations performed in this section. Input parameters and $\dot{Q}_{net,ref}$ time-series for both simulations were identical.

Heating curve switching Heating curve switching was validated with the heat network model for the exergy losses problem from fig. 29.

The heat flow rate for the case with the switching ("case 2" curves) and the case without switching ("case 1" curves) are given in fig. 41. It can be seen that heating curve switching mechanism can evade energy flow limitation: the actual heat flow rate $\dot{Q}_{net}$ finally meets the reference $\dot{Q}_{net,ref}$ in the steady state.

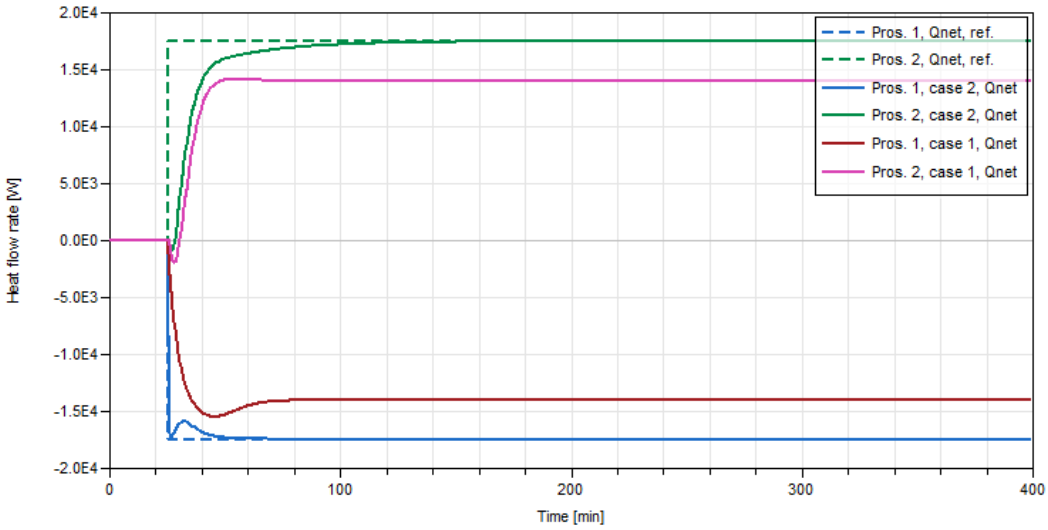

Figure 41: Heat flow rate between prosumers with and without heating curve switching

The temperatures on the secondary and primary sides are shown in fig. B.5. Compared to fig. B.4, the values from two different heating curves are observable. Outlet temperature coming from the heat source was set according to the heating curve 70/30 °C (curve "Pros. 1, temSecHot"). Thus, "heat extraction controller" that utilizes the heating curve 50/30 °C, can achieve its reference (curves "Pros. 2, temSecHot" and "Pros. 2, contExtr, ref."), and the required heat demand is fulfilled.

Rosemann's controller Heat flow rate for prosumers equipped with the Rosemann's controllers is given in fig. 42. The reference flow rate was finally reached.

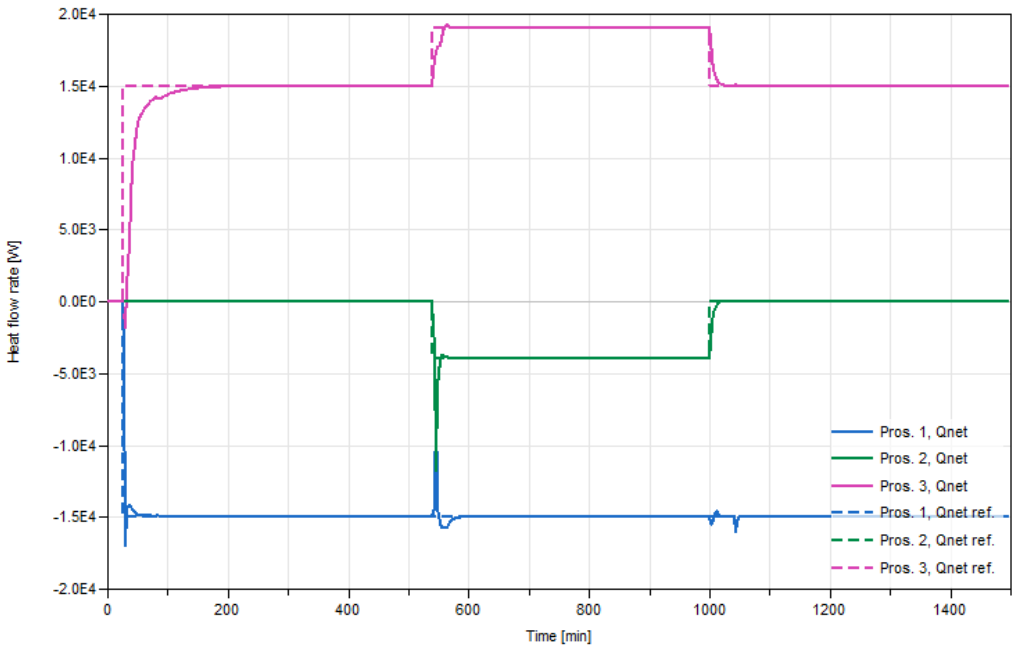

Figure 42: Heat flow rate between prosumers for the Rosemann's controller

Comparing the flow conditions from fig. 43 and fig. 33 in between 540 min and 1040 min, the Rosemann's controller restricts head developed by the first feed-in pump to 15.4 kPa. This allows prosumer 2 to operate in the network.

The Rosemann's controller does not control prosumers undergoing blocking. The set point temperature and mass flow were not met (see fig. 44) for the prosumer facing blocking. Consequently, it cannot be a part of a comprehensive control strategy for prosumer-based heat networks. However, with the help of prosumer 2 where the Rosemann's controller governed its operation, the minimum mass flow rate $\dot{m}^{pri}_{min,\,set}$ was achieved at prosumer 1, and the reference heat flow rate $\dot{Q}_{net,\,ref}$ was met. This was due to the thermodynamic balancing of Rosemann's controller.

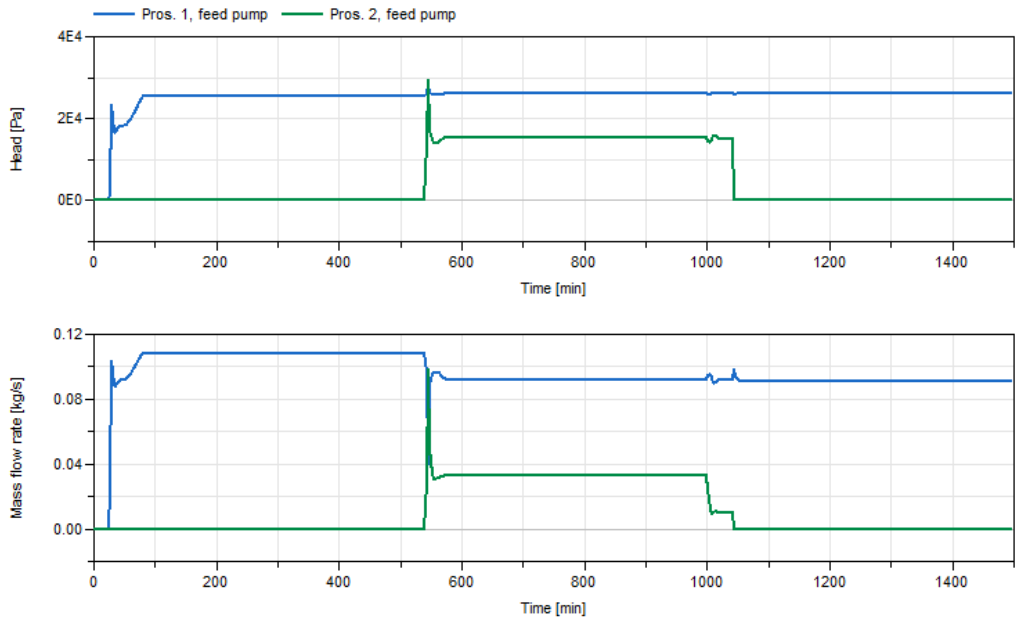

Figure 43: Head and mass flow rates for prosumers operated by the Rosemann's controller

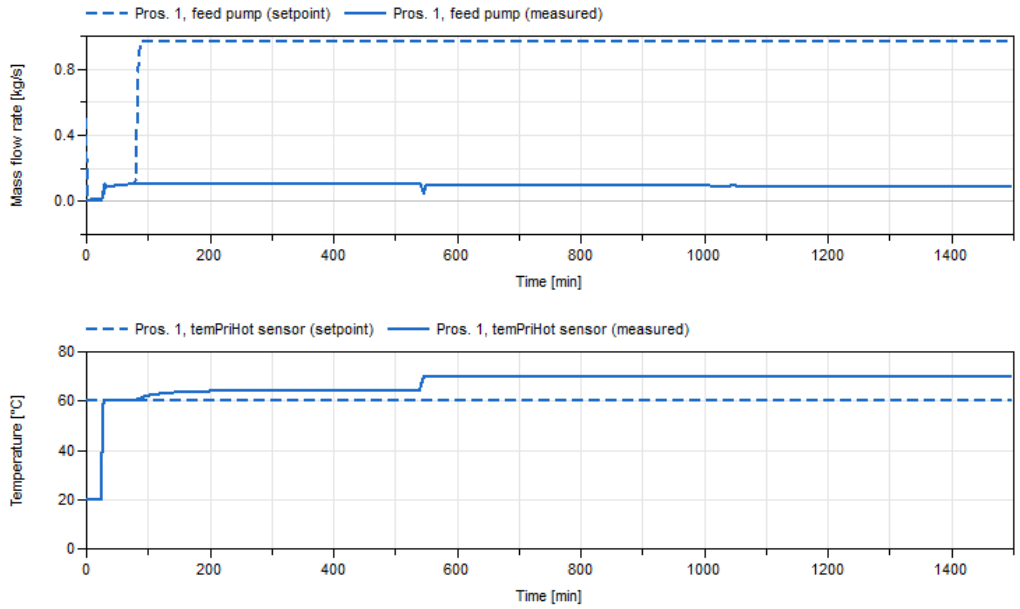

Figure 44: Set point and measured value for inner controller (above); set point and measured value for outer controller (below) for the Rosemann's controller of prosumer 1

Minimal flow controller Adequate operation of "minimal flow controller" depends on redundancy coefficient k_r. As expected, the simulations showed that $k_r = 1$ restrained heat transfer from prosumer 1. The value $k_r = 3$ provoked undesirable flow reduction from prosumer 1.

Electricity consumption was increasing with decreasing k_r as it is demonstrated in table 7. Although energy consumption of the feed-in pump was low for $k_r = 1$, the simulations showed that low mass flow rates on the primary side causes large mass flow on the secondary side according to eq. (54). It was founded that the value $k_r = 1.15$ was the least from blocking risk and energy consumption view.

Table 7: Electric energy consumption depending on redundancy coefficient k_r for the "minimal flow controller"

Redundancy coefficient, k_r	Total power consumed [W h]	Power consumed by a feed-in pump [W h]
1	1841	83
1.15	1352	119
3	1208	122

Heat flow rate with respect to the network is shown in fig. 45 for the "minimal flow controller". The plot is distinguished by long-lasting transient states between 540 min and 680 min.

As well as the Rosemann's controller, the "minimal flow controller" did not follow the mass flow rate set point for prosumer 1 as it can be seen in fig. 46, so it cannot be a part of the comprehensive control strategy. Despite this fact, the required heat transfer was possible due to maintaining minimal flow rate. That is because this controller is also driven by thermodynamic equilibrium.

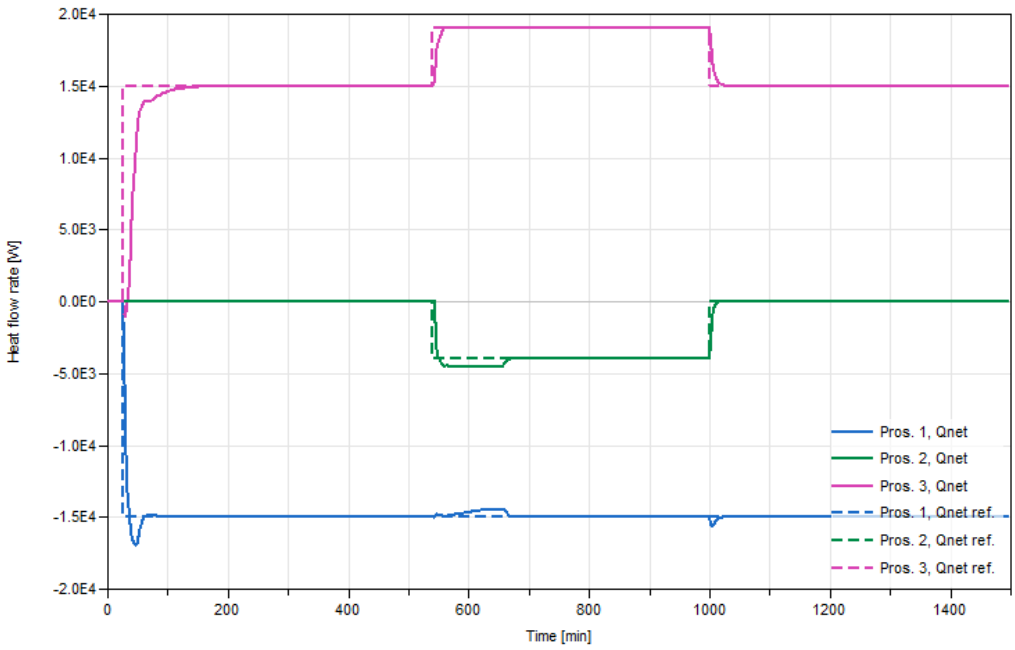

Figure 45: Heat flow rate between prosumers for the "minimal flow controller"

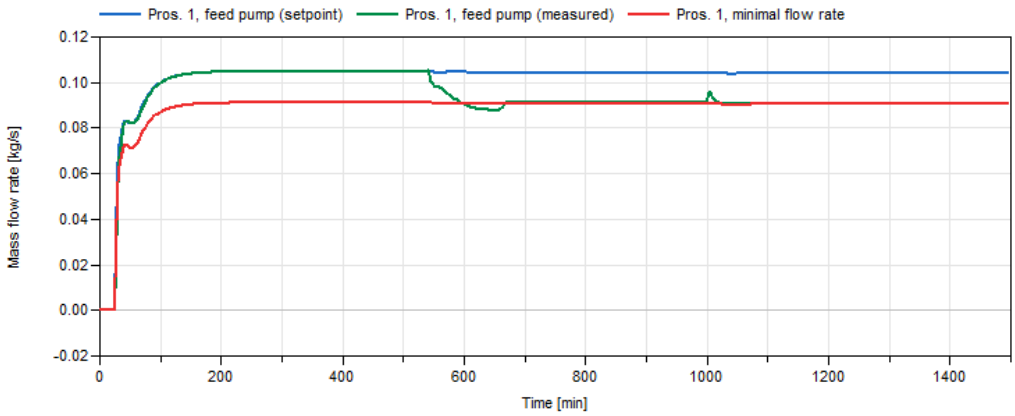

Figure 46: Set point and mass flow rate of "minimal flow controller" for prosumer 1

"Suppression controller" A validation of "suppression controller" required communication lines between prosumers. A corresponding heat network model is given in fig. 47. A block *commutator*, developed in this thesis, was responsible for transferring control signals between prosumers. The diagram of *commutator* is given in fig. B.1.

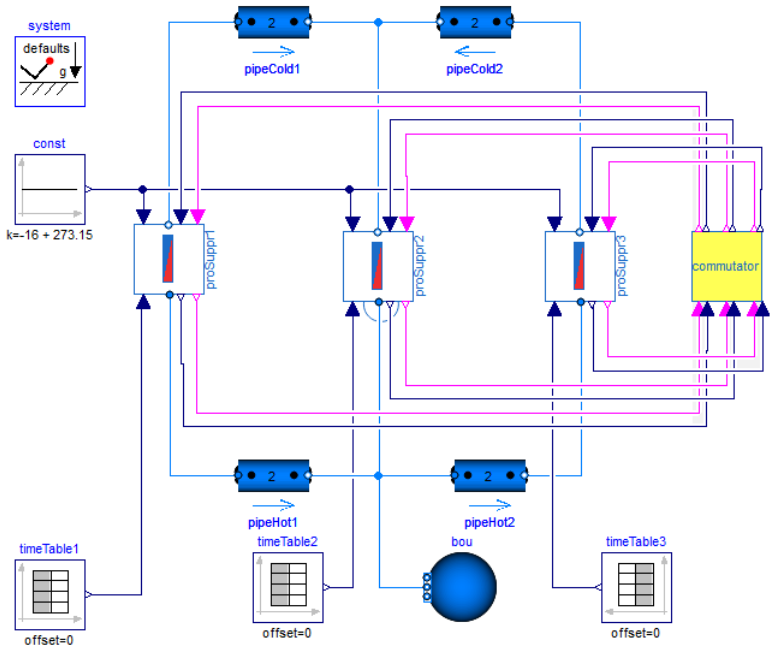

Figure 47: Diagram of the prosumer-based heat network with "suppression controllers"

The reference and actual heat flow rates are shown in fig. 48 for the "suppression controller": the reference was met with extremely brief transient states.

The plot of control signals for the feed-in pump of prosumer 2 is given in fig. 49. Reduction signal is coming from prosumer 1 and have negative sign. At 540 min, it starts to slow the second feed-in pump. The state of the controller is in the same plot: it is active during 'true' value.

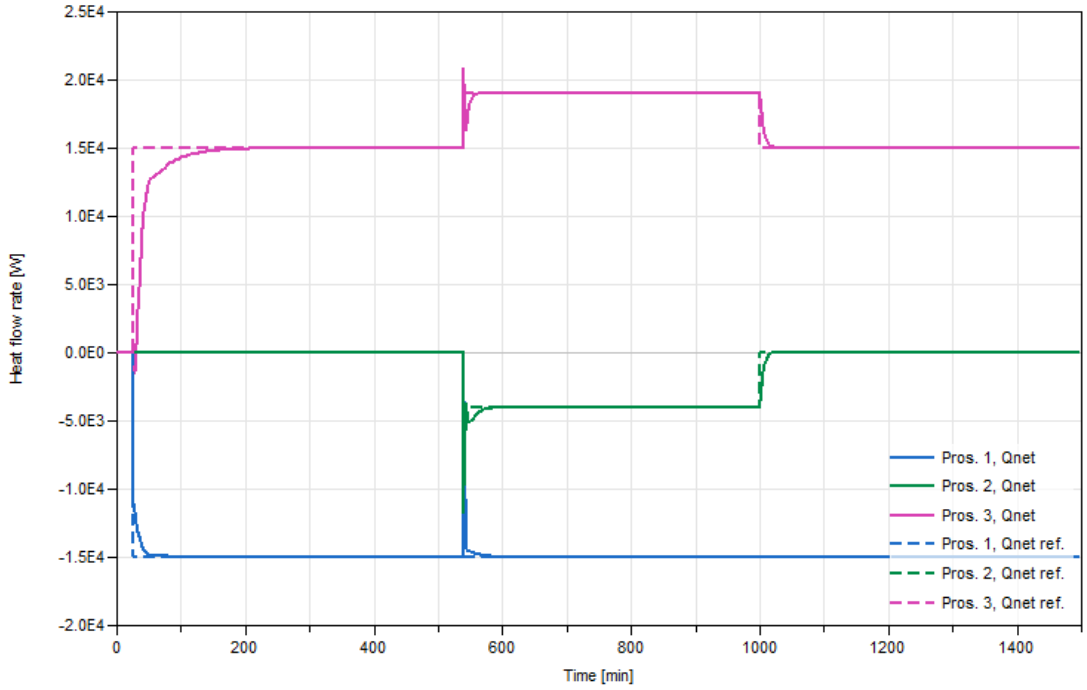

Figure 48: "Suppression controller": heat flow rate with respect to the network

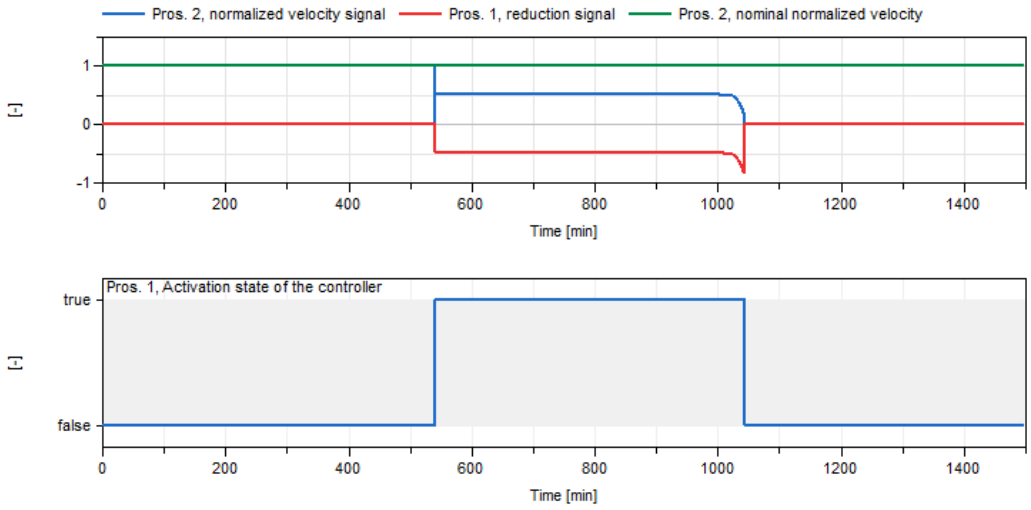

Figure 49: Control signals for the feed-in pump of prosumer 2 (above) and state of the controller at prosumer 1 (below)

5.4. Evaluation of flow control mechanism

While heating curve switching mechanism and the "heat extraction controller" had no alternatives in the considered control strategy development, the flow controllers were represented by three different options: the Rosemann's controller, "minimal flow controller", and "suppression controller". For the next stage, it was reasonable to select one type of the flow controllers.

Evaluation of controllers with respect to the various criteria are given in table 8. As it was mentioned before, the Rosemann's controller relied on thermodynamic equilibrium, which might take a long time to reach, especially for a big network. The "minimal flow controller" was also driven by thermodynamic equilibrium, but with lower flow rate $\dot{m}^{pri}_{min}$. This made it even longer to reach the equilibrium as can be seen in fig. 45.

In addition, the Rosemann's controller and the "minimal flow controller" do not control prosumers undergoing blocking, so they cannot be a part of the comprehensive control strategy for prosumer-based heat networks.

Along with other physical quantities, only the "suppression controller" uses pressure, which propagates much faster than temperature change, as a measured variable. It means that the "suppression controller" reacted faster to flow conditions, which is demonstrated by the least disruption to the room air temperature in fig. 50).

Table 8: Evaluation of flow controllers

Control mechanism	Measured quantities	Error w.r.t. the reference $\dot{Q}_{net}$	Error w.r.t. room air temperature	Total power consumption [W h]
Rosemann's controller	T, $\dot{m}$	Identical	Fair	1086
"Minimal flow controller"	T, $\dot{m}$	Poor	Worst	1352
"Suppression controller"	T, $\dot{m}$, Δp	Identical	Best	986

To conclude, the "suppression controller" demonstrated the finest performance, and was accepted as a part of the developed control strategy.

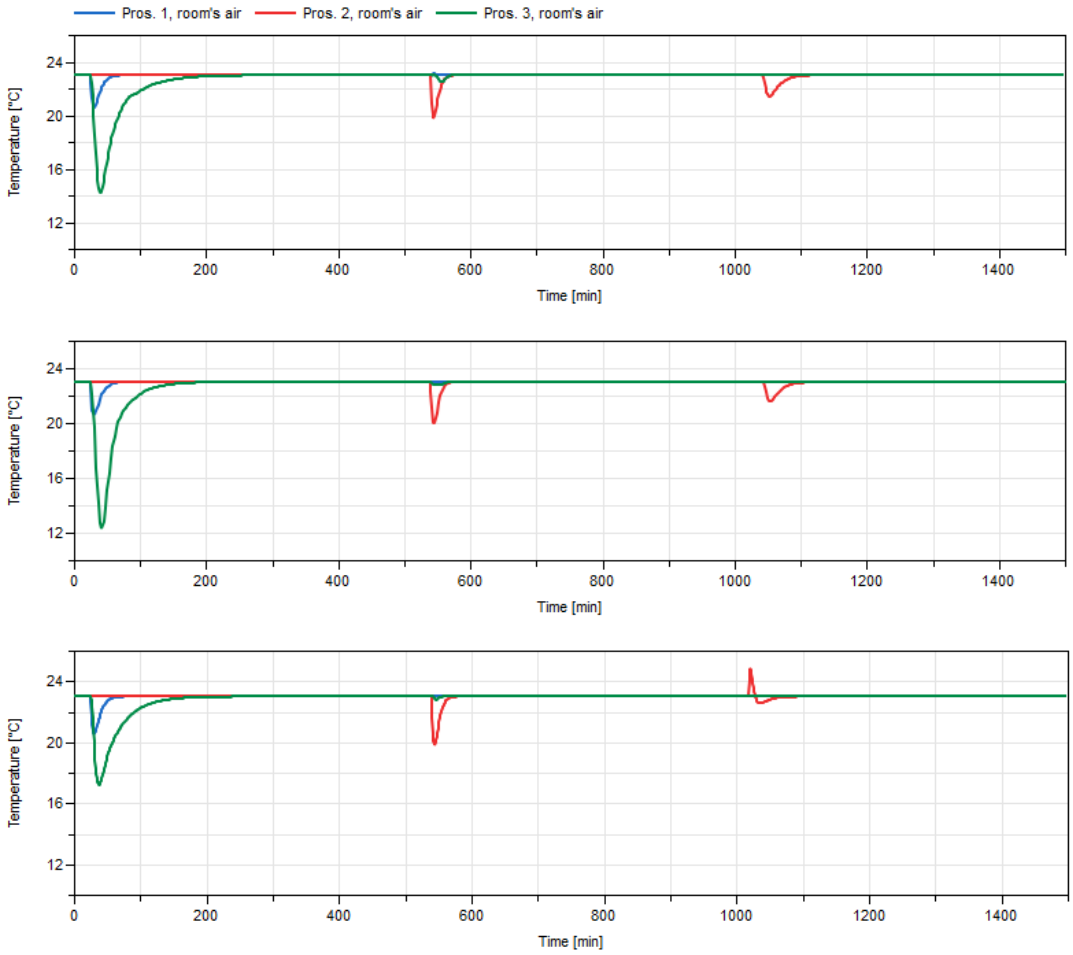

Figure 50: Room air temperature for the flow controllers, the reference is 23 ℃ : Rosemann's controller (above), "minimal flow controller" (middle), "suppression controller" (bottom)

6. Simulation results

This chapter presents a comprehensive hydrodynamic and thermodynamic analysis of a prosumer-based heat network under the developed control strategy. A specific sequence of alternating states of the system was achieved by applying scenarios. A description of scenarios and their results are given in section 6.1.

Transient states that were observed during simulations were divided into two groups. The first, generic states, present intrinsic properties of prosumers. The second, non-generic states, present properties that could only be observed within interactions between prosumers. The first group is described separately in section 6.2. The analysis of the second group of the transients is given along with scenarios in section 6.1.

6.1. Scenarios

The following scenarios are suggested for thermohydraulic analysis:

1. Reaching targeted number of prosumers operating in production / consumption mode (Scenarios A. 1 – A. 2)
2. Unbalanced heat distribution (Scenarios B. 1 – B. 3)
3. Influence of network topology (Scenario C)

For all scenarios, the outdoor air temperature $\vartheta_o = \vartheta_{o,d} = -16$ ℃ was taken. The overview of network configuration is shown in fig. 28. Applied network topology model is radial, except for scenario C. Parameters of the model are given in appendix C.

6.1.1. Reaching targeted operating modes

Scenario A. 1 A goal of scenario A. 1 was to reach a state when two prosumers were operating in consumption mode simultaneously. In addition, prosumer 1 and prosumer 2 exchanged their roles in this scenario. Fig. 51 demonstrates a reference heat flow rate time-series for this scenario.

Heat flow rate $\dot{Q}_{net}$ with respect to the network is given in fig. 52. After transient processes faded away, a desired operating state was successfully achieved at 430 min. Generic transient states are marked in the plot and have the following designation: R – "heat transfer reversal", O – "overproduction", "C-On" and "C-Off" – onset and "fading" transient state for consumption mode, "P-On" and "C-Off" – onset and "fading" transient state for production mode. These transient states are described in section 6.2. Point *a* represents a non-generic transient state that clarified later in this scenario.

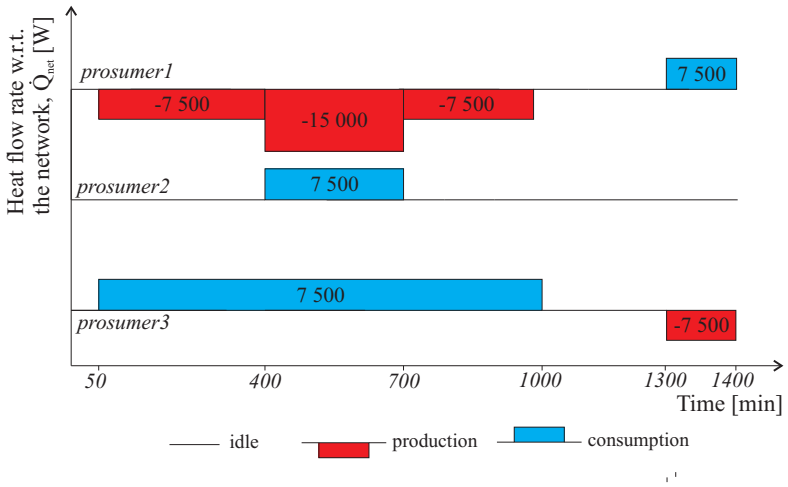

Figure 51: Scenario A. 1: the reference heat flow rate time-series

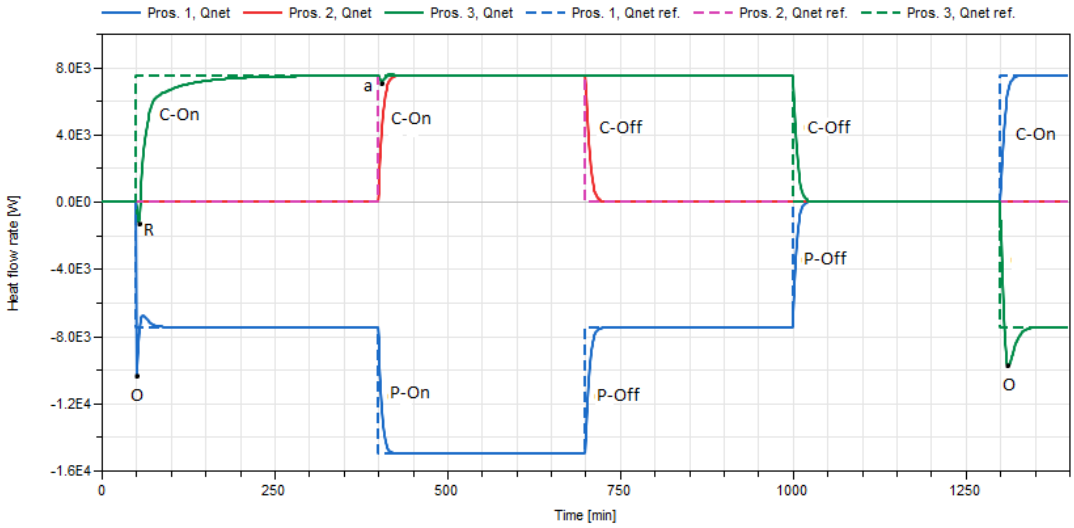

Figure 52: Scenario A. 1: heat flow rate with respect to the network

The performance of the heat network is shown in fig. 53. When prosumer 2 is switched to consumption mode at 400 min, the "heat extraction controller" started modulating a control valve. Since prosumer 3 was already in consumption mode, hydraulic conductance of the network increases. As a result, the working point of the feed-in pump at prosumer 1 shifts to the right, which can be seen by the head decrease and the mass flow increase until 700 min. Due to the thermal inertia of the heat source at prosumer 1, temperatures in the network develop slower than the flow propagation.

The non-generic transient state was observed at 400 min at prosumer 3 (see point *a* in

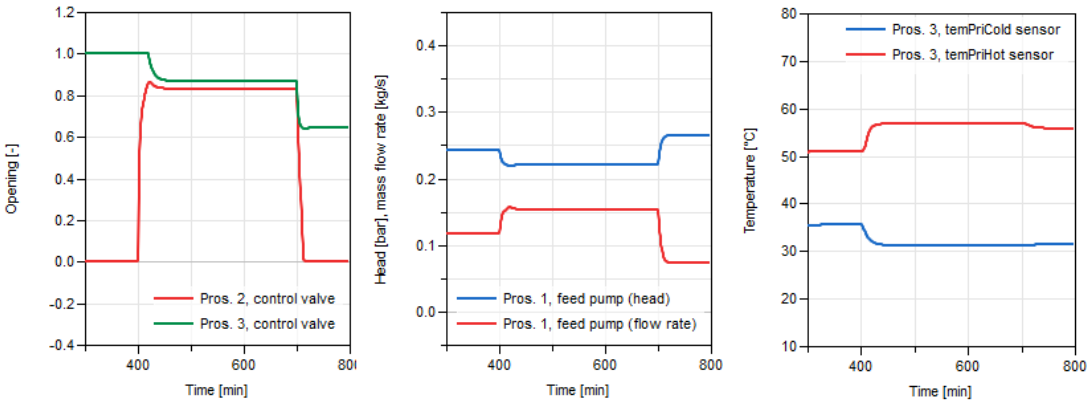

Figure 53: Scenario A. 1: control valve opening (left), performance of the feed-in pump of prosumer 1 (center), temperature in the network for prosumer 3 (right)

fig. 55). This slight drop of $\dot{Q}_{net}$ was caused by the decrease of effectiveness (ε) in the heat exchanger according to eq. (12). A new flow distribution in the network leads flow reduction at prosumer 3. At the moment when both mass flow rates at prosumer 3 are equal (point *b*), the minimum of ε is observed (point *c*). This minimum can be predicted by eqs. (13) – (16). The recovery of $\dot{Q}_{net}$ was associated with increasing temperature difference in the network.

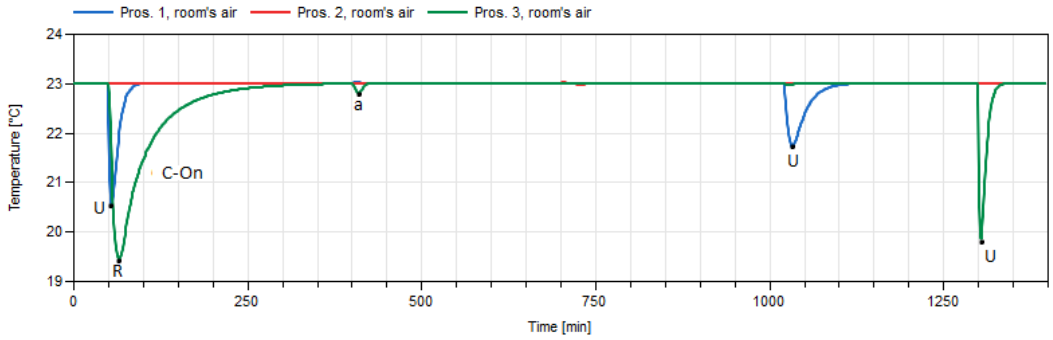

Figure 54: Scenario A. 1: room air temperature

The room air temperature of the prosumers are given in fig. 54. Generic transient states that can be observed in the figure are: U – "unbalanced mixing", "C-On" – onset state for consumption mode. The decrease of ε at the heat exchanger also had an effect on room air temperature. It is designated as *a* in fig. 54.

The difference in the results for operation starting at 50 min and 1400 min was caused by changing the state of the network from "cold" to "warm". This change is described later in section 6.2. The plot demonstrating temperatures in the network is given in fig. 56: "tem-

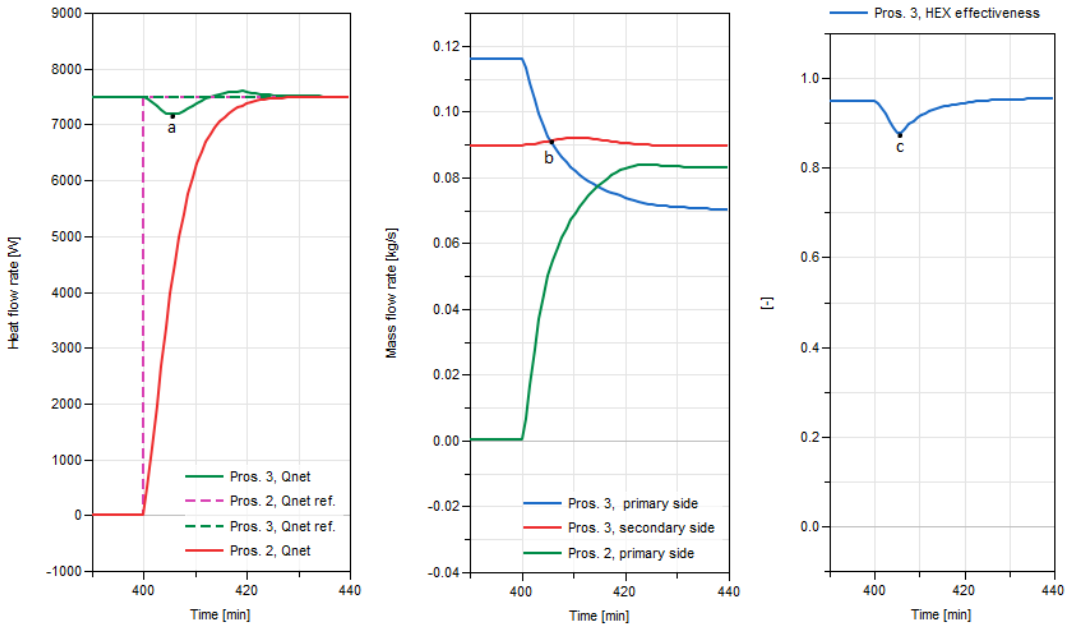

Figure 55: Scenario A. 1: heat flow rate $\dot{Q}_{net}$ (left), mass flow rates for demonstrating heat flow drop (center), effectiveness of the heat exchanger at prosumer 3 (right)

PriHot sensor" curve is the inlet temperature on the primary side, "temPriCold sensor" curve is inlet temperature on the secondary side.

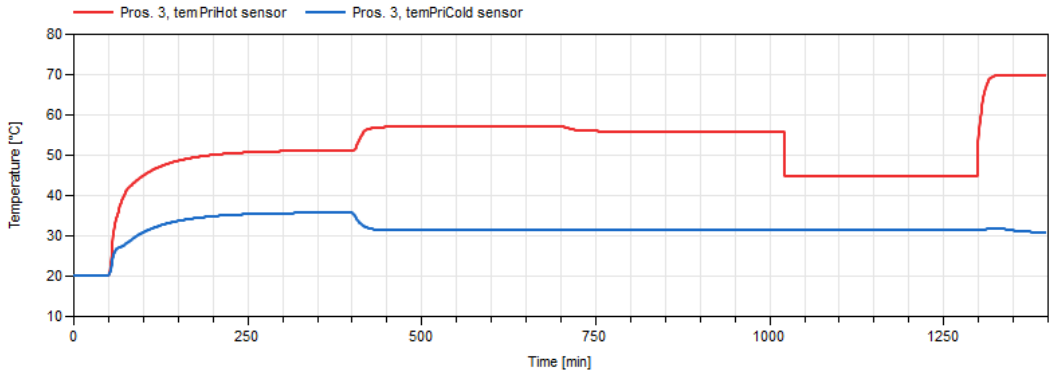

Figure 56: Scenario A. 1: water temperature in the network for prosumer 3

Scenario A. 2 This scenario was similar to A. 2 except that the goal was to reach a state when two prosumers were operating in production mode simultaneously. The reference heat flow rate is given in fig. 57.

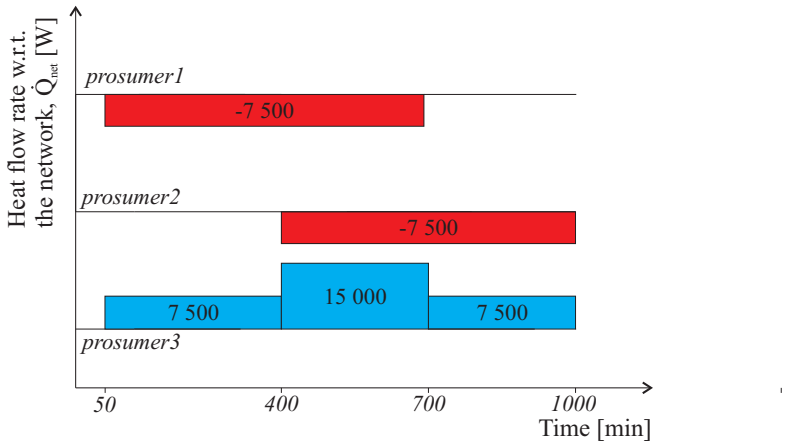

Figure 57: Scenario A. 2: the reference heat flow rate time-series

Actual heat flow rate values are given in fig. 58. The targeted state was successfully at 420 min. Generic and non-generic transient states are marked in the plot. New non-generic transient states are the "switching-on" of "suppression controller" (point *s*) and the "unleashing" of the feed-in pump (point *p*).

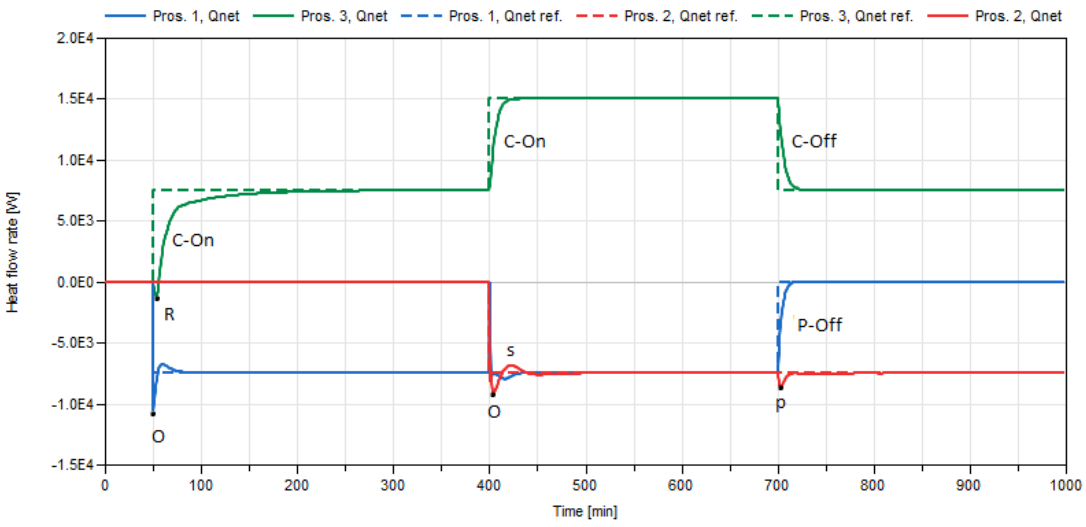

Figure 58: Scenario A. 2: heat flow rate with respect to the network

For clarifying the "switching-on" state (point *s*), a closer look on thermohydraulic performance is given in fig. 59 (below). Immediately after the second feed-in pump was turned on, the first pump undergoes blocking state (point *a*), but the "suppression controller" unblocks it. This can be observed by the drastic decrease in mass flow rate from the prosumer 2 (point

b). A consequent decline in mass flow until point *c* is explained by the partial closure of the control valve at prosumer 3 due to the temperature growth in the network (see fig. B.3).

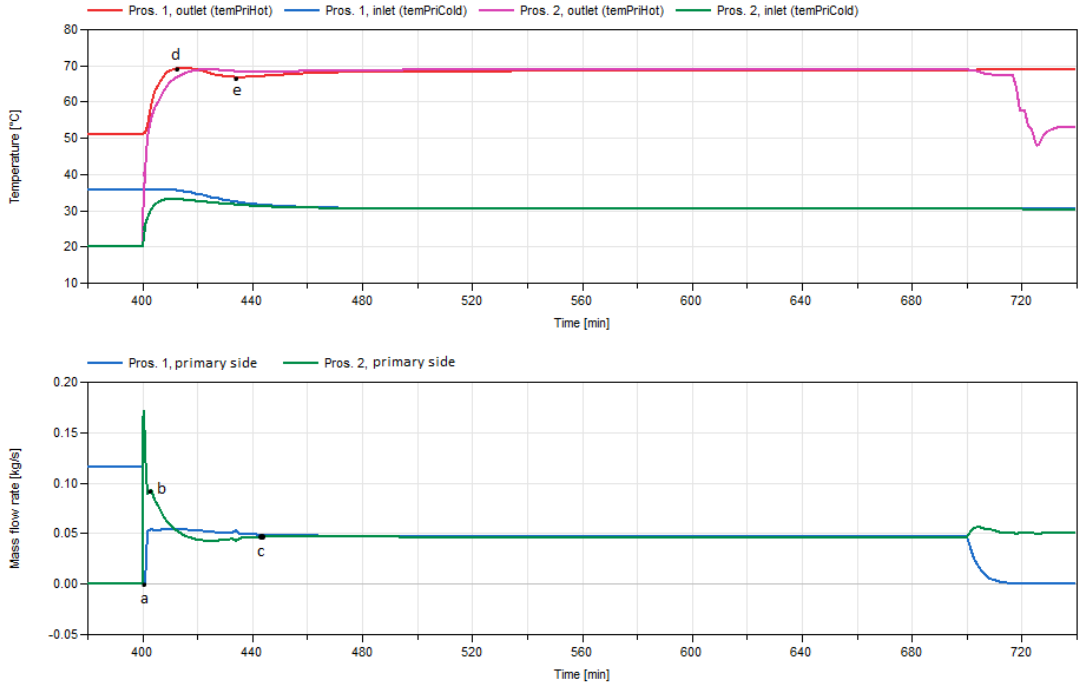

Figure 59: Scenario A. 2: temperatures in the heat network (above), mass flows at prosumer 1 and 2 (below)

The overview of the temperatures at prosumers is given in fig. 59 (above). The outlet temperature growth from prosumer 1 (point *d*) was due to the mass flow rate reduction. Here, the "suppression controller" switches to the minimal mass flow rate $\dot{m}^{pri}_{min,\,set}$. At point *e* temperature is slightly falling as a response to a moderate decrease in the minimal mass flow rate. It is going down with descending of the inlet temperature as can be seen from eq. (68).

The "unleashing" transient process (point *p* in fig. 58) was associated with exponential decrease of the minimal mass flow rate as it can be seen in fig. 60. Reduction signal from prosumer 1 allows the second feed-in pump to accelerate (point *f*), and excessive mass flow is generated, which, in turn, is the source of excessive heat flow rate through the heat exchanger.

The room air temperature of prosumers are given fig. 61. Generic transient states are marked. A temperature increase to 23.5 °C at 700 min was also caused by the "unbalanced mixing".

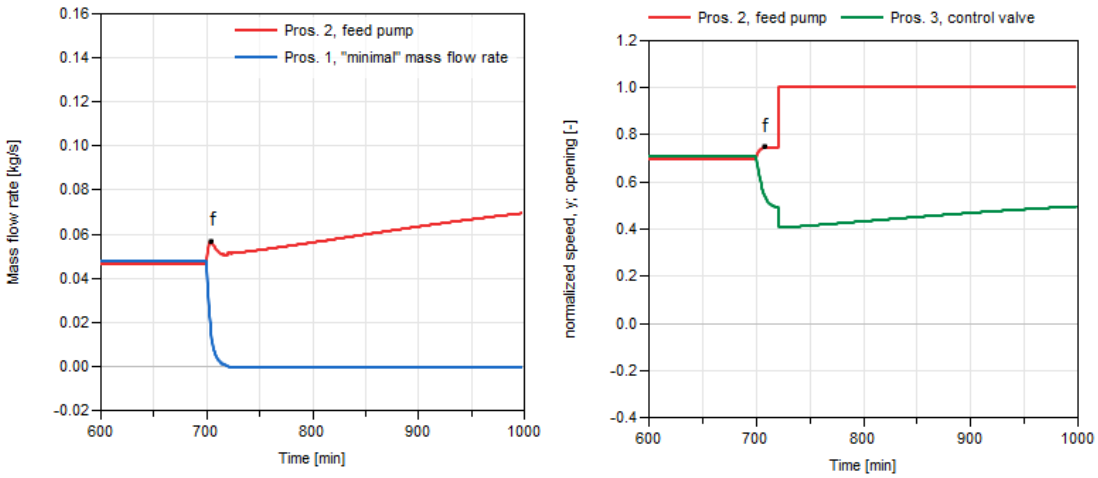

Figure 60: Scenario A. 2: flow rates for showing the "unleashing" transient state (left), normalized speed signal and control valve opening (right)

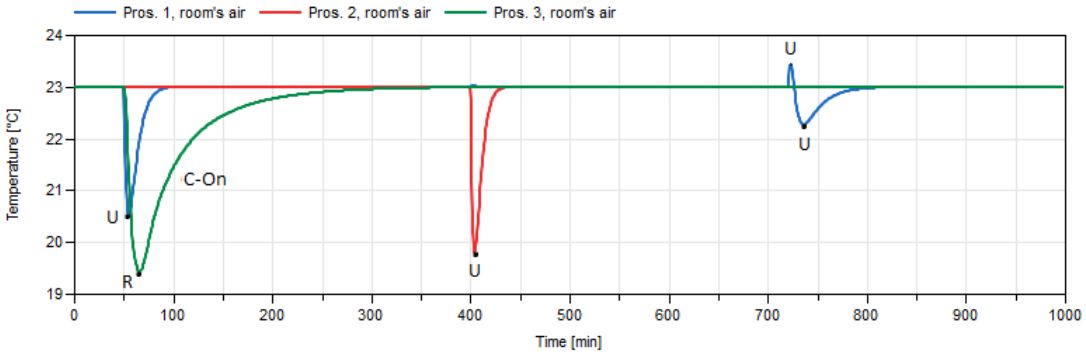

Figure 61: Scenario A. 2: room air temperature

Water temperatures and mass flows in the network are given in fig. 62. Starting from 700 min mass flow in the network gradually increases due to the valve opening. This was caused by the movement to a new thermodynamic equilibrium. As a result, temperature in the "hot" pipeline is decreasing.

In fig. 63, the pressure plot is provided for prosumer 1 . Initially, pressure in the network was static and solely determined by the boundary, *bou* (see fig. 47). Between 50 min and 400 min, the pressure difference in the network was 0.241 bar. It corresponded to 2.49 mWc generated by the feed-in pump, considering the hydraulic losses in the check valve *cheVal1*. Shut-off head of the pump is 3 mWc. At 400 min, a pressure spike (point *m*), which was higher than the shut-off head activated the "suppression controller", and it immediately equalizes the head of the second feed-in pump.

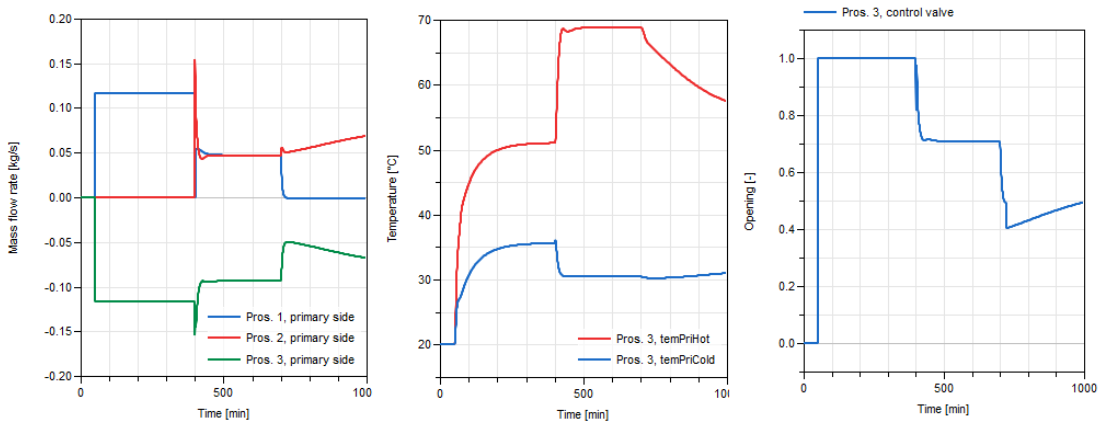

Figure 62: Scenario A. 2: mass flows (left), water temperature in the network (center), control valve opening of prosumer 3 (right)

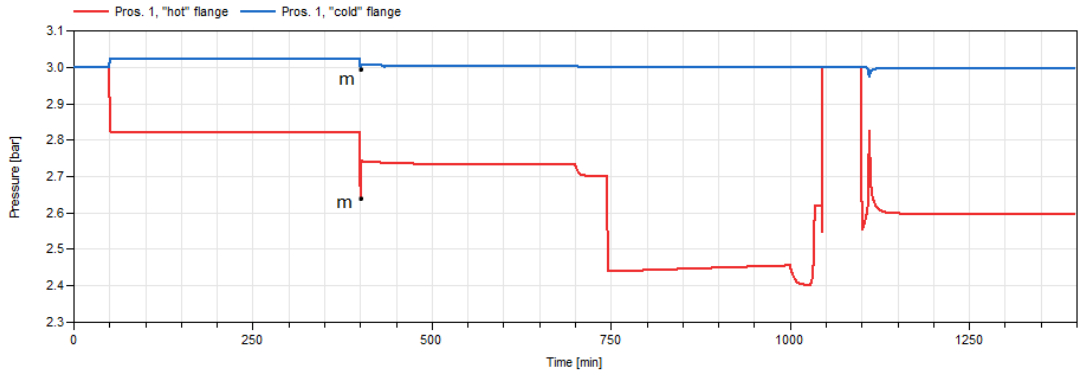

Figure 63: Scenario A. 2: pressure in the network

6.1.2. Unbalanced heat distribution

Scenarios B. 1 and B. 2 These two scenarios represented unbalanced heat flow distribution while new prosumers were being introduced to the network. The supply surpassed the demand for scenario B. 1 and vice versa for scenario B. 2. The reference heat flow rate time-series for both scenarios are shown in fig. 64.

The analysis of heat flow rate with respect to the network, $\dot{Q}_{net}$, (see fig. 65) illustrate that for the case when supply surpassed from 600 min, excessive heat flow from prosumer 2 is not transferred to the network.

However, the suggested control strategy did not embrace all aspects of an unbalanced heat distribution. The plot of mass flows in the network that is given in fig. 66 demonstrates this. As usual, the start-up of the second feed-in pump causes blocking of the first feed-

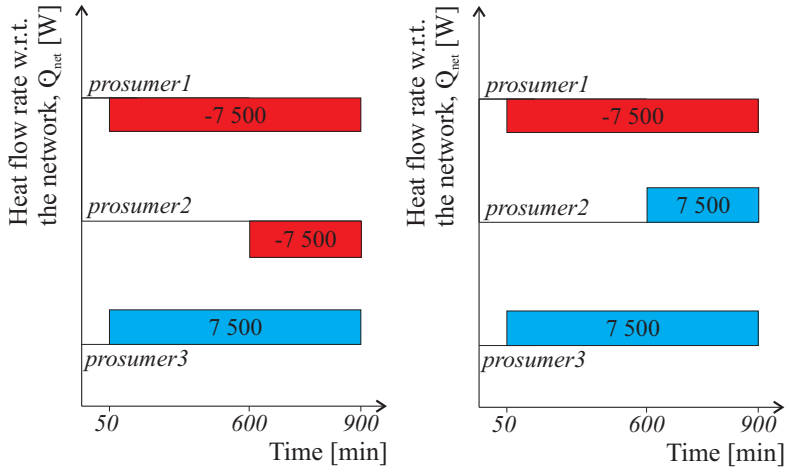

Figure 64: The reference heat flow rate time-series for scenario B. 1 (left) and scenario B. 2 (right)

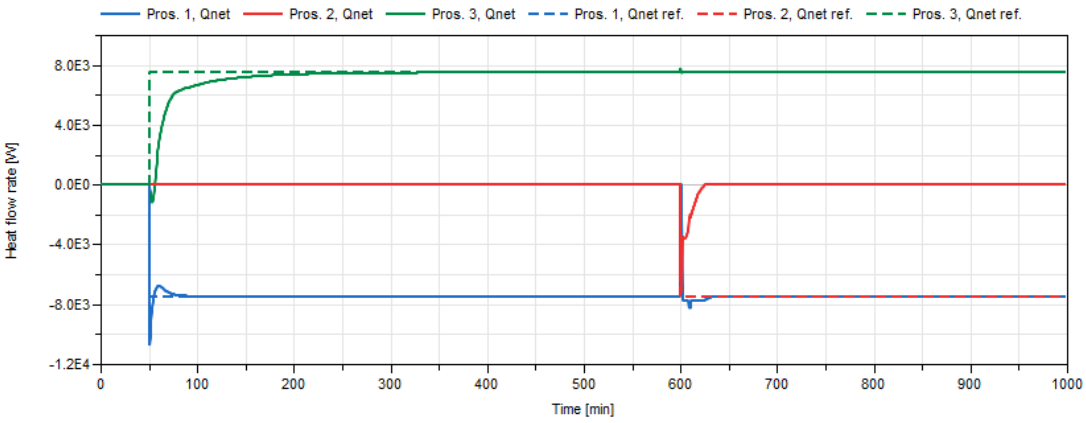

Figure 65: Scenario B. 1: heat flow rate with respect to the network

in pump (point *a*). At prosumer 1, this leads to activation of "suppression controller" that forces the feed-in pump to follow the minimal flow rate ($\dot{m}^{pri}_{min,\,set}$) by using feed-in pump at prosumer 2 as a source of back pressure. This is not correct.

In order to avoid irrational operation, the control strategy needs to be complemented. A solution could be introducing a centralized moderator (energy management) that will assign $\dot{Q}_{net}$ to every prosumer, so that prosumers will not transfer excessive heat to the network.

Heat flow rate, $\dot{Q}_{net}$, for scenario B. 2 is shown in fig. 67. After 600 min, the heat inflow from prosumer 1 is spread between the two other prosumers.

Thus, temperature in the network and in the room decreased (see fig. 68). Eventually, the system is brought to a new thermodynamic equilibrium with lower room air temperature.

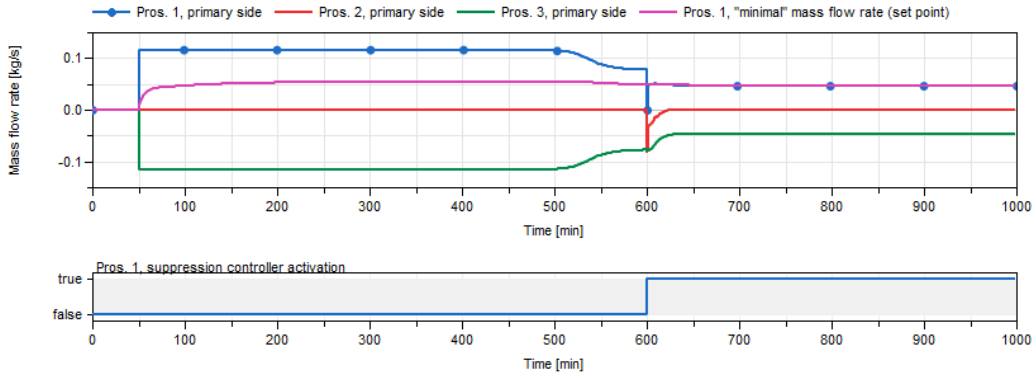

Figure 66: Scenario B. 1: mass flows in the network (above), activation status of "suppression" controller

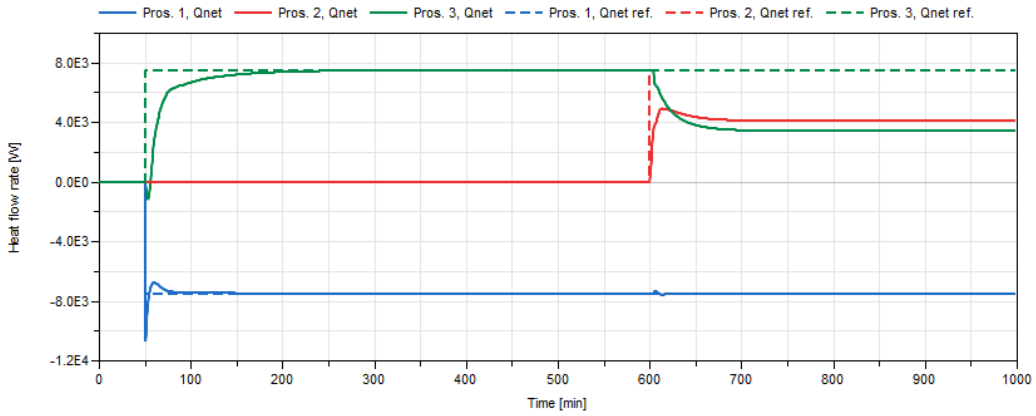

Figure 67: Scenario B. 2: heat flow rate with respect to the network

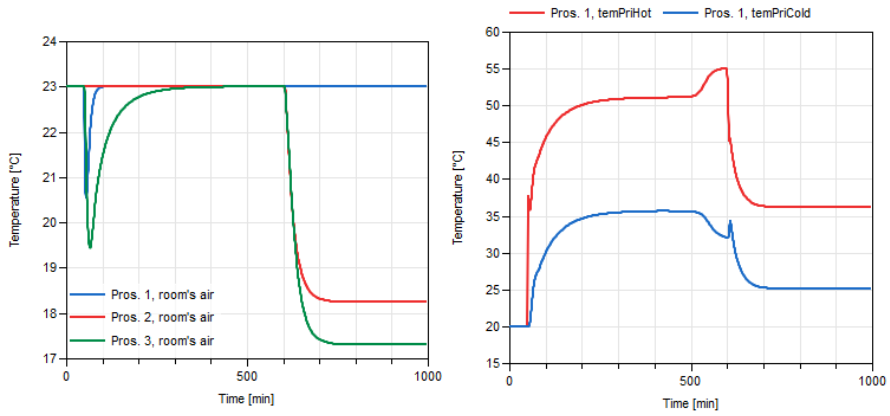

Figure 68: Scenario B. 2: room air temperature (left), water temperature in the network (right)

Scenario B. 3 Scenario B. 3 describes another case for unbalanced heat distribution when one of the prosumers started to generate a surplus of thermal power. The reference heat flow rate for this case is given in fig. 69.

Actual heat flow rates, $\dot{Q}_{net}$, that correspond to the investigated scenario are given in fig. 70. Although starting from 600 min the reference $\dot{Q}_{net,net}$ requires to inject bigger heat flow rate, the actual heat flow from prosumer 1 was limited by the demand from prosumers 2 and 3.

After 600 min, temperature difference in the network starts to increase (see fig. 71) due to a non-steady heat transfer. As well as inlet temperature on the primary side, T^{pri}_{cold}, inlet temperature at the heat source, T^{b}_{1}, is increasing. However, this growth is limited by maximum allowed temperature $T^{b}_{1,max}$ (see eq. (63)). Eventually, the network was brought to a new thermodynamic equilibrium with much bigger temperature difference in the network.

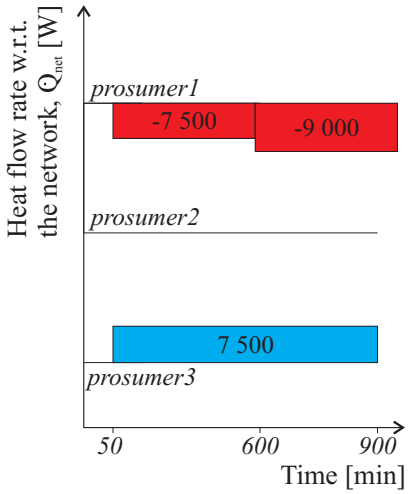

Figure 69: Scenario B. 3: heat flow rate with respect to the network

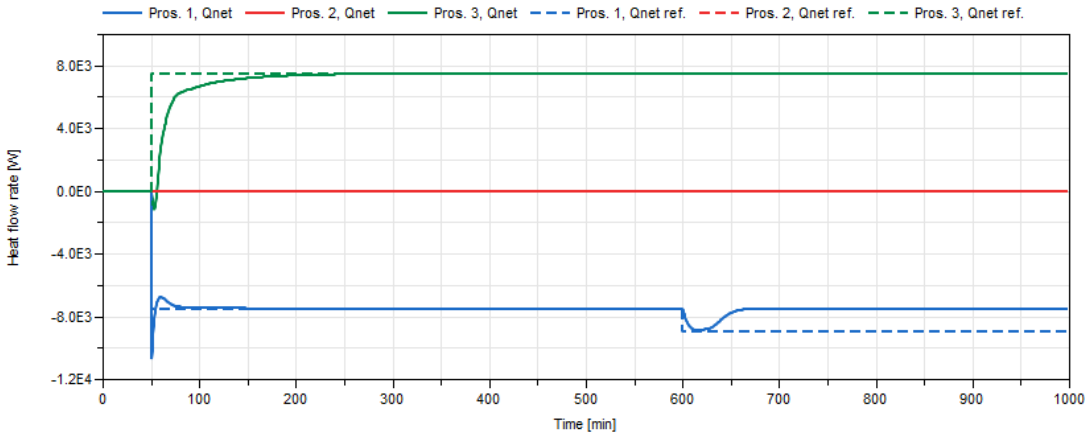

Figure 70: Scenario B. 3: heat flow rate with respect to the network

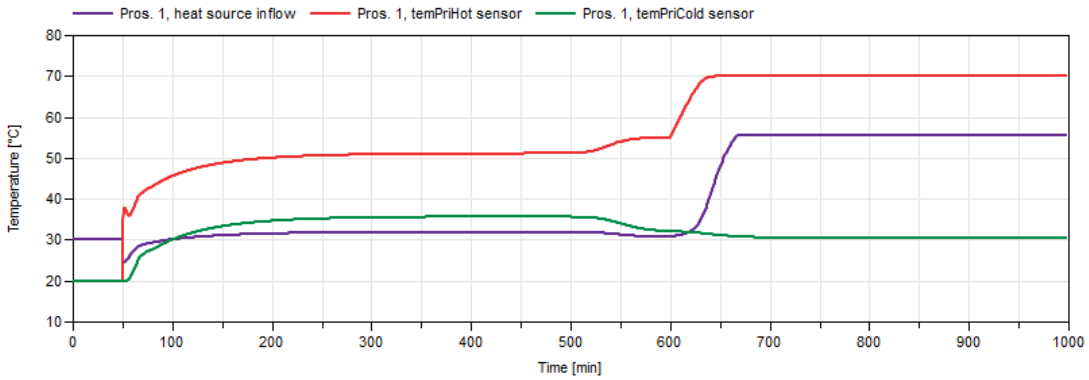

Figure 71: Scenario B. 3: temperature in the network and at the heat source of prosumer 1

6.1.3. Influence of network topology

Scenario C For scenario C, a meshed grid topology from fig. 27 was used instead of the radial one. The reference heat flow rate is the same as in scenario A.2 (see fig. 57).

Actual heat flow rates $\dot{Q}_{net}$ for this scenario are given in fig. 72. The diagram contains the same generic transient states as in scenario A.2. The only difference is that the "unleashing" transient state is not observed.

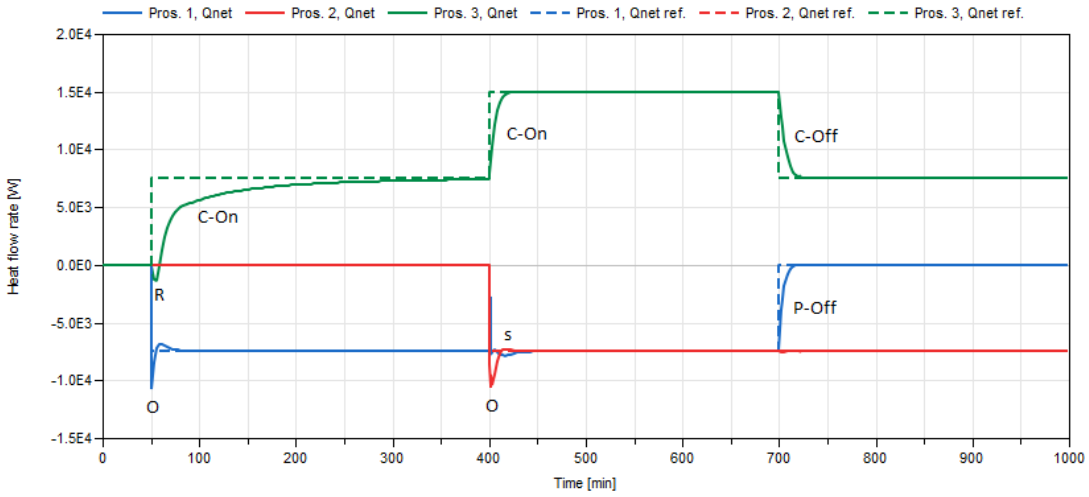

Figure 72: Scenario C: heat flow rate with respect to the network

Pressure difference in the network for a meshed grid network was less than in the radial one as can be seen in fig. 73. The meshed grid had higher hydraulic conductance due to additional pipes C1 and C2. This means that the blocking state is less likely to occur in such

a network: a pressure difference spike that caused blocking in scenario A. 2 is 0.33 bar (point *a*), but in a meshed grid, it was 0.29 bar (point *b*). Obviously, shut-off head (H_{max}) was no longer a valid parameter for "suppression controller". Therefore, the maximum allowed head for a long-lived operation of the pump was chosen.

Feed-in pump at prosumer 1 generates higher mass flow rate due to higher conductance in the network, and thus, the temperature in the network is reaching steady-state slower and with lower values as shown in fig. 73.

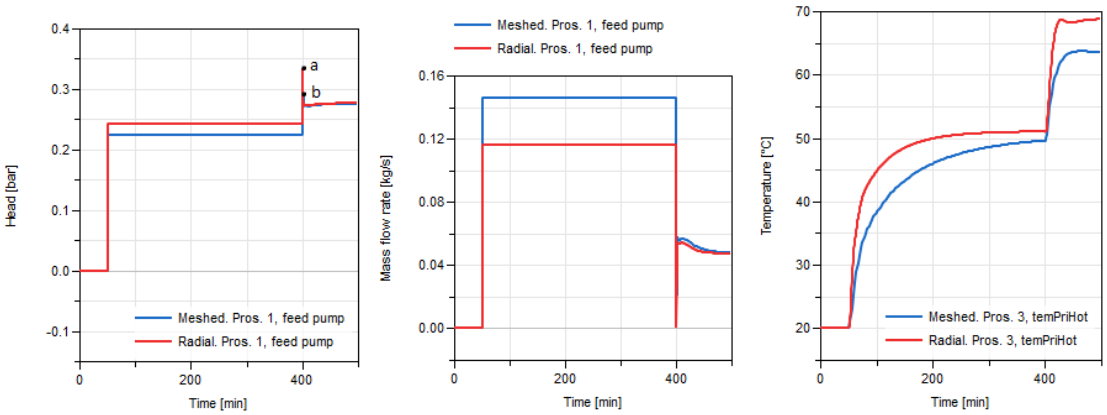

Figure 73: Scenario C: pressure difference (head) (left), mass flow rates (center), temperatures in the network (right)

Therefore, the "heat transfer reversal" (state R) in fig. 72 lasts longer than in scenario A. 2 (see fig. 74). The effect it has on the room air temperature is shown in the same plot: the temperature drops lower for the meshed grid (point *c*) for prosumer 3. Apart from this, no other changes were observed.

To conclude, the meshed grid network topology caused deeper fall with respect to the room air temperature for prosumer 3, but the error between $\dot{Q}_{net,ref}$ and $\dot{Q}_{net}$ was less for prosumer 2 due to the absence of "unleashing" transient state. Potentially, if the feed-in pump at prosumer 1 was chosen with bigger sizing, the negative effect of the meshed topology could have been avoided.

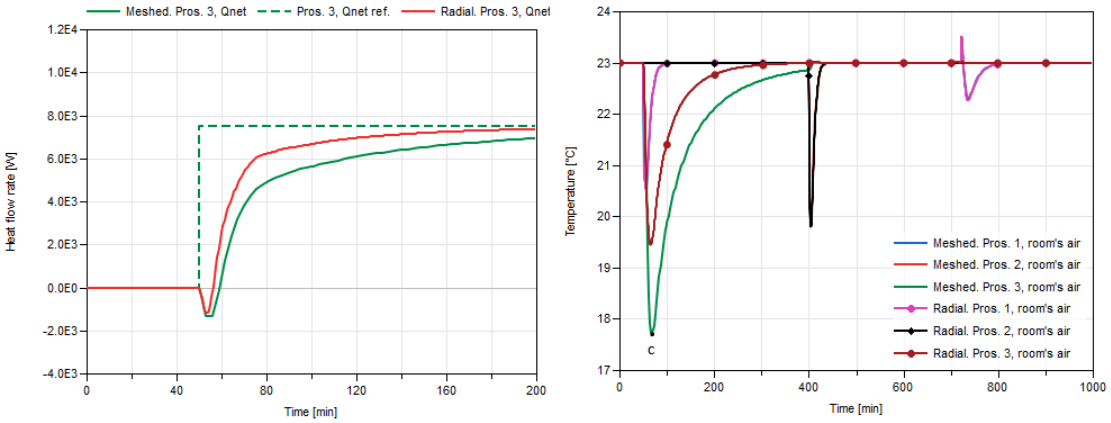

Figure 74: Scenario C: heat flow for the "heat transfer reversal" transient process (left), room air temperature (right)

6.2. Generic transient states

In subsections section 6.2.1 and section 6.2.1, transient states observed during the simulation are classified according to the underlying mode of operation. Moreover, the origin of transient states and their evaluation is provided.

6.2.1. Consumption mode

When switching from idle to consumption mode took place, observed transient states were the "heat transfer reversal" (state R) and the onset state (state C-On). The "fading" state (state C-Off) was formulated for turning from consumption to idle mode.

"Heat transfer reversal" transient state (state R) Although consumption mode was described as heat extraction from the network, heat flow reversal occurs when the network is in the "cold" state. In general, the state of the network is determined by the temperature difference between primary and secondary sides. For "cold" state, temperature on the primary side is lower than on the secondary side.

As it can be seen in fig. 75 (left), heat transfer reversal within the interval marked by point *a* and *b* at prosumer 3. The plot of corresponding inlet temperature T_{hot}^{pri} (curve "temPriHot") on the primary side and inlet temperature T_{cold}^{sec} (curve "temSecCold") on the secondary side of the heat exchanger are shows in fig. 75 (right).

Initially, the inlet temperature on the secondary side was 40 °C although there was no water flow in the *secondary side* module in appendix A. This happened because for no-

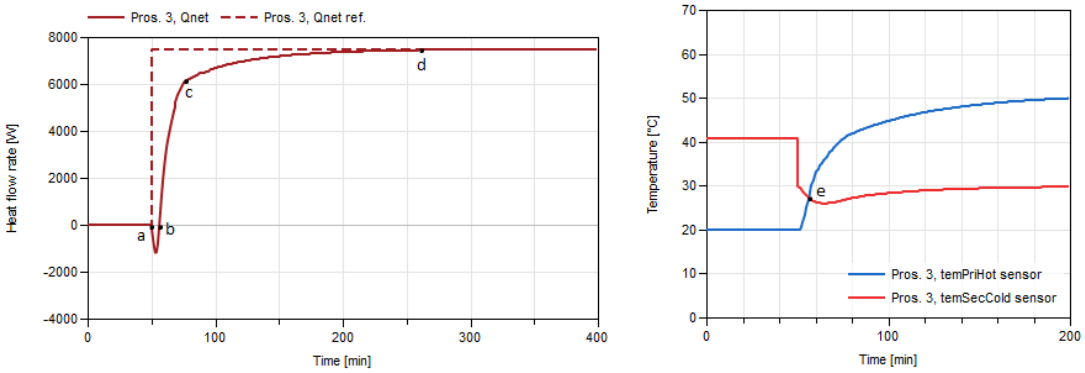

Figure 75: "Heat transfer reversal" transient state: heat flow rate with respect to the network (left), inlet temperature on primary and secondary side of the heat exchanger (right)

flow, Fluid library from Modelica takes an average temperature between two connectors at the *temSecCold* sensor in appendix A, which correspond to outlet (50 °C) and inlet (30 °C) temperature at the heat source. After consumption mode is activated at 50 min, T_{cold}^{sec} is higher than T_{hot}^{pri} during the "heat transfer reversal" until point *e*. At point *e* the heat network is brought to a "warm" state, when T_{hot}^{pri} becomes equal to T_{cold}^{sec}. Thus, after this moment the direction of heat transfer comes back to normal.

Under the assumption that the heat losses in the network were negligible, the injected heat to the network is not lost. However, sudden heat outflow from the prosumer, provokes a drastic room air temperature fall as it can be seen in fig. 76 (left).

Remarkably, after changing operating modes at 1300 min (see Scenario A. 1 in fig. 51), the "heat transfer reversal" does not occur. It can be observed by comparison of fig. 76 (right) and fig. 75 (left).

The heat network can change its state from "warm" to "cold" because of cooling caused by the heat losses during intermittent break of operation. Another opportunity is the outdoor air temperature ϑ_o decrease, which will cause increase of T_{cold}^{sec} because of the heating curve.

To conclude, "heat transfer reversal" transient state has an effect on both $\dot{Q}_{net}$ and room air temperature plots. Future work must be done to take measures to avoid the reversal of heat transfer.

Onset transient state (state "C-On") The onset state can be distinguished between the points *b* and *d* in fig. 75, and is split into "fast" (*b* ... *c*) and "slow" phases (*c* ... *d*). The heat source needs to reduce thermal power $\dot{Q}^b$ to give a way to the heat flow from the heat exchanger (see eq. (50)). Since the mass flow $\dot{m}^c$ on the secondary side is determined by

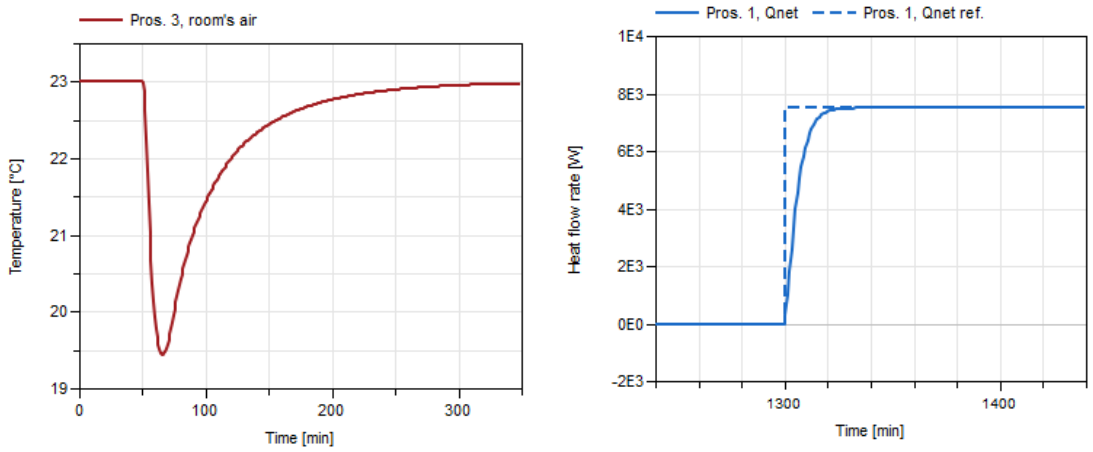

Figure 76: "Heat transfer reversal" transient state: room air temperature (left), heat flow rate with respect to the network in "warm" state (right)

the heat source (see eq. (54) and eq. (58)), the "fast" phase is caused by the thermal inertia of the source. This can be clearly seen in fig. 77: "fast" phase settles at the same time as $\dot{Q}^b$ (points *f* and *g* respectively). The reason for "slow" phase is thermal inertia of the heat network that can be expressed through the temperature plot in fig. 77.

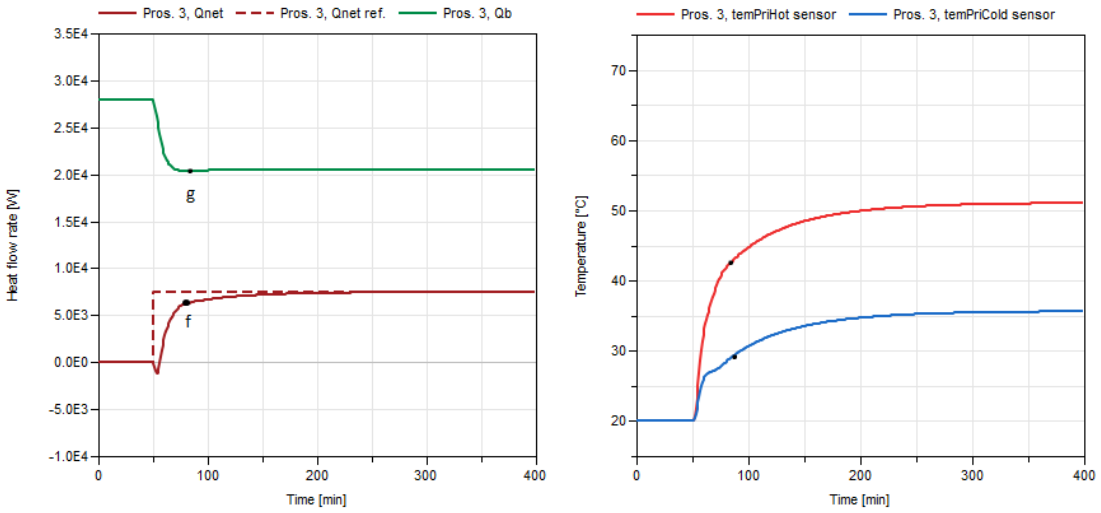

Figure 77: Onset transient state: heat flows at prosumer (left), supply and return temperatures in the network (right)

Note that when a prosumer is set to consumption mode in the "warm" state of the network, the "slow" phase is not observed (see fig. 76). Only "slow" phase of onset state has an effect

on the room air temperature plot.

To sum up, bringing the network from the "cold" to the "warm" states provoke very slow recovery of the room air temperature.

"Fading" transient state (state "C-Off") During the "fading", heat flow $\dot{Q}_{net}$ from the network is substituted with that from the heat source $\dot{Q}^b$ according to eq. (50). The shape of the "fading" curve is determined by thermal inertia of the source. It is demonstrated in fig. 78 that $\dot{Q}_{net}$ reaches steady state at the same time as $\dot{Q}^b$ (compare the points *a* and *b*).

The "fading" state of consumption mode has no effect on the room air temperature plot, and is only observed in the $\dot{Q}_{net}$ plots.

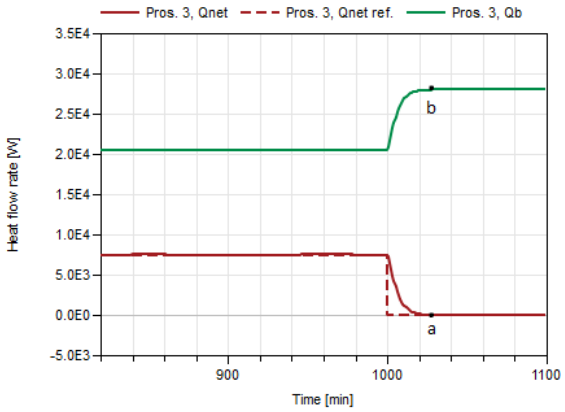

Figure 78: Off-set transient state: heat flows at prosumer

6.2.2. Production mode

For switching from idle to consumption mode and vice versa, the following transient states were identified: "unbalanced mixing" (state U), "overproduction" (state O), onset (state P-On), and off-set (state P-Off).

"Unbalanced mixing" transient state (state U) The effect of "unbalanced mixing" is expressed in the room air temperature drop when the prosumer is switched between production and idle modes, This is given in fig. 79 (above): the first point *a* is for the case of "cold" network, the second point *a'* is for "warm" network case. The "unbalanced mixing" is a transient process that stems from heating curve switching. It does not have any an effect on $\dot{Q}_{net}$ plot.

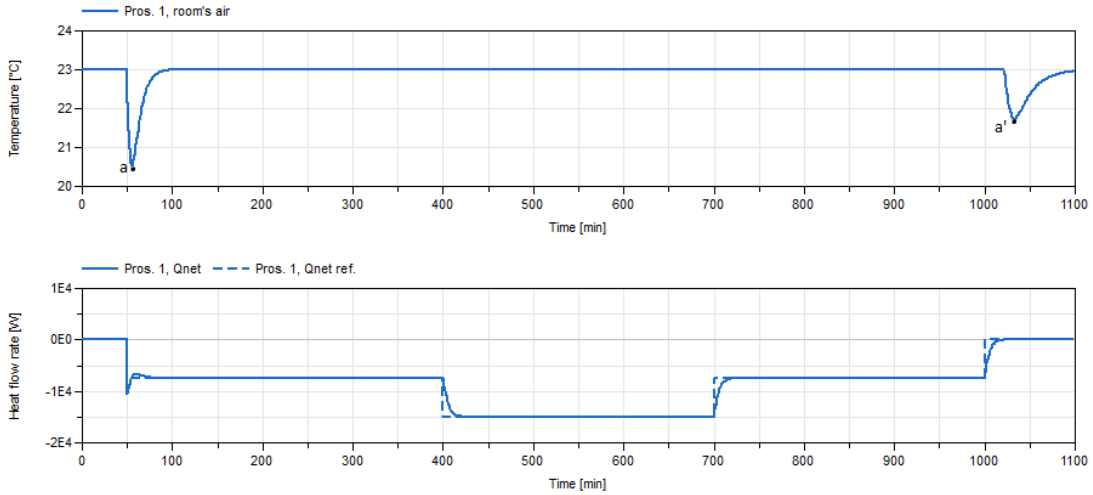

Figure 79: "Unbalanced mixing" transient state: room air temperature (above), heat flow rate with respect to the network (below)

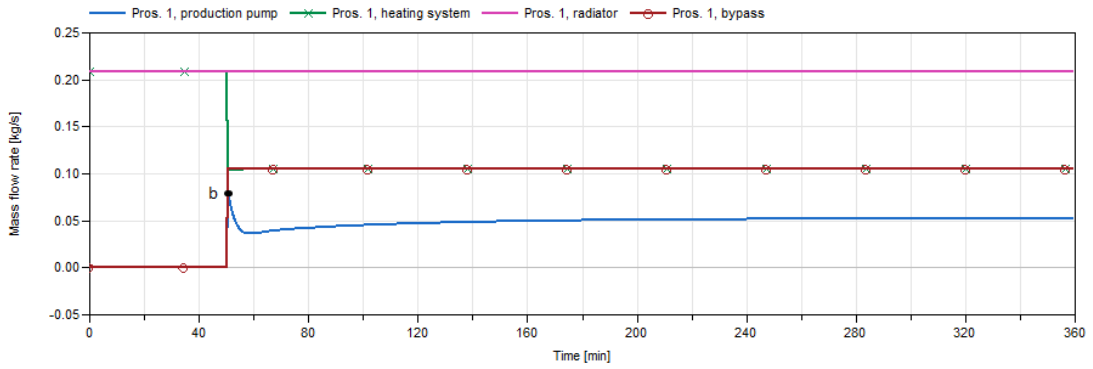

Figure 80: Switching to production mode: mass flow rates on the secondary side in appendix A

For switching from idle to production mode at 50 min (see fig. 79 (below)), mass flow $\dot{m}^p$ on the secondary side changes stepwise from zero to point *b* as it is given in fig. 80. This is due to the fact that $\dot{m}^p$ is determined by the formula eq. (57) for *contSecPumps* controller in appendix A. Mass flow $\dot{m}^{heaSys}$ through the heating system is kept constant and determined by eq. (61). As a step response, $\dot{m}^{heaSys}$ drops, and the flow $\dot{m}^{bypass}$ through the bypass is instantly activated. However, the outlet temperature T_2^b at the heat source does not catch up with this abrupt change of $\dot{m}^{bypass}$ due to the thermal inertia. Therefore, an abrupt activation of the bypass causes the "unbalanced mixing" transient state, which can be demonstrated by the decline of the inflow temperature T_1^r of the radiator in fig. 81 (above), and a subsequent

drop of the room air temperature (point *a*) in fig. 79 (above).

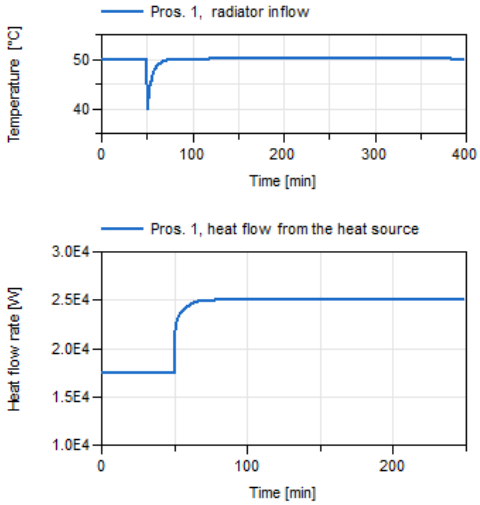

Figure 81: Temperature of inflow at the radiator (above) and heat flow rate from the heat source (below)

Eventually, when heat flow $\dot{Q}^b$ from the heat source, reaches steady state (see fig. 81 (below), T_1^r, the room air temperature comes back to the desired value.

The second drop of the room air temperature at point *a'* in fig. 79 happens 20 min later than the reference $\dot{Q}_{net,\,net}$ drops to zero. Again, the reason for this trait is thermal inertia of the heat source as it is shown in fig. 82. As a reminder, the actual condition for the mode switching was $\dot{Q}_{net} \leq 0.1$ as it can be seen in *mode definer* module in appendix A.

In order to sustain desired T_1^r, which is 50 °C during the entire transient process, "balanced mixing" must be sustained. This condition can be expressed through energy and mass balance for the inlet of the radiator (see fig. 25). Assuming that c_p is almost the same for every flow, one can write:

$$\begin{aligned} T_1^r\,\dot{m}^r &= T_2^r\,\dot{m}^{bypass} + T_1^{heaSys}\,\dot{m}^{heaSys} \\ \dot{m}^r &= \dot{m}^{bypass} + \dot{m}^{heaSys} \end{aligned} \tag{71}$$

Solving eq. (71) for $\dot{m}^{heaSys}$:

$$\dot{m}^{heaSys} = \frac{\dot{m}^r\,(T_1^r - T_2^r)}{T_1^{heaSys} - T_2^r} \tag{72}$$

By substituting parameters and input value for prosumer 1 in eq. (72), the condition for the "balanced mixing" is derived:

$$\dot{m}^{heaSys} = \frac{0.209\,(50-30)}{T_1^{heaSys} - 30} = \frac{4.18}{T_1^{heaSys} - 30}$$

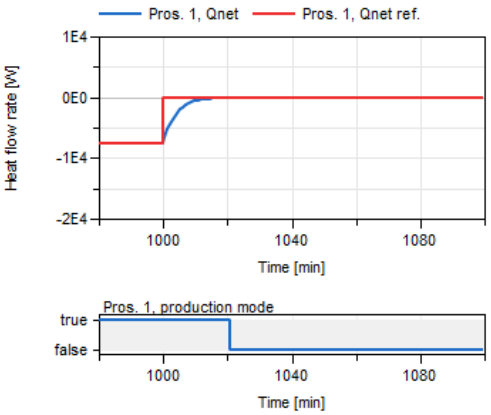

Figure 82: Demonstration of mode switching condition

Every deviation of either $\dot{m}^{heaSys}$ or T_1^{heaSys} from eq. (72) leads to overheating or cooling the room air temperature from the reference 23 °C . It can be seen in fig. 83 (above), where eq. (72) is plotted along the actual $\dot{m}^{heaSys}$. At 1025 min, the difference between the two achieves the maximum, which corre-

sponded to the minimum of T_1^r (below). Nevertheless, the temperature drop for the point *a'* is less than for the point *a*.

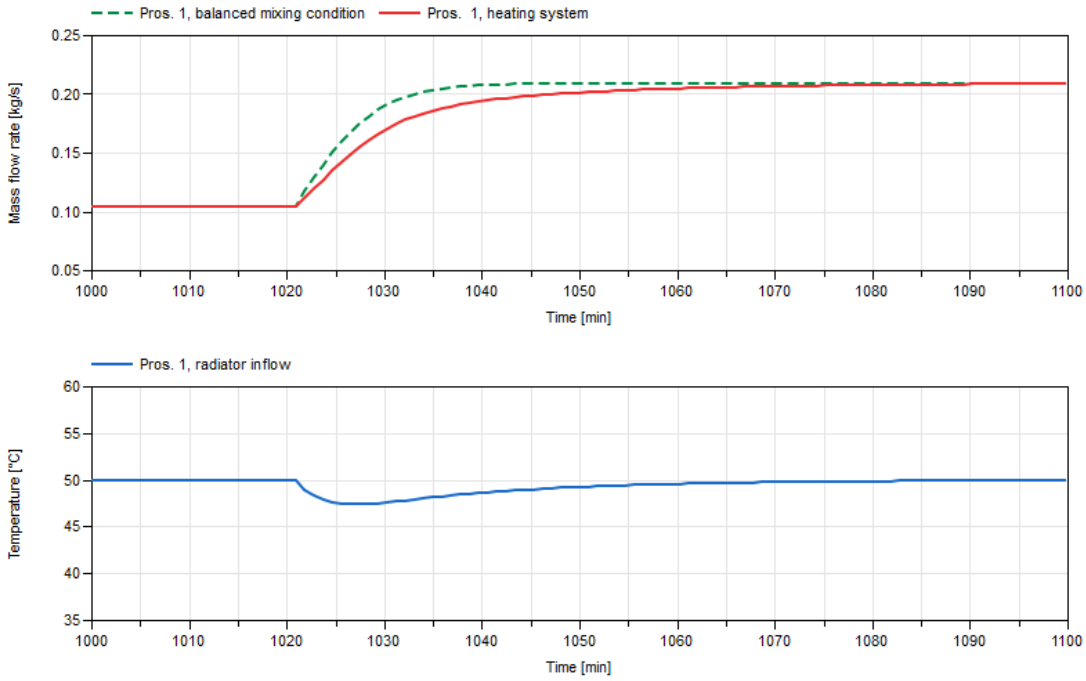

Figure 83: Switching from production to idle mode: "balanced mixing" condition and actual mass flow rate $\dot{m}^{heaSys}$ in the heating system (above), temperature of the inflow at the radiator (below)

Again, as in the case of "heat transfer reversal", "unbalanced mixing" is an undesirable effect, and must be avoided in the improved version of the considered control strategy.

"Overproduction" transient state (state O) Every start of production mode is accompanied with the "overproduction" transient state.

In the case of a "cold" network, immediately after a prosumer is brought to production mode at 50 min, $\dot{Q}_{net}$ demonstrates a rapid, spike-like decrease (point *a*) as it is given in fig. 84 (left). This decrease contradicts "inertial" development of $\dot{Q}_{net}$ explained in section 4.2.2 for $\dot{Q}_{net,ref}^{w/inert}$ in *mode definer* module.

A control valve at prosumer 3 is fully open (see fig. B.2) due to the low temperature in the network; consequently, the flow on the primary side is not limited. The feed-in pump quickly achieves nominal flow rate $\dot{m}_{nom}^f$ at prosumer 1 as it is demonstrated in fig. 84 (right). On the secondary side, mass flow, $\dot{m}^p$ changes stepwise (point *b*) due to the same reason that was already mentioned in the "unbalanced mixing". At the very beginning of the transient

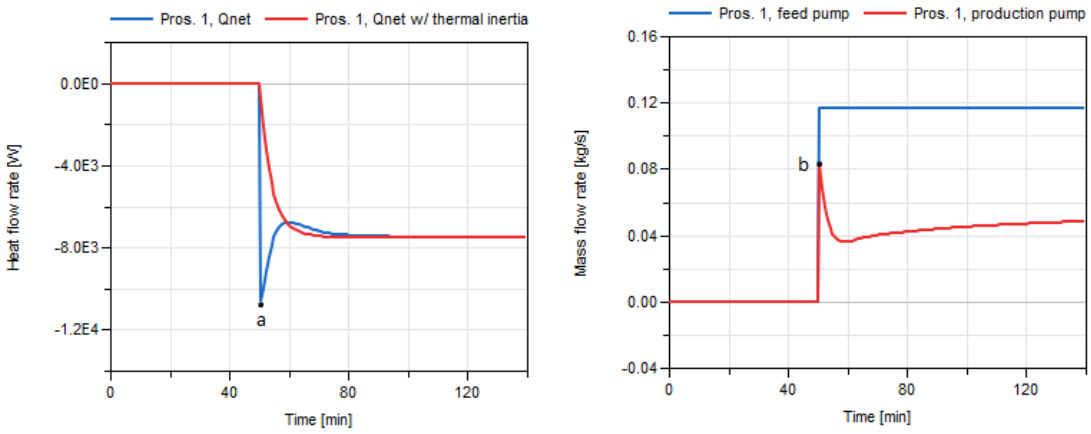

Figure 84: Switching from idle to production mode, "cold" network case: heat flow rate with respect to the network (left), mass flow rates of the pumps on both sides of the heat exchange (right)

state, an opportunity for heat transfer through the heat exchanger is created. At the same time, the "unbalanced mixing" transient state limited heat transportation to the radiator, so that the heat flow is redirected to the network:

$$\dot{Q}_{net} = \dot{Q}^b - \dot{Q}^r$$

where $\dot{Q}^r$ is the heat flow rate at the radiator.

As a result, the spike-like drop of absolute $\dot{Q}_{net}$ is caused, which can be found among heat flows at the prosumer in fig. 85 (left, point *e*).

The convex after the spike (left, point *c*) in fig. 85 was caused by the thermal inertia of the room air. It is given in the plot of inlet T_1^r and outlet T_2^r temperatures at the radiator in fig. 85 (right). The augmentation of T_2^r was different from T_1^r, which implied heat storage in the volume of air. Finally, when the room air temperature came back to the desired 23 ℃ , the steady state was reached.

The case of "hot" network is distinguished by less heat transfer availability through the heat exchanger. Thus, a spike-like decrease of $\dot{Q}_{net}$ is not observed at 1100 min in fig. 86.

The smaller heat transfer availability was caused by the activation of the control valve at prosumer 3. After switching prosumer 1 to consumption mode, the "warm" state in the network eased to normal operation when the "heat extraction controller" is required to limit the flow. As a consequence, the flow through the primary side (feed-in pump $\dot{m}^f$) does not catch up with the flow $\dot{m}^p$ on the secondary side (production pump) as shown in fig. 86 (right, compare with fig. 84). It means that the heat transfer through the heat exchanger is not yet

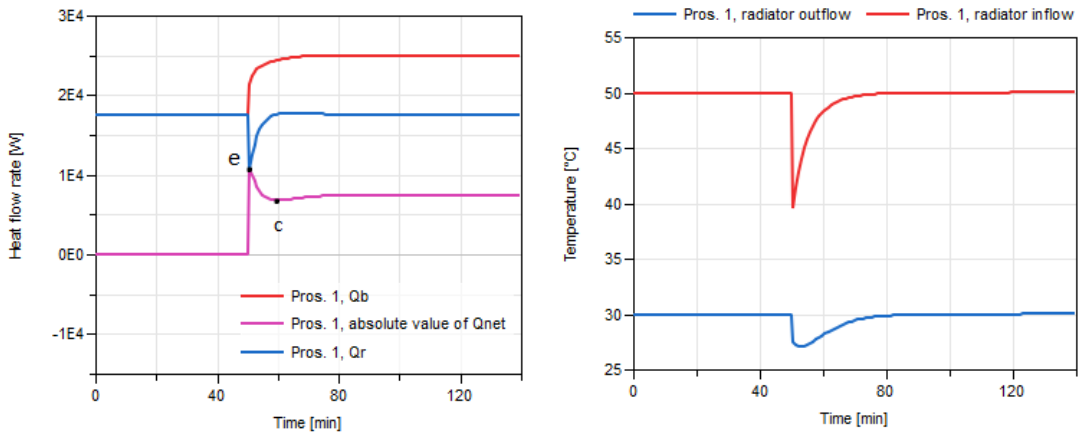

Figure 85: "Overproduction" transient state, "cold" network case: heat flows at the prosumer (left), inlet and outlet temperatures of the radiator (right)

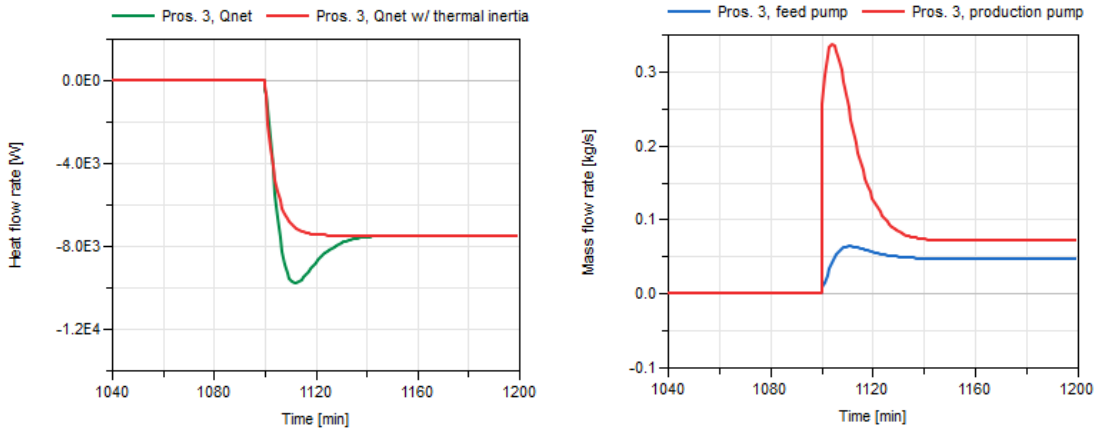

Figure 86: "Overproduction" transient state, "hot" network case: heat flow rate with respect to the network (left), mass flow rates of the pumps on both sides of the heat exchange (right)

developed at the cutting-in.

As well as for the "cold" case, the "unbalanced mixing" limits heat transportation to the radiator, but in "warm" state, heat transfer through the heat exchanger is limited too. As a result, the heat flow $\dot{Q}^b$ from the source itself drops (see fig. 87). An embedded controller at the heat source responds in a rough way to the drop of $\dot{Q}^b$, which, in turn, resulted in overshooting of mass flow through the source's pump $\dot{m}^b$ and consequently of $\dot{Q}_{net}$ (point *d*).

To sum up, this transient state has an effect only on $\dot{Q}_{net}$ plot.

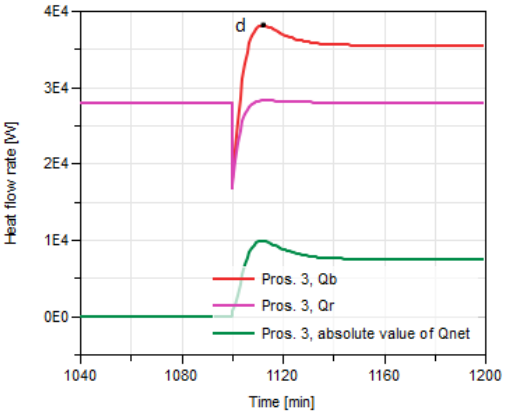

Figure 87: "Overproduction" transient state, "hot" network case: heat flows at prosumer

Onset (state "P-On") and fading transient state (state "P-Off") Onset transient state is different from "overproduction" state, which is accompanied by the every turn-on of production mode. Onset state is just a response to the thermal power increase. It has the same origin as in the case of consumption mode, namely, thermal inertia of the heat source. "Fading" transient state for production mode is analogous to that of consumption mode.

To conclude, onset and "fading" transient states of production mode find their representation in $\dot{Q}_{net}$ plots only and has no effect on the room air temperature plot.

6.3. Summary

Simulation results confirmed the capability of a developed control strategy to operate the heat network with prosumers. Moreover, a few distinctive transient states were observed and investigated. They were arranged according to their effect on prosumers.

The states that influenced the room air temperature were the following:

1. For prosumers operating in consumption mode, "heat transfer reversal" transient state caused the most significant room air temperature drop (from 23 ℃ to 18 ℃) and was associated with transition of the heat network from "cold" to "warm" state. This state also had influence on the heat transfer $\dot{Q}_{net}$ with respect to the network.
2. In every case of mode switching from idle to production mode and vice versa, the "unbalanced mixing" transient process was the origin of another room air temperature falling (from 23 ℃ to 20.5 ℃ and 21.7 ℃ respectively). This was caused by non-synchronous alternation of mass flow on the secondary side and outlet temperature at the heat source due to the thermal inertia.
3. In scenario A. 1 with two consumers as the targeted state, the room air temperature decrease to 22.8 ℃ was detected due to the altering of flow condition, which had an effect on $\dot{Q}_{net}$ as well.

The following transient states interfered heat flow rate with respect to the reference $\dot{Q}_{net}$:

1. "Overproduction" state was seen during transition from idle to production mode. It was characterised by significant and abrupt heat flow injection to the network more than the the reference. However, this state lasted for 5 min and 15 min respectively in scenario A. 1. It was caused by the undesired heat flow redistribution of prosumers due to the "unbalanced mixing".
2. Onset and "fading" transient states represented natural thermal inertia of the prosumer heat source.
3. Turning-on of the "suppression" controller caused a slight swinging of $\dot{Q}_{net}$ around the reference, which was the consequence of blocked – unblocked sequence at prosumer 1 and the actuator (control valve) modulating at prosumer 3 in scenario A. 2.
4. A certain excessive mass flow rate was generated during the "unleashing" state of a feed-in pump due to a rapid decline of reduction signal from prosumer 1 in scenario A. 2.

Unbalanced heat flow distribution scenarios B. 1 – B. 3 revealed important insights on the control strategy operation. When the supply surpassed the demand for new prosumers in the network, the mismatch of $\dot{Q}_{net}$ caused false activation of the "suppression controller" that utilized the second feed-in pump in the network as a source of back pressure to maintain a "minimal flow" rate at the first feed-in pump. For gradual unbalanced increase of heat injection from one of the prosumers in production mode, the consequence was different: the growth of $\dot{Q}_{net}$ was limited by the current demand, and the network came back to the balanced state. For the case when demand is higher than supply, temperature in the network decreased, and the system came to the new thermodynamic state with the lower room air temperature at the demand side.

The meshed grid network in scenario C had lower pressure losses than the radial one. As a result, the mass flow rates were higher, and the temperatures in the network were lower. Although the meshed grid alleviated the "unleashing" transient state, room air temperature dropped to 17.8 ℃ due to the "heat transfer reversal". This drop was deeper than in the radial grid scenarios.

7. Conclusion

To begin with, the role of a district heating system was evaluated in the view of transition towards renewable energy. Nowadays, it is estimated that fossil fuels account for 66 % of energy production for heating purpose in the EU. One of the measures taken for decarbonisation could be an expansion of district heating networks that would connect local renewable and waste heat sources with consumers in cities. The idea of the heating network expansion can be implemented with existing state-of-the-art technology. However, there is an opportunity to further integrate local heat sources with so-called "prosumers". A prosumer is a customer that can both produce and consume heat with respect to the heat network. A building with a heat source, for instance a solar collector, could be a prosumer. The prosumer concept imposed new challenges on the customers' heating system and the heat network operation.

As a basis for the research, a scheme and the characteristics of the experimental set-up for prosumers at Combined Smart Energy Systems (CoSES) center at the Technical University of Munich were used. The experimental set-up was designed for bidirectional energy and non-directional medium flow. The heat transfer with respect to the network took place with the help of the heat exchanger, which separated heat network from the prosumer.

A preliminary analysis of operational modes of prosumers in the heat network focused on both energy and medium flow conditions. It was examined that the exergy losses in the heat exchanger limited the heat flow, and certain pressure conditions caused a flow blocking state for prosumers.

The scientific method was presented by computer simulation done in Modelica language in Dassault Systèmes Dymola software. Firstly, a general prosumer model was developed. This model combined a heat source and heating load. The reference heat flow rate with respect to the network was equal to the difference between heat flow rate of the source and the load. A distinctive feature of the model was the ability to present room's air temperature. Secondly, appropriate control mechanisms were modelled as a response to the problems identified in the preliminary analysis.

A control mechanism that targeted the exergy losses was heating curve switching. It essentially utilized a heating curve with higher supply temperature to compensate the exergy losses in production mode. For solving the flow blocking problem, three control mechanisms were proposed. Eventually, all proposed control mechanisms were validated. By evaluating the performance of the flow controllers, one of them, namely the "suppression controller", was accepted as a part of the concluding control strategy. The "suppression controller" was activated in case of the blocking state. The controller then suppressed shaft velocity of the

feed-in pump that was causing the blocking. By means of the velocity reduction signal, it released prosumers from the blocking state.

The major results were received when scenarios were applied to the heat network with three prosumers driven by the concluding control strategy. Those scenarios aimed to demonstrate sequence of alternating modes of operation, unbalanced heat distribution, and the influence of the network topology (meshed and radial).

The simulation results allowed to analyse thermohydraulic states of the prosumer-based heat network and determine crucial transient processes during mode activation and operation. The goal of the control strategy was met: the actual heat flow rate with respect to the network followed the reference one for a steady state. Transient states had an effect on both room temperature and error between the reference heat flow rate and the actual one. Unbalanced heat distribution scenarios caused a false activation of "suppression controller", which, in turn, caused utilizing one of the other pumps as a source of back-pressure. When demand surpassed supply, the heat flow in the network was restricted by the current value of the load. Finally, the meshed grid scenario was characterized by higher mass flow rates, and consequently, lower temperatures in the network. This had a negative effect on room air temperature during one of the transient states.

To sum up, the capability of a developed control strategy in response to the challenges was confirmed. However, the analysis of the transient states revealed that the control strategy needs to be improved to avoid the decrease in room air temperature.

8. Outlook

For prosumers operating in consumption mode, measures must be developed to avoid or lessen the "heat transfer reversal" transient state, which caused the most significant room air temperature drop. To avoid this state the network should be brought from the "cold" to "warm" state before turning on consumption mode. To compensate the "unbalanced mixing" transient state, it is required synchronizing mass flow change on the secondary side with the thermal inertia of the heat source.

In addition, the influence of the heat losses should be investigated, and domestic hot water (DHW) load could be added.

Finally, the simulation results could be tested in the experimental set-up.

List of Figures

List of Tables

Nomenclature of Variables

Variable	Description	Unit
$\dot{Q}$	Heat flow rate	$[W]$
U	Internal energy	$[J]$
u	Specific internal energy	$[J/kg]$
Ex	Exergy flow rate	$[W]$
h	Specific enthalpy	$[J/kg]$
T	Water temperature	$[°C]$
ϑ	Air temperature	$[°C]$
$\dot{m}$	Mass flow rate	$[kg/s]$
$\dot{V}$	Volume flow rate	$[m^3/s]$
V	Volume	$[m^3]$
v	Velocity	$[m/s]$
p	Pressure	$[Pa]$
H	Head	$[mWc]$
n	Rotational speed	$[rpm]$
P	Electric power	$[W]$
$\dot{W}_{flow}$	Flow power	$[W]$
h	Overall heat transfer coefficient	$[W/(m^2K)]$
α	Convection heat transfer coefficient	$[W/(m^2K)]$
C	Heat capacity rate	$[W/K]$
A	Heat transfer area	$[m^2]$
G	Thermal conductance	$[W/°C]$
Δx	Heat surface wall thickness	$[m]$
l	Length	$[m]$
S	Circumference	$[m]$
d	Diameter	$[m]$
K_{vs}	Flow coefficient of a valve	$[m^3/h]$
ϵ	Absolute roughness	$[m]$
ρ	Density	$[kg/m^3]$
c_p	Specific heat capacity	$[J/(K\,kg)]$
μ	Kinematic viscosity	$[m^2/s]$
g	Gravity	$[m/s^2]$

References

[1] Javier Bonilla, Alberto de la Calle, Margarita M Rodríguez-García, Lidia Roca, and Loreto Valenzuela. Study on shell-and-tube heat exchanger models with different degree of complexity for process simulation and control design. *Applied Thermal Engineering*, 124:1425–1440, 2017.

[2] Lisa Brand, Alexandra Calvén, Jessica Englund, Henrik Landersjö, and Patrick Lauenburg. Smart district heating networks–a simulation study of prosumers' impact on technical parameters in distribution networks. *Applied Energy*, 129:39–48, 2014.

[3] Simone Buffa, Marco Cozzini, Matteo D'Antoni, Marco Baratieri, and Roberto Fedrizzi. 5th generation district heating and cooling systems: A review of existing cases in europe. *Renewable and Sustainable Energy Reviews*, 104:504–522, 2019.

[4] Michael Chertkov and Nikolai N Novitsky. Thermal transients in district heating systems. *Energy*, 184:22–33, 2019.

[5] David Connolly, Henrik Lund, Brian Vad Mathiesen, Sven Werner, Bernd Möller, Urban Persson, Thomas Boermans, Daniel Trier, Poul Alberg Østergaard, and Steffen Nielsen. Heat roadmap europe: Combining district heating with heat savings to decarbonise the eu energy system. *Energy policy*, 65:475–489, 2014.

[6] M Decker, L Vasakova, et al. Energy roadmap 2050. impact assessment and scenario analysis. *European Commission, Energy, unit A1 Energy policy and analysis*, 2011.

[7] Tobias Fleiter, Rainer Elsland, Matthias Rehfeldt, Jan Steinbach, Ulrich Reiter, Giacomo Catenazzi, Martin Jakob, C Rutten, R Harmsen, F Dittmann, et al. Profile of heating and cooling demand in 2015. *Heat Roadmap Europe Deliverable*, 3(1), 2017.

[8] Peter Fritzson. *Principles of object-oriented modeling and simulation with Modelica 2.1*. John Wiley & Sons, 2010.

[9] Martin Heymann, Karin Rühling, and Clemens Felsmann. Integration of solar thermal systems into district heating–dh system simulation. *Energy Procedia*, 116:394–402, 2017.

[10] Hanne Kauko, Karoline Husevåg Kvalsvik, Daniel Rohde, Natasa Nord, and Åmund Utne. Dynamic modeling of local district heating grids with prosumers: A case study for norway. *Energy*, 151:261–271, 2018.

[11] MM Koceva, T Brandmüller, I Lupu, Å Önnerfors, L Corselli-Nordblad, C Coyette, and P Wolff. Urban europe: statistics on cities, towns and suburbs (2016 edition). *Luxembourg: Publications Office of the European Union*, 2016.

[12] Wetter Michael. Simulation model air to air plate heat exchanger. *Energy*, 13(32):49–54, 1998.

[13] Alfonso Urquía Moraleda and Carla Martín Villalba. *Modeling and simulation in engineering using Modelica*. Universidad Nacional de Educación a Distancia, 2018.

[14] Damian Piotr Muniak. Regulation fixtures in hydronic heating installations: Types, structures, characteristics and applications. 187, 2018.

[15] S Paulick, C Schroth, S Guddusch, and K Rühling. Resulting effects on decentralized feed-in into district heating networks–a simulation study. *Energy Procedia*, 149:49–58, 2018.

[16] Urban Persson, Bernd Möller, and Sven Werner. Heat roadmap europe: Identifying strategic heat synergy regions. *Energy Policy*, 74:663–681, 2014.

[17] Toni Rosemann, Jan Löser, and Karin Rühling. A new dh control algorithm for a combined supply and feed-in substation and testing through hardware-in-the-loop. *Energy Procedia*, 116:416–425, 2017.

[18] E Ya Sokolov. Teplofikatsiya i teplovye seti. *District heating and heat networks]. Moscow, MEI Publ*, 2001.

[19] Thermohydraulic modelling of decentral, bidirectional district heating networks: presentation. Technical Univeristy of Munich, 2019.

[20] Michael Wetter and Jianjun Hu. Quayside energy system analysis. *Energy Technologies Area*, 2019.

[21] Jie Yang, Anthony Jacobi, and Wei Liu. Heat transfer correlations for single-phase flow in plate heat exchangers based on experimental data. *Applied Thermal Engineering*, 113:1547–1557, 2017.

A. Prosumer Model

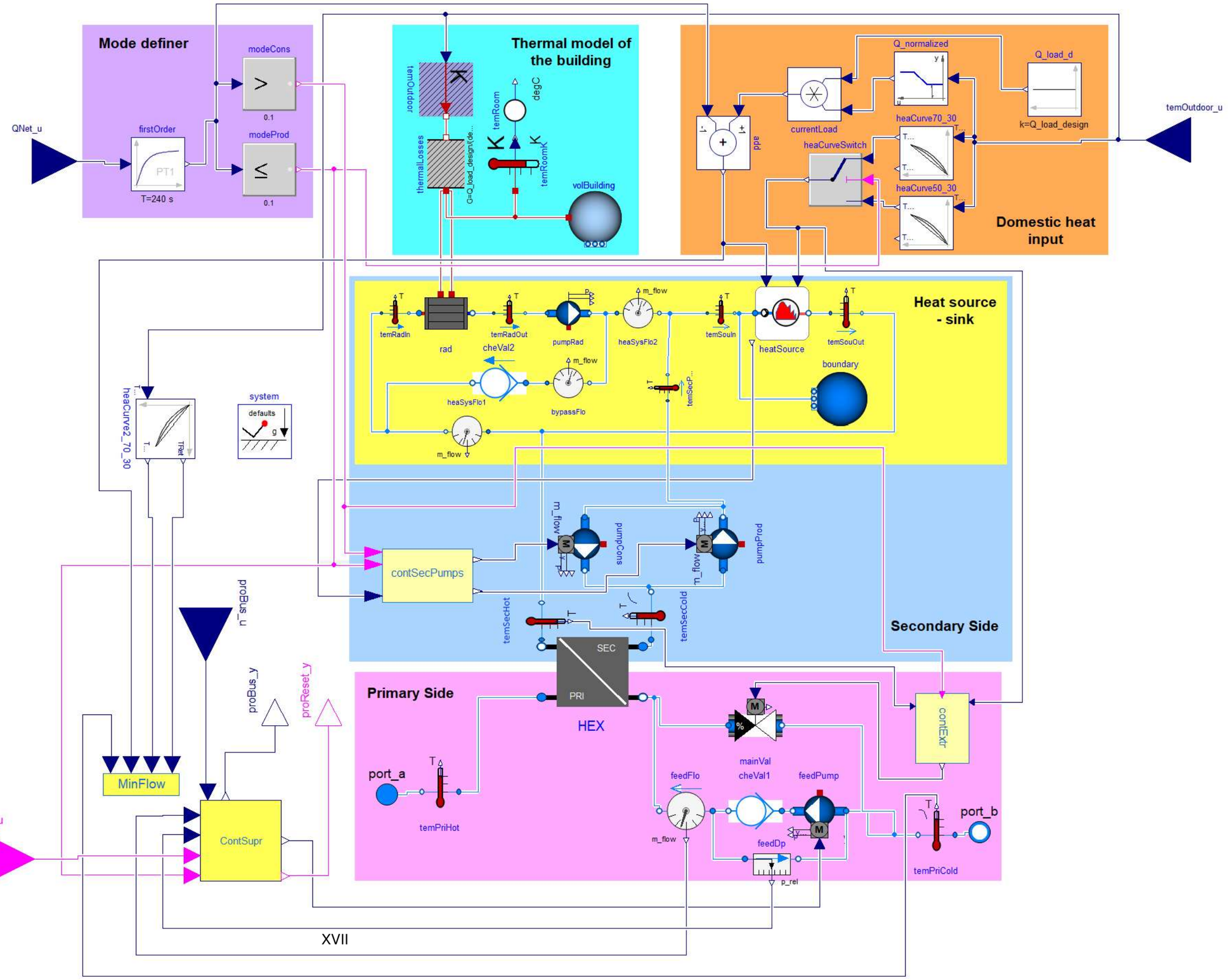

B. Supplementary Modelling and Simulation Results

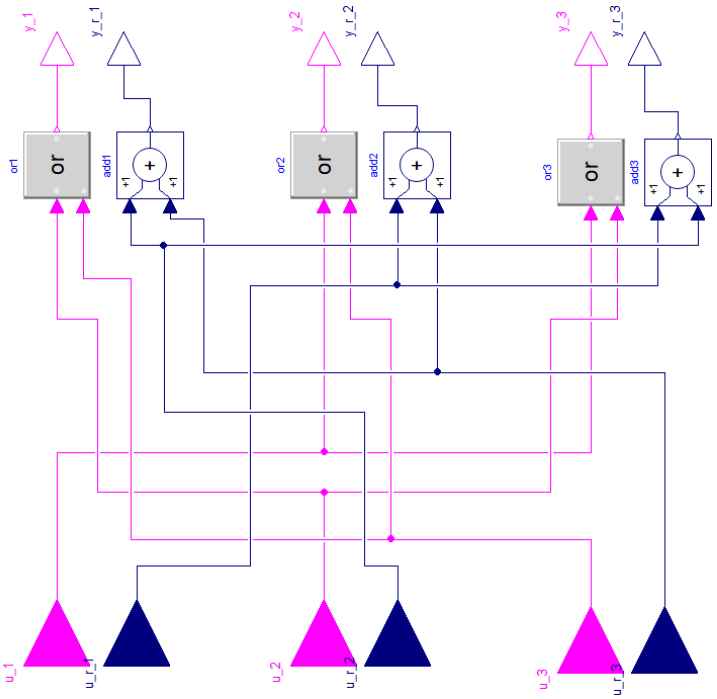

Figure B.1: Commutator block for "suppression controller"

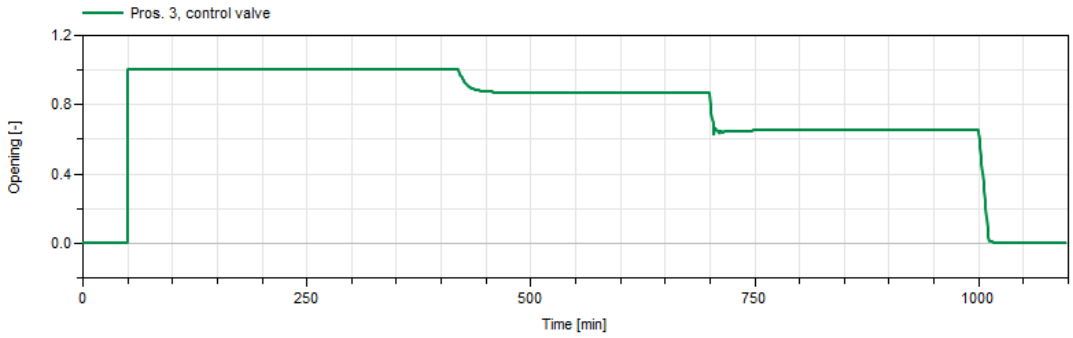

Figure B.2: Control valve opening at prosumer 3 for "overproduction" transient state

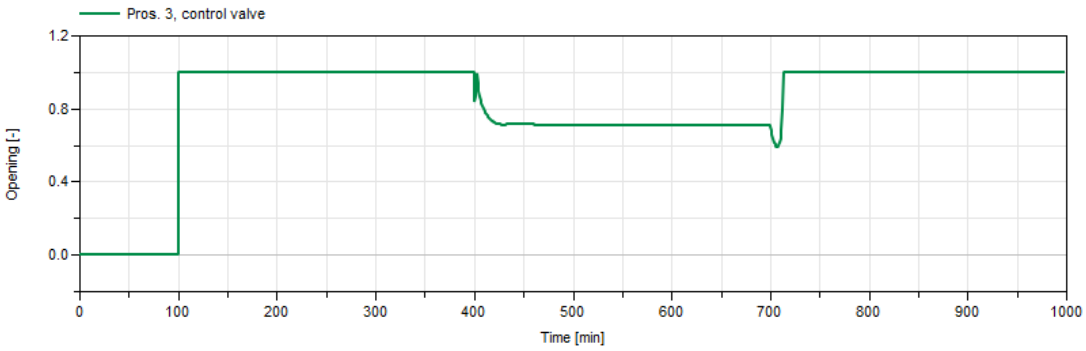

Figure B.3: Control valve opening at prosumer 3 for scenario A. 2

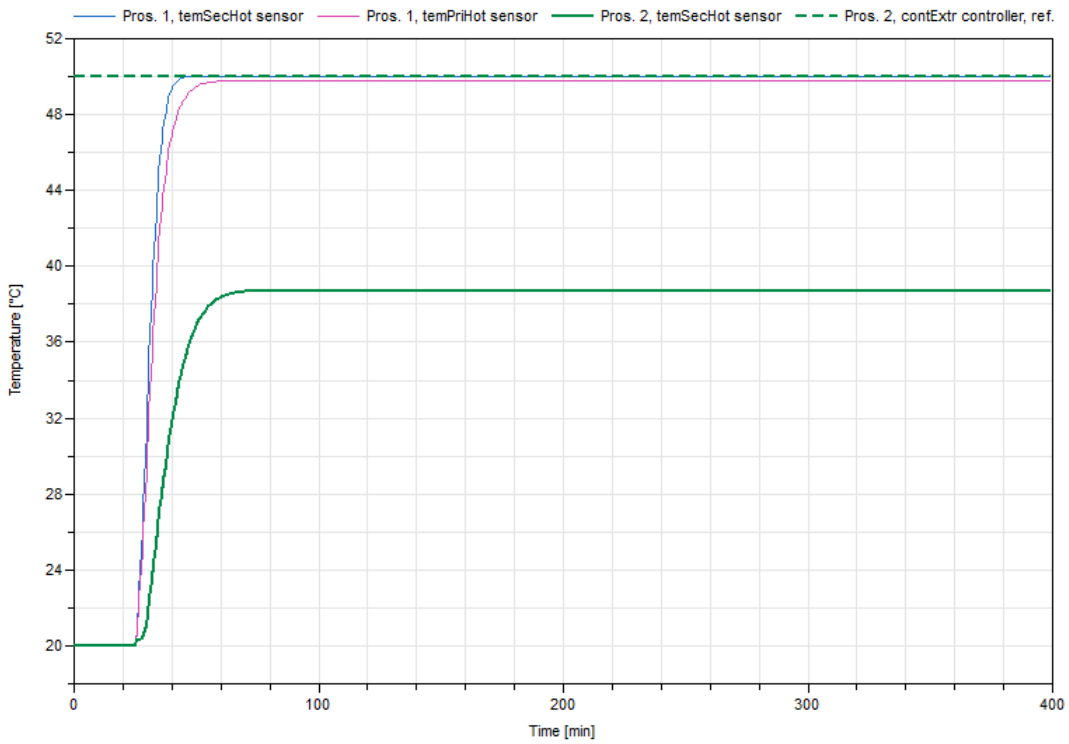

Figure B.4: Temperatures plot on secondary and primary sides of prosumers without heating curve switching

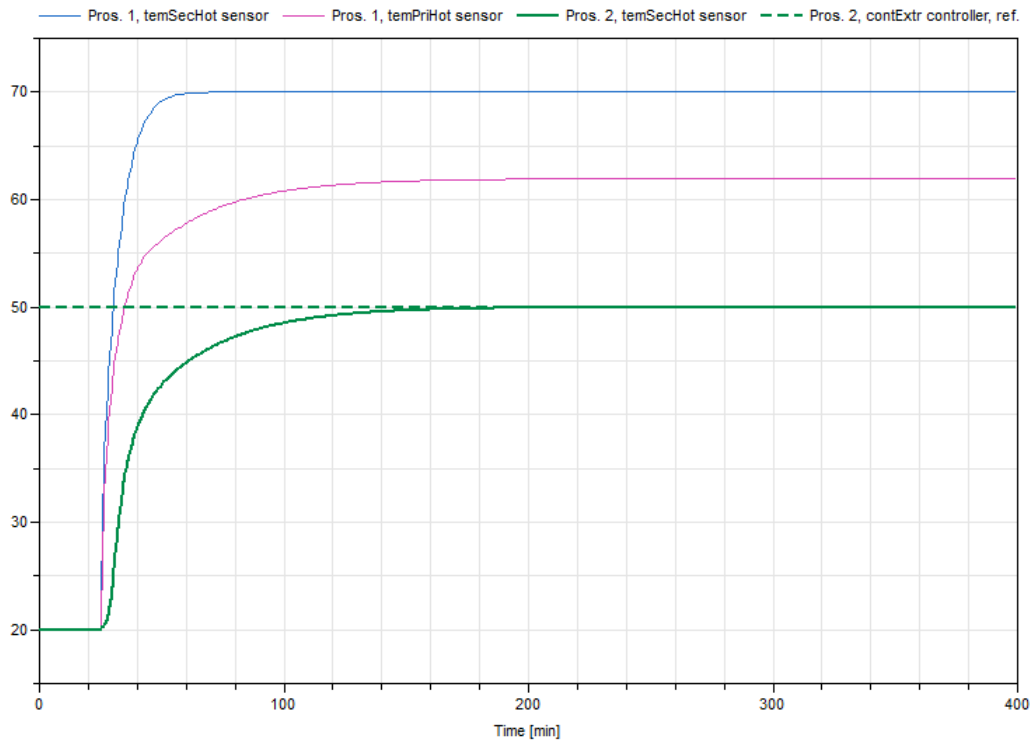

Figure B.5: Temperature plot in secondary and primary sides of prosumers with heating curve switching

C. Parameters of the Model

In this appendix, parameters that were not mentioned in chapters 4 and 5 are given in table 9. If a parameter is not mention, then the default value was taken.

For water properties, i.e. ρ, c_p, μ, a package 'Media.Water' with a model for liquid water with constant density was used from the IBPSA library.

Table 9: Parameters of the model

Parameter	Variable	Description	Value	Unit
		Time constants		
riseTime	τ_{pump}	Feed-in pump (*feedPump*)	$35/20$	$[s]$
riseTime	τ_{pump}	Production pump (*pumpProd*)	5	$[s]$
riseTime	τ_{pump}	Consumption pump (*pumpCons*)	5	$[s]$
riseTime	τ_{pump}	Heat source pump (*pump*)	5	$[s]$
riseTime	τ_{valve}	Control valve (*mainVal*)	5	$[s]$
tau	-	"Cold" pipeline temperature sensor (*temPriCold*)	5	$[s]$
T	$\tau_{b,Q}$	First order system (*firstOrder*) for modelling thermal inertia	240	$[s]$
tau	$\tau_{b,T}$	*heater* control volume inside *heatSource* model	240	$[s]$
use_inputFilter	-	Dynamic speed change for radiator pump (*pumpRad*)	'false'	$[-]$
		Control valve (*mainVal*)		
Kv	K_{vs}	Flow coefficient	2.5	$[m^3/h]$
l	-	Leakage	$2.5 \cdot 10^{-3}$	$[-]$
		Module *thermal model of the buiding*		
V	V_{air}	Air volume of the building	300	$[m^3]$
		Check valve 1 (*cheVal1*)		
m_flow_nominal	-	Nominal mass flow rate	0.134	$[kg/s]$
dpValve_nominal	-	Nominal pressure drop of fully open valve	0.01	$[bar]$
		Check valve 2 (*cheVal2*)		
m_flow_nominal	-	Nominal mass flow rate	0.134	$[kg/s]$

Continued on next page

Parameter	Variable	Description	Value	Unit
dpValve_nominal	-	Nominal pressure drop of fully open valve	0.01	$[bar]$
		Heat exchanger (*HEX*)		
Q_flow_nominal	$\dot{Q}_{nom}$	Nominal heat transfer	30000	$[W]$
T_a1_nominal	$T^{pri}_{nom,\,in}$	Nominal inlet temperature on primary side	70	$°C$
T_a2_nominal	$T^{sec}_{nom,\,in}$	Nominal inlet temperature on secondary side	45	$°C$
m1_flow_nominal	$\dot{m}^{pri}_{nom}$	Nominal mass flow rate on primary side	0.3585	$[kg/s]$
m2_flow_nominal	$\dot{m}^{pri}_{nom}$	Nominal mass flow rate on secondary side	0.3585	$[kg/s]$
dp1_nominal	Δp^{pri}_{nom}	Nominal pressure loss on primary side	$4 \cdot 10^4$	$[Pa]$
dp1_nominal	Δp^{pri}_{nom}	Nominal pressure loss on secondary side	$4 \cdot 10^4$	$[Pa]$
		Internal *PI* controller of "heat extraction controller" (*contExtr*)		
K	-	Gain of controller	0.05	$[-]$
Ti	-	Time constant of integral block	5	$[s]$
		Internal *contPID* controller of "suppression controller" (*contSupr*)		
K	-	Gain of controller	1	$[-]$
Ti	-	Time constant of integral block	10	$[s]$
Td	-	Time constant of derivative block	0.1	$[s]$
		Prosumer 1		
Q_boiler_load	$\dot{Q}_{b,\,nom}$	Nominal thermal power of the heat source	35000	$[W]$
Q_load_design	$\dot{Q}_{l,\,d}$	Design heating load	17500	$[W]$
		Prosumer 2		
Q_boiler_load	$\dot{Q}_{b,\,nom}$	Nominal thermal power of the heat source	56000	$[W]$
Q_load_design	$\dot{Q}_{l,\,d}$	Design heating load	28000	$[W]$

Continued on next page

Parameter	Variable	Description	Value	Unit
		Prosumer 3		
Q_boiler_load	$\dot{Q}_{b,\,nom}$	Nominal thermal power of the heat source	56000	$[W]$
Q_load_design	$\dot{Q}_{l,\,d}$	Design heating load	28000	$[W]$